DNS of biomass pyrolysis and combustion in co-firing power plants

DNS of Biomass Pyrolysis and Combustion In Co-firing Power Plants

PROEFSCHRIFT

ter verkrijging van de graad van doctor aan de Technische Universiteit Eindhoven, op gezag van de rector magnificus prof.dr.ir. F.P.T. Baaijens, voor een commissie aangewezen door het College voor Promoties, in het openbaar te verdedigen op 15 januari 2018 om 16:00 uur

door

Abhijay Awasthi

geboren te Delhi, India

Dit proefschrift is goedgekeurd door de promotoren en de samenstelling van de promotiecommissie is als volgt:

voorzitter:	prof.dr. L.P.H. de Goey
1e promotor:	prof.dr. J. G. M. Kuerten
2e promotor:	prof.dr.ir. B. J. Geurts (UT)
leden:	prof.dr.ir. B.J. Boersma (TUD)
	prof.dr.ir. G. Brem (UT)
	prof.dr.ir. B. Koren
	dr.ir. J.A. van Oijen
	prof.dr. M.E.Z. Golombok

Het onderzoek dat in dit proefschrift wordt beschreven is uitgevoerd in overeenstemming met de TU/e Gedragscode Wetenschapsbeoefening.

Dedicated to the memory of my father

and

to my mother, to whom I owe everything

This work is part of the Industrial Partnership Programme (IPP) Computational Sciences for Energy Research (project code: 12CSER013) of the (former) Foundation for Fundamental Research on Matter (FOM), which is (now) part of the Netherlands Organization for Scientific Research (NWO). This research programme is co-financed by Shell Global Solutions International B.V.

Cover design by: A. Awasthi
Printed by IPSKAMP Printing, Enschede, The Netherlands

A catalogue record is available from the Eindhoven University of Technology Library
ISBN: 978-90-386-4436-3

Summary

Particle-laden turbulent flows can be found in many engineering applications and natural processes. These include internal combustion engines, coal-fired furnaces, and formation of aerosols. Modeling of particle-laden turbulent flows remains a challenging topic due to the dynamic nature of the dispersed phase that modulates the turbulent characterstics of the continuous phase through two-way coupling. Despite the many advancements in computing power, it is still very difficult to simulate millions of particles in a turbulent gas flow. The computing cost for simulating the flow around each individual particle is prohibitively expensive if a large number of particles is present.

The main objective of this thesis is to develop a computational model to simulate the co-firing of coal and biomass. We also do not want to increase the computational costs to unrealistic levels. To do this we adopt a point-particle approach. This approach has been widely used in direct numerical simulation (DNS) of particle laden flows. The particle is treated as a point and correlations are used to compute forces acting on the particle and the heat transfer to the particle. The gas phase is solved within a Eulerian framework, while the dispersed phase (particles) is solved using Lagrangian tracking of particles and solving equations for mass, temperature, and velocity of each individual particle.

In the past, several studies in literature have focussed on coal particle combustion modeling using DNS and large-eddy simulation (LES). Several commercial CFD codes also include models for coal particle conversion. However, these models can not be adopted directly to biomass, since these models make some fundamental assumptions about coal particles that are not valid for biomass particles. The most notable of these are the kinetic models for reactions on the solid particle surface. Moreover, as stated earlier, there are significant differences in chemical composition and thermal properties between coal and biomass particles. These differences in fuel characterstics require a different treatment of biomass particles while modeling their conversion. In this thesis, we use previously developed and validated models for single particle biomass conversion. We adopt these single particle models for their use in a point-particle DNS CFD model. The developed DNS model captures the main qualitative nature of the biomass and coal conversion processes. We use the DNS model to study the effect of various operating parameters like particle size

and solid volume fraction on the solid conversion process.

One of the main parameters of interest in the design of industrial furnaces is the conversion time of solid fuel. The feed rate and sizing of the furnace is primarily determined by the conversion time of solid fuel under given operating conditions. In this thesis, we analyze the effect of different model parameters on the conversion time of solid particles.

In the first part of the thesis (chapter 2 and chapter 3), we focus our attention on DNS of the biomass conversion process. From our simulation results, we observe that the heat exchange between the gas and the particles strongly influences the particle conversion during pyrolysis and combustion. It was observed that the effect of two-way coupling in the energy equation is significant for particle volume fractions $\phi > 1 \times 10^{-5}$. At lower volume fractions $\phi < 10^{-6}$, the effect of particles on the gas is negligible and at such low volume fractions, particles can be modelled by just including one-way coupling to reduce the computational costs. However, typical industrial furnaces have particle volume fractions on the higher side with $\phi > 1 \times 10^{-3}$ and hence the effect of two-way coupling becomes important.

We also find that the conversion time of biomass particles is sensitive to their diameter and increases for larger particles. One of the main findings of the thesis is that at constant particle volume fraction the effect of two-way coupling is higher for smaller particles due to their higher total heat exchange area.

We also study the effect of homogeneous gas phase reactions on the biomass conversion process. We select a relatively simple model for gas phase reactions and qualitatively study the effect of these reactions on the biomass conversion process. It is observed that the inclusion of gas phase reactions in the DNS model decreases the biomass pyrolysis time due to higher gas temperatures. In contrast, including gas phase reactions increases the combustion time of biomass due to the lower availability of oxygen at the particle surface.

The DNS model is also used to perform simulations of realistic biomass particle size distributions (PSD) to compare the particle conversion times for mono-dispersed with PSD cases. We analyze the interactions between particles of different sizes in the PSD case and find that the presence of smaller particles in the distribution speeds up the conversion process of larger particles.

After analyzing the biomass conversion process using the DNS model, we present the model for DNS of coal pyrolysis and combustion. We use single particle coal conversion models from literature for the DNS of coal particles in a turbulent channel flow. As the size of coal particles is very small compared to the biomass particles, the number of coal particles in our simulations is very large. Solving the equations for all the coal particles during the simulation is computationally very expensive and takes a large amount of memory. To overcome this problem we adopt a particle grouping method where a virtual particle represents a number of real coal particles with the same properties. In order to model the interaction between the two phases, we multiply the two way coupling terms between the gas and particles with the

particle grouping factor.

We analyze the accuracy of this particle grouping method by running simulations at varying values of the particle grouping factor (ζ). We observe that a value of $\zeta = N_p/N_{cell}$, where N_p is the number of real particles and N_{cell} the number of grid cells, results in a good approximation for the simulation with no particle grouping. This is true for all the particle sizes and solid volume fractions used in our study. We also observe that the errors due to larger values of ζ are low for simulations with high solid volume fractions, irrespective of the size of the particles.

Finally, we present the model for DNS of co-firing of coal and biomass. We use the models developed for sole firing of coal and biomass for the DNS of co-firing. We define a mass based blending ratio as the ratio between the amount of coal which is substituted by biomass and the original amount of coal. We study the effect of the blending ratio on the conversion of coal and biomass in co-firing. It was observed that during co-firing the presence of coal particles decreases the pyrolysis time of biomass particles, whereas it increases the combustion time of biomass particles. In contrast, the presence of biomass particles increases both the pyrolysis and combustion time of coal particles.

We also study the effect of varying blending ratio on the maximum temperature inside the furnace as it is one of the critical operating parameters for a furnace. Using the co-firing model, we find that as the blending ratio increases the maximum temperature of the gas phase decreases. This is because of the difference in heating values of the coal and biomass. Coal has a higher heating value than biomass, so as the blending ratio, i.e., the fraction of biomass in the solid feed increases, the total heating value of the solid fuel decreases. This causes the maximum temperature of the gas phase to decrease.

We conclude the thesis in the last chapter where we list the capabilities of the DNS model. The main limitations of the DNS model are also presented and a scheme for further improvement of the model in the future is outlined.

List of Symbols

A	Pre-exponential or frequency factor, $kg/m^2/s/atm$
A_ν	Arrhenius parameter for stoichiometric coefficient calculation in char oxidation reaction, $1/Pa$
A_p	Particle surface area, m^2
$a_{g,i}$	Stoichiometric coefficient of the gas in char-gas reactions
c_p	Specific heat, $J/kg/K$
c_v	Specific heat capacity at constant volume, $J/kg/K$
$D_{gi,m}$	Effective diffusion coefficient of the gas species in gas mixture, m^2/s
D_{ij}	Binary diffusion coefficient, m^2/s
d	Particle diameter, m
E	Activation energy, J/mol
e	Gas phase total energy density, J/m^3
e_{int}	Gas phase internal energy density, J/m^3
e_{kin}	Gas phase kinetic energy density, J/m^3
H	Half the channel height, m
h_m	Convective heat transfer coefficient, $W/m^2/K$
j_{gi}	species mass diffusive flux, $kg/m/s$
k_d	Mass transfer coefficient, m/s
k_b	Thermal conductivity of biomass, $W/m/K$
M	Molecular weight, g/mol
m	Mass, kg
N_p	Number of particles
N_{cell}	Number of computational cells in domain
n	Reaction order
P	Pressure, Pa
Pr	Prandtl number
q	Heat Flux, W/m^2
R	Particle radius, m
Re	Reynolds number

r	Surface reaction rate, kg/m^2/s
r	Gas phase reaction rate, kg/m^3/s
r	Radial coordinate
r_c	Char front location, m
r_t	Thermal front location, m
T	Temperature, K
t	Time, s
t_{conv}	Conversion time, s
t_{pyro}	Pyrolysis time, s
t_{comb}	Combustion time, s
$\mathbf{u}$	Gas velocity vector, m/s
V	Volume, m^3
$\mathbf{v}$	Particle velocity vector, m/s
X	Mole fraction
$\mathbf{x}$	Particle position vector, m
x	Streamwise coordinate
Y	Mass fraction
y	Spanwise coordinate
z	Wall-normal coordinate

Greek letters

α	Thermal diffusivity, m^2/s
δ	Average distance between the particles (dimensionless)
ΔH	Heat of reaction, J/kg
ϵ	Emissivity
λ	Thermal conductivity of the gas mixture, W/m/K
μ	Viscosity, kg/m/s
ν	Stoichiometric coefficient in char oxidation reaction
ϕ	Solid volume fraction
ρ	Density, kg/m^3
σ	Stefan-Boltzmann constant, W/m^2/K^4
τ	Stress tensor, Pa
τ_p	Particle relaxation time, s
θ	Blending ratio
ζ	Particle grouping factor

Subscripts

b	Bulk gas phase
c	Char
core	Reactive core (for shrinking core model)
D	Domain
db	Dry basis

g	Gas phase
m	Gas mixture
p	Particle
s	Particle surface
w	Wall
wb	Wet basis

Contents

Chapter 1

Introduction

1.1 Background to biomass co-firing

Renewable energy is key to meet the ever increasing needs in a climate-constrained world. An increased awareness about the depleting fossil fuel resources coupled with a higher sensibility towards environmental pollution has made biomass an attractive alternative energy source. Being the only carbon based renewable fuel in our fossil fuel based economy and due to its large availability in many regions of the world, biomass has attracted the attention of both scientific researchers and industrial companies [1]. Consequently, biomass utilization, as an energy source, has continued to increase and now accounts for over 10% of global primary energy supply [2].

The word biomass refers to all kinds of materials derived from living organisms. This includes plant matter and its derivatives, such as wood, wood-derived fuels, fuel crops, agricultural wastes and by-products, and animal waste [29]. This list comprises the solid, liquid, and gaseous forms of biomass. All these forms of biomass are used to generate energy in the form of renewable energy sources.

The solid biomass, mainly wood and wood-derived fuels, can be burned in furnaces to generate power. This is one of the main, and more mature, biomass-to-energy pathways. It involves generation of power by burning solid biomass along with coal in commercial power plants [3, 7]. This process of co-firing biomass with coal is one of the most economic and easily adaptable methods to increase the proportion of energy generated from renewable sources [4]. The carbon neutrality of biomass is instrumental in reducing the carbon footprint of these co-firing plants [8]. This is particularly beneficial if the biomass used in co-firing is a waste agricultural residue. The idea behind coal-biomass co-firing is to utilize existing coal combustion equipment for burning biomass in order to save on new capital expenditure. Experimental studies have also shown improvement in NOx and SOx emissions when comparing coal firing and co-firing [5, 6].

Biomass, like coal, consists of different groups of chemical compounds which

Table 1.1: Proximate and Ultimate analysis of torrified wood, as an example of biomass fuel, and sub-bituminous coal [29]; db: dry basis, wb: wet basis

	Torrified Wood	Coal
Proximate analysis		
Moisture (wt%, wb)	1.01	2.0
Volatile Matter (wt%, db)	71.5	30.1
Fixed Carbon (wt%, db)	27.6	57.9
Ash (wt%, db)	0.91	12.0
Ultimate analysis		
C	49.9	66.2
H	4.9	4.7
N	0.17	1.4
O (by difference)	44.09	15.7

are classified under the proximate analysis of fuel [83]. These groups - moisture, volatile matter, fixed-carbon, and ash - undergo chemical conversion in a sequence of steps inside a furnace. However, biomass differs significantly from coal in its low carbon, high volatile matter and higher oxygen content [9]. This results in lower heating values for biomass as compared to coal [8], and significant differences in conversion times of the fuel particles during co-firing. A comparison of biomass and coal propreties is given in Table 1.1. These differences in fuel properties result in suboptimal utilization of biomass while burning it in equipment primarily designed for coal [10].

To achieve higher efficiencies in the co-firing process, a better understanding of biomass particle behavior and gas-particle interactions inside the furnace is desired. A deeper knowledge of biomass particle interactions with the gas inside the furnace will be helpful in improving the design of furnaces and optimizing operating conditions by changing for example the properties of the biomass particles. In this thesis, we focus our attention on studying the biomass-coal co-firing by developing a computational model for the process.

1.2 Modeling of particle-laden channel-flow

Particle-laden turbulent flows can be found in many engineering applications and natural processes. These include internal combustion engines, coal-fired furnaces, and formation of aerosols [29]. Modeling of particle-laden turbulent flows remains a challenging topic due to the dynamic nature of the dispersed phase that modulates the turbulent characterstics of the continuous phase through two-way coupling. Despite the many advancements in computing power, it is still very difficult to simulate

millions of particles in a turbulent gas flow. The computing cost for simulating the flow around each individual particle is prohibitively expensive if a large number of particles is present [17, 18].

The main objective of this thesis is to develop a computational model to simulate the co-firing of coal and biomass. We also do not want to increase the computational costs to unrealistic levels. To do this we adopt a point-particle approach. This approach has been widely used in direct numerical simulation (DNS) of particle laden flows [18, 23]. The particle is treated as a point and correlations are used to compute forces acting on the particle and the heat transfer to the particle. The gas phase is solved within a Eulerian framework, while the dispersed phase (particles) is solved using Lagrangian tracking of particles and solving equations for mass, temperature, and velocity of each individual particle.

In the past, several studies in literature have focussed on coal particle combustion modeling using DNS and large-eddy simulation (LES) [18, 19, 20]. Several commercial CFD codes also include models for coal particle conversion. However, these models can not be adopted directly to biomass, since these models make some fundamental assumptions about coal particles that are not valid for biomass particles. The most notable of these assumptions are the kinetic models for reactions on the solid particle surface. Moreover, as stated earlier, there are significant differences in chemical composition and thermal properties between coal and biomass particles. These differences in fuel characterstics require a different treatment of biomass particles while modeling their conversion. In this thesis, we use previously developed and validated models for single particle biomass conversion [12]. We adopt these single particle models for their use in a point-particle DNS CFD model.

1.3 Objectives

The objectives of this thesis are as follows:

- Study the existing models for biomass particle conversion and adopt them for their use in a CFD code
- Develop a DNS model for biomass conversion in a turbulent channel-flow and study the effect of model parameters on the biomass conversion process
- Develop a DNS model for coal conversion in a turbulent channel flow and study the effect of model parameters on the coal conversion process
- Study the coal-biomass co-firing process by varying the coal-biomass blend ratio

1.4 Outline of the thesis

Based on the above objectives, this thesis is organized into different chapters. Chapter 1 presents a general introduction of the problem and motivation for coal-biomass co-firing. Chapter 2 starts off with a literature survey of CFD studies on biomass and coal conversion. This is followed by a description of the biomass conversion process. Next, the single particle biomass pyrolysis and combustion models developed by Haseli [12] are described in detail. After this, the DNS model for the continuous phase (gas) is described. The model development is followed by an analysis of results where we study the effect of varying model parameters like solid volume fraction, particle size, and two-way coupling on the biomass conversion process.

One of the main parameters of interest in the design of industrial furnaces is the conversion time of solid fuel. The feed rate and sizing of the furnace is primarily determined by the conversion time of solid fuel under given operating conditions. In chapter 2, and also in other chapters of this thesis, we analyze the effect of different model parameters on the conversion time of solid particles.

In chapter 2, we focus our attention only on the solid-gas heterogeneous reactions. In chapter 3, we further improve the DNS model by including the homogeneous gas phase reactions. We select a relatively simple model for gas phase reactions and qualitatively study the effect of these reactions on the solid conversion process. In this chapter, we also run simulations by including a particle size distribution for the biomass particles and analyze the interactions between particles of different sizes.

Chapter 4 describes the model development for coal particle conversion. First a short literature survey of LES and DNS studies of coal conversion is presented. This is followed by the description of the DNS model for coal conversion used in this thesis. This includes details of the single particle models for coal pyrolysis and combustion. The coal particles are generally much smaller than biomass particles. For the same particle volume fraction, the number of coal particles is very large as compared to the number of biomass particles and solving equations for all the coal particles in the simulation becomes computationally very expensive. To avoid this, we use a particle grouping method where a number of real coal particles is represented by a single virtual particle. In chapter 4, we study the application of this particle grouping method on the DNS of coal particle conversion. In particular we determine the number of real particles that can be represented by a single virtual particle without significantly changing the results of the simulation.

In chapter 5, we first present the simulation of a particle-size distribution of coal particles. After this, we move to the study of the coal-biomass co-firing process. We use the models developed in previous chapters to simulate the process of co-firing. In particular, we study the co-pyrolysis process by varying the coal-biomass blending ratio. The blending ratio is defined as the ratio between the amount of coal which is substituted by biomass and the original amount of coal. This blending ratio can be mass-based, if the coal is replaced by the same amount of biomass, or energy-

based, if the total heating value of the fuel is kept the same. In this thesis, we study the effects of mass-based blending ratio on the co-firing process, as in most of the industrial settings the mass flow rate of solid fuel is a more relevant and controlled parameter [13].

Finally, we conclude the thesis in chapter 6. Here we list the capabilities of the DNS model and the major conclusions of this work. The main limitations of the DNS model are also presented and a scheme for further improvement of the model in the future is outlined.

Chapter 2

Biomass particle pyrolysis and combustion

2.1 Introduction

Biomass conversion is a complex process where a number of heterogeneous (solid-gas) and homogeneous (gas-gas) reactions take place inside the furnace. Inside a furnace, the biomass particle first undergoes drying where the moisture inside the particle evaporates. This is then followed by pyrolysis/devolatilization of the fuel particle. Upon being heated, the volatile matter in the biomass breaks down and volatile gases are released [13]. The amount and composition of the released volatile gases during pyrolysis vary widely with fuel type, temperature and pressure conditions, and heating rates [14]. Once the volatile gases are released, the virgin biomass is converted into char which mainly consists of the fixed-carbon part of the fuel. Finally, the solid char-particle is converted into gaseous products through heterogeneous combustion reactions. These reactions take place at the char-particle surface where carbon reacts with oxygen and other gases [15].

Various models of biomass conversion processes - pyrolysis and combustion - are available in the literature. Haseli has presented an overview of single-particle models for biomass pyrolysis and combustion [12]. A detailed review of single-particle biomass pyrolysis models is also presented by Di Blasi [13]. The combustion behavior of biomass particles has been extensively investigated by a number of research groups [16, 17]. These single-particle models are usually focussed on the chemistry of the biomass particle reactions and are able to capture variations in important particle quantities - such as particle temperature, mass, and composition - during pyrolysis and combustion. However, in an industrial furnace, the chemical reactions of the biomass particles are always coupled with interphase interactions - in terms of mass, momentum, and heat transfer - between the particles and the gas phase. To capture all physical and chemical phenomena during the biomass combustion inside

a furnace, a model needs to include the interaction of biomass particles with the surrounding gas. The complex two-phase flow with the chemically reacting particles makes Computational Fluid Dynamics (CFD) an ideal choice to study this process [18]. A comprehensive CFD model can complement the costly full (or even small) scale laboratory experiments and measurements that are required in the design and prediction of an efficient biomass combustion process.

In literature, a number of studies on numerical simulations [15-18] of pulverized-coal-fired furnaces can be found. These studies comprise different levels of detail in terms of resolving the length and time scales of turbulence with Reynolds-averaged Navier-Stokes (RANS) equations [19], Large Eddy Simulation [20, 21], and Direct Numerical Simulation [18]. However, similar studies for biomass combustion are relatively few. A 2D simulation of biomass co-firing with coal using a detailed burner geometry is presented by Ghenai and Janajreh [22]. They model turbulence using the RANS equations with the $k-\epsilon$ turbulence model and adopt a stochastic tracking model to predict particle dispersion. Hara et al. [23] present a DNS of a turbulent pulverized-coal jet flame using a two-step global reaction scheme for pyrolysis of coal. Brosch et al. [24] present the DNS of pulverized coal combustion with detailed explanations for the observed effects of root mean square velocity fluctuations of the gas phase and particle size on the coal particle combustion. To the best of the author's knowledge, the present work is the first to investigate biomass combustion in a 3D turbulent gas flow by means of DNS, thereby extending our understanding from pulverized-coal-fired furnaces to furnaces suitable for biomass conversion.

The method of Direct Numerical Simulation has the unique advantage, over other methods, of resolving all length and time scales involved in the turbulence. In order to model the thermo-chemical conversion of the biomass particles at realistic volume fractions, and their interaction with the surrounding turbulent gas flow, the DNS model for the gas phase needs to be coupled with single particle chemistry models of a biomass particle. To simulate the gas flow with a large number of biomass particles, simplified models of biomass pyrolysis and combustion are required to reduce the computation time to acceptable levels. The single-particle models available in literature [25, 26] are very complex and will result in very high computational costs. Haseli et al. [27, 30] developed simplified models for biomass pyrolysis and combustion based on some key parameters of interest, like the surface temperature of particles, the amount of volatiles released, and the conversion time of particles. Russo et al. [28] combined Haseli's pyrolysis model [12] with a model for particle tracking and simulated 3D turbulent particle-laden channel flow by including the two-way interactions of particles with the gas phase.

Here, we extend Russo's model for biomass pyrolysis in a channel flow [29] by adding the relevant solid-gas heterogeneous reactions. The turbulent gas flow is solved in an Eulerian manner while the particles are tracked in a Lagrangian framework. The two-way gas-particle interactions are modeled in detail. It should be noted that the presence of particles in turbulent gas flow in principle requires the

flow around each particle to be resolved in order to be truly called DNS. However, to simulate millions of chemically reacting particles which interact with a turbulent gas flow, the computational power required to resolve all details of the flow around the particles would be impossibly high [31, 32]. It is a common practice to adopt a point-particle approach for simulating flows with a large number of particles. This approach is particularly suitable where particle sizes are smaller than the Kolmogorov scale η of the turbulent flow [33, 34], which is satisfied in all simulations presented in this chapter. The typical size of biomass particles in this work is less than 1 mm. Luo et al. [18] employ this point-particle approach in their DNS model for pulverized-coal combustion. Several other studies have adopted this approach to perform DNS and LES [36, 37, 38] of particle-laden turbulent gas flows.

Our aim is to develop a DNS model for biomass conversion in a turbulent gas flow, which can help to better understand the process inside a furnace. The results of the DNS model can be used for the development of engineering models of the process, thus facilitating the optimization of the co-firing process parameters like conversion time, oxygen-fuel ratio and biomass-coal ratio. The interaction between turbulence and chemistry in solid-fuel combustion systems is very important but still not well understood [39]. A DNS model can be instrumental in analyzing the effects of turbulence on the reaction chemistry inside a combustor. In this chapter, the framework for the development of such a DNS model, involving the two-way interactions of chemically reacting particles with the gas, is presented. In order to establish the need for a detailed DNS model, including in particular the gas phase transport and interactions, over the single-particle models for the biomass conversion, we analyze the effects of two-way interactions on the biomass conversion process.

In section 2.2 we describe the biomass conversion and particle tracking models used in the DNS. Section 2.3 outlines the gas phase equations including the two-way coupling terms between the solid and the gas phase. This is followed by the details of numerical method (section 2.4) and the setup of simulation (section 2.5). Finally, we end this chapter with the analysis of the DNS results and concluding remarks in section 2.6.

2.2 Biomass particle model

This section presents the pyrolysis and combustion models for biomass particles used in the DNS. The equations of motion for Lagrangian tracking of particles are also presented in this section.

When simulating a large number of particles undergoing thermochemical conversion, the usage of detailed models for particle conversion would cost considerable computational efforts and time. These detailed models would solve transport equations and chemical kinetics to compute time and space evolution of temperature and

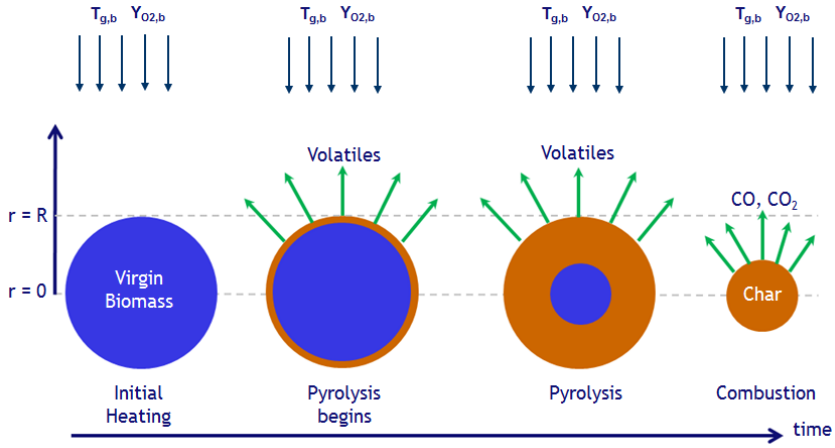

Figure 2.1: Stages of the biomass conversion process - pyrolysis and combustion; $T_{g,b}$ and $Y_{O2,b}$ are the bulk gas temperature and bulk gas oxygen concentration respectively; R is the initial radius of the biomass particle.

species mass inside each particle. However, for many industrial applications, only a few key parameters - such as particle surface temperature, rate and amount of particle mass loss, and the duration of conversion processes - are of interest. In this work, simplified models for particle conversion which include equations for particle surface temperature, surface reaction rates, and mass loss from particles are used. These models have sufficient accuracy for engineering purposes of predicting particle conversion times and gas temperatures [12].

The type of biomass in the simulations is torrified wood. The torrefaction of biomass is essentially a drying process, which involves thermo-chemical treatment of biomass particles at 200-300 ^{o}C. Drying, in absence of oxygen, evaporates the moisture content of the biomass particle and therefore the quality of fuel, in terms of its grindability and hydrophobicity, is improved. After torrefaction, the biomass is milled to fine particles before being fed into the furnace. The key differences between wood and torrified wood, after milling, are the smaller size and the more spherical shape of the torrified fuel particles [40] which is convienient as the biomass pyrolysis and combustion models that follow are based on the assumption of a spherical shape of the particle. Biomass particles can be of complex shape and structure [13] and can even have anisotropic properties [41]. Nevertheless, for torrified wood particles, the assumption of a spherical shape is better justified than for untorrefied wood.

Figure 2.1 shows the sequence of steps in the biomass conversion process. In the present model, biomass pyrolysis and char combustion reactions take place in sequence and not simultaneously, i.e., pyrolysis is followed by combustion. A justification for this, as offered by Haseli [12], is that during pyrolysis the outward flux of volatile gases released during pyrolysis from the particle is rather strong and

hence significantly delays the diffusion of oxygen from the bulk gas to the particle surface. This prevents combustion reactions at the solid surface from happening until pyrolysis is finished. Hence, our choice for a sequential treatment of pyrolysis and combustion reactions.

2.2.1 Biomass pyrolysis model

Pyrolysis of a solid fuel - biomass or coal - is the thermal degradation of the solid in the absence of oxidizing agents. This thermo-chemical conversion results into many products that are, for simplicity, lumped into three groups: permanent gases, a pyrolytic tar, and char [42]. The permanent gases and tar are the volatiles evolved from the solid upon heating. The remaining solid gets converted into char subsequently. The relative amount of volatile gases and char produced during pyrolysis depends on the type of fuel. Torrified biomass contains a high percentage, typically about 70% [13], of volatile matter with the rest being fixed-carbon and ash. In light of this fact, the process of pyrolysis becomes very important particularly for biomass in order to contribute to effective co-firing.

We adopt the model developed by Haseli [27] for the pyrolysis of biomass particles. The model consists of several phases during which the biomass particle evolves from virgin biomass to char. Although we adopt a point-particle assumption which usually implies a uniform temperature inside the particle, the pyrolysis model developed by Haseli [27] is based on thermal diffusion inside the particle which results in temperature variations within the particle. Another key aspect of the model is the assumption of a pyrolysis temperature, i.e., the temperature at which the virgin biomass is converted into char with the release of volatile gases. As soon as the temperature of a layer of virgin biomass inside the particle reaches this pyrolysis temperature, biomass breaks down into volatile gases and char. The choice of the pyrolysis temperature has been a matter of debate in literature, and some studies [43] justify this assumption by choosing a suitable value for the pyrolysis temperature such that the overall energy balance agrees well with experimental data.

In Appendix A, we present in detail the pyrolysis model of Russo et al. [28] which is a further computational development of Haseli's work [12]. The model considers a spherical biomass particle with uniform initial temperature. The particle is subjected to an inward heat flux at its surface, due to the hot surrounding gas, and the surface temperature of the particle starts to rise. The temperature profile inside the particle evolves as well due to its thermal diffusivity. This phase is called *heating of the virgin biomass* and involves two distinct regions inside the particle - an outer region close to the surface where the temperature has changed, and an inner region where the temperature is still at its initial value. The position of the moving *thermal front*, i.e., the position inside the solid particle where the temperature is still at its initial value is tracked during this phase.

At some point the *thermal front* reaches the particle centre and the second phase

Table 2.1: Kinetic data for char oxidation and char gasification used in this study [12]

Reaction	Pre-exponential factor ($kg/m^2/s/atm^n$)	Activation energy (kJ/kmol)
Oxidation	382	70810
Gasification	362	165050

- *pre-pyrolysis heating* - starts. The only difference between the first two phases is in their mathematical formulation. Once the temperature of the particle surface reaches the pyrolysis temperature, volatiles are released and biomass is converted into char. This third phase of *pyrolysis* is marked by the movement of a char front from the particle surface towards the particle center. The thin layer which has reached the cut-off pyrolysis temperature is instantaneously converted into char and volatile gases. The char front separates the volume of the particle - which remains constant during the pyrolysis - into two regions: an outer region of char and an inner region of virgin biomass.

Once the pyrolysis stage has finished completely, the biomass has been converted into char. The solid char then reacts with gases through heterogeneous solid gas reactions which are described in the next section.

2.2.2 Biomass combustion model

The last stage during biomass particle conversion includes char oxidation and char gasification reactions with carbon dioxide. The combustion model of Haseli et al. [30], used for the DNS, is presented in this section. For simplicity, the char obtained after pyrolysis is treated as pure carbon. We only consider the two most relevant heterogeneous reactions of solid char with gases - char oxidation with oxygen and char gasification with carbon dioxide:

$$C + \nu O_2 \rightarrow 2(1-\nu)CO + (2\nu - 1)CO_2 \tag{2.1}$$

$$C + CO_2 \rightarrow 2CO \tag{2.2}$$

In the above equations the stoichiometric coefficient, ν, of oxygen in the char oxidation reaction (1) determines the molar ratio of CO and CO_2 in the reaction products. This coefficient, which satisfies $0.5 < \nu < 1$, depends on the temperature and is given by an Arrhenius type equation:

$$\frac{2(1-\nu)}{(2\nu-1)} = A_\nu \exp\left(-\frac{E_\nu}{RT_s}\right) P_{O2,s} \tag{2.3}$$

where A_ν and E_ν are Arrhenius parameters, R is the universal gas constant, T_s is the particle surface temperature, and $P_{O2,s}$ is the partial pressure of oxygen at the particle surface.

The combustion model is formulated based on the traditional shrinking core approximation. This implies that the char-gas reaction front, where reactions (1) and (2) take place, starts at the surface of the particle and progresses towards the center as the reactions take place. This results in a decreasing particle size with continuing reactions. However, the mass density of the shrinking reactive core remains unchanged throughout the combustion process. In the shrinking core model, the radius of the reactive core of the particle, R_{core}, is calculated as follows:

$$\frac{dR_{core}}{dt} = \frac{-\sum_i r_i}{\rho_c} \tag{2.4}$$

where ρ_c is the density of the char, and r_i are the rates of surface reactions (1) and (2) of the char particle with the gases. The reactions rates are described by an Arrhenius law in the following way:

$$r_i = A_i \exp\left(-\frac{E_i}{RT_s}\right) P_{i,s} \tag{2.5}$$

The kinetic data, i.e., pre-exponential factors (A_i), and the activation energies (E_i), are selected from a wide range of experimental data [12, 30] and are given in Table 2.1. To calculate the surface reaction rates, the partial pressures of various gases at the particle surface ($P_{i,s}$) need to be determined. We adopt the following approach for this. Using a quasi steady-state assumption the conservation of mass of O_2 and CO_2 leads to the following balance equations:

$$\rho_g k_{d,O_2}(Y_{O_2,b} - Y_{O_2,s}) - (r_1 + r_2)Y_{O_2,s} = \frac{M_{O_2}}{M_c}\nu r_1 \tag{2.6}$$

$$\rho_g k_{d,CO_2}(Y_{CO_2,b} - Y_{CO_2,s}) - (r_1 + r_2)Y_{CO_2,s} = \frac{M_{CO_2}}{M_c}(r_2 - (2\nu - 1)r_1) \tag{2.7}$$

where ρ_g is the gas mass density, k_d is mass transfer coefficient, Y is the gas species mass fraction, M_c is the molecular weight of char (carbon), and M is the molecular weight of the gas species. In the above equations, the first term on the L.H.S. represents the mass flux of gas due to diffusion from the bulk gas phase (subscript 'b') to the particle surface (subscript 's'). The second term denotes the convective flux of gases leaving the particle surface. The term on the R.H.S. equals the net rate of mass consumption of the gas species due to the surface reactions. The above balance equations are used to calculate mass fractions Y of the gases at the particle surface. Subsequently, the partial pressures of gases at the particle surface are determined for calculating the reaction rates. To calculate the rates of reactions (1) and (2), we only need to calculate the partial pressures of O_2 and CO_2 at the particle surface.

Apart from the partial pressure of gas species, the combustion model also requires the calculation of the particle surface temperature (T_s) at which the chemical reactions take place. During the combustion stage, the temperature of a particle is calculated from the principle of conservation of energy with an assumption of uniform temperature inside the particle [12, 15]. The particle exchanges heat with its surroundings - wall and the gases - through convection and radiation. Apart from this, there is also heat generation due to the exothermic char oxidation reaction (1) and heat consumption due to the endothermic char gasification reaction (2). The net enthalpy balance over the particle surface is described in the following way:

$$m_p c_{pc} \frac{dT_s}{dt} = h_m A_p (T_g - T_s) + \sigma \epsilon A_p (T_w^4 - T_s^4) + \sum_i r_i A_p \Delta H_i \tag{2.8}$$

where m_p is the mass of the particle and A_p is its surface area, c_{pc} is the specific heat capacity of char, σ is the Stefan-Boltzmann constant, ϵ is the emissivity, ΔH_i is the heat of reaction for the char-gas reactions, and T_w is the reactor wall temperature.

We model radiation only between particles and channel walls. The gas radiation has been neglected and the gases are considered to be non-gray [44]. We model biomass combustion in air whose combustion characterstics are very different from oxy-fuel combustion [44, 45]. In fact, in oxy-fuel combustion, considerably higher partial pressures of CO_2 and H_2O emerge in the product gas, which sum up to almost 1 atm even for operation of the furnace at atmospheric pressure. This means that radiative emissions from gases are significant and the gases should be considered as 'gray' as far as gas radiation is concerned. Correspondingly, gas radiation should be explicitly included in models for oxy-fuel combustion. However, during combustion in air, the lower concentrations of O_2 result in much lower radiative emissions from gases. Here, the initial concentration of O_2 results in a maximum partial pressure of CO_2 of only 0.15 atm , i.e., much smaller than in oxy-fuel combustion. Hence we neglect gas radiation and treat the gas as transparent. A similar approach has recently been employed in the Direct Numerical Simulation studies of combustion of coal particles [47].

Substituting $m_p = \rho_c V_p$ with ρ_c the char mass density, particle volume $V_p = \frac{4}{3}\pi R_{core}^3$ and $A_p = 4\pi R_{core}^2$ in the above equation, we get:

$$\frac{1}{3} R_{core} \rho_c c_{pc} \frac{dT_s}{dt} = h_m (T_g - T_s) + \sigma \epsilon (T_w^4 - T_s^4) + \sum_i r_i \Delta H_i \tag{2.9}$$

In this subsection, we described the particle conversion model for the combustion stage. The model includes char-combustion and char-gasification reaction with CO_2 and is based on a shrinking core approximation. During the DNS we calculate the surface temperature for all particles separately. Each particle is characterized by its location, velocity, temperature, radius, and its char and biomass content. A

summarized scheme of the biomass pyrolysis and combustion models used in this work is illustrated in Figure 2.2.

In the next subsection, we describe the equations used for tracking solid particles in the DNS model.

2.2.3 Particle tracking model

For particle tracking a Lagrangian formulation is used. We use the formulation for drag force on a spherical particle in a gas flow. Similar assumptions were adopted by Ma et al. [48] who use a shape factor to incorporate effects of non-spherical particles. We assume the particle to be spherical while non-sphericity of the particle will be a future model improvement. As the focus of the study is not on the settling of particles, and due to the small sizes and short residence time of the particles inside the reactor furnace, we do not take gravity into account. Newton's law applied to a particle which experiences a drag force in a gas flow field can be written as:

$$\frac{d(m_i \mathbf{v}_i)}{dt} = m_i(\mathbf{u}(\mathbf{x}_i, t) - \mathbf{v}_i)\frac{1 + 0.15Re_p^{0.687}}{\tau_p} + \mathbf{v}_i\frac{dm_i}{dt} \tag{2.10}$$

where m_i is the mass of the particle, $\mathbf{v}_i$ its velocity, and τ_p is the particle relaxation time. The velocity of the gas at the particle position $\mathbf{x}_i$ is represented by $\mathbf{u}(\mathbf{x}_i, t)$. The two terms on the R.H.S of equation (2.10) are the drag force and the change in momentum of the particle due to mass loss from the particle during the pyrolysis and combustion stages. We use the Schiller-Naumann drag correlation which is valid for particle Reynolds numbers between 0 and 1000. Another way of writing Eq. (2.10) is in terms of acceleration which directly yields the particle equation of motion:

$$\frac{d\mathbf{v}_i}{dt} = (\mathbf{u}(\mathbf{x}_i, t) - \mathbf{v}_i)\frac{1 + 0.15Re_p^{0.687}}{\tau_p} \tag{2.11}$$

where the particle relaxation time, τ_p, is calculated based on the mass density (ρ_p) and size (d_p) of the particle as $\tau_p = d_p^2\rho_p/(18\mu_g)$, where μ_g is the viscosity of the gas. The particle size d_p remains constant during the pyrolysis stage, whereas it varies during the combustion stage according to the shrinking core model. The position of the particle is obtained by integration of the trajectory equation in time, where the particle velocity is calculated from Eq. (2.11):

$$\frac{d\mathbf{x}_i(t)}{dt} = \mathbf{v}_i \tag{2.12}$$

with $\mathbf{x}_i$ and $\mathbf{v}_i$ the position and the velocity of the particle, respectively.

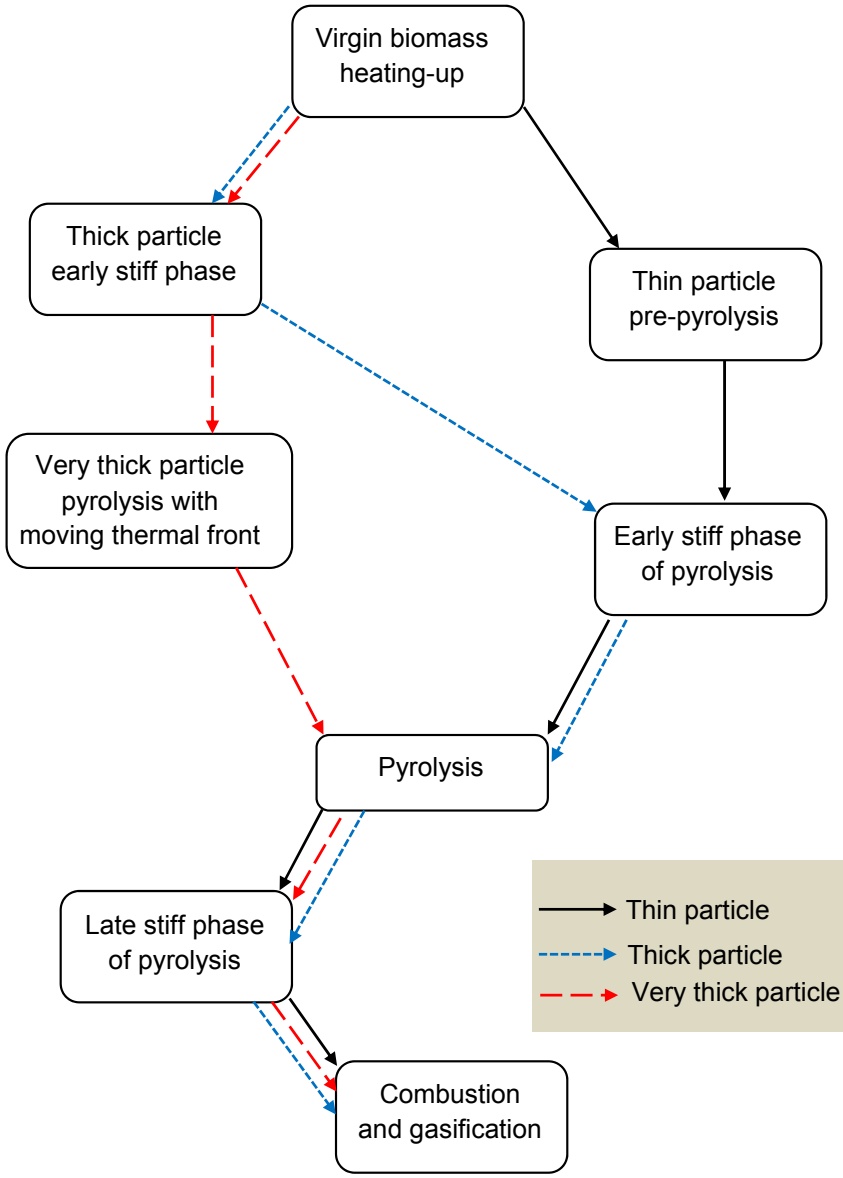

Figure 2.2: Scheme of the routes of a biomass particle undergoing pyrolysis and combustion; in the flow diagram the conversion routes followed by the particle are dictated by the different criteria. Details of the biomass pyrolysis model are given in Appendix A.

2.3 Gas model

The evolution of the flow in the gas phase is governed by a set of transport equations describing conservation of mass, momentum, energy, and gas species mass. In this

section, we formulate these conservation laws as well as the constitutive equations required to complete their formulation. The continuous gas phase is treated in an Eulerian way. The range of temperatures involved in the process of biomass pyrolysis and combustion is quite high (500-1500 ^{o}C). This results in large variations in mass density of the gas phase which is treated as a compressible Newtonian fluid.

Presently, the model includes 6 gas species - O_2, CO_2, CO, CH_4, H_2O, and N_2. We consider all the volatiles released during pyrolysis as methane. In the present chapter, homogeneous gas phase reactions have been neglected, i.e., we consider the gas mixture to be inert. We will discuss the effects of homogeneous gas phase reactions on the biomass conversion process in the next chapter.

The governing equations for the gas can be written as the volume integral of conservation laws over an arbitrary volume V with boundary S:

$$\int_V \frac{\partial \mathbf{w}}{\partial t} \mathrm{dV} + \int_{\partial V} \hat{n}.f_c \, dS = \int_{\partial V} \hat{n}.f_v \, dS + \int_V L_{2way} \, dV + \int_V F \, dV \tag{2.13}$$

with $\mathbf{w}(\mathbf{x},t) = [\rho u, \rho v, \rho w, \rho, e, \rho_{O2}, \rho_{CO2}, \rho_{CO}, \rho_{CH4}, \rho_{H2O}]^T$ the vector of dependent variables. Here, ρ is the total mass density of the gas; u, v, and w are the Cartesian components of the velocity vector; e is the total energy density; $[\rho_{O_2}$,ρ_{CO_2},$\rho_{CO}, \rho_{CH4}, \rho_{H2O}]$ are the mass densities of individual gas species, t denotes the time, and $\mathbf{x} = [x, y, z]^T$ is the vector of Cartesian co-ordinates. These governing equations express that the rate of change of $\mathbf{w}$ in the volume V is due to the convective fluxes (f_c), the diffusive fluxes (f_v), the two-way coupling terms (L_{2way}) which account for the presence of the particles, and F the source terms in the gas phase. The source term F consists of a driving force, for the channel flow, that is added to the streamwise momentum equation in such a way that the total mass flow rate in the streamwise direction is kept exactly constant.

The above set of differential equations is completed with an equation of state for the gas. In most combustion problems where the temperatures are quite high, the gas mixture and its components are treated as ideal gases. Therefore, the thermal equation of state is given by the ideal-gas law:

$$\rho = \frac{P\bar{M}}{RT} \tag{2.14}$$

with R the universal gas constant, and $\bar{M}$ the average molar mass which is defined as

$$\bar{M} = \left(\sum_i^{N_g} \frac{Y_i}{M_i} \right)^{-1} \tag{2.15}$$

with N_g the number of gas species, M_i the molar mass of gas species i and Y_i its mass fraction in the gas mixture. The vector of dependent variables $\mathbf{w}(\mathbf{x},t)$ in eq.

(2.13) contains $5 + N_g - 1$ components. The mass fractions of gas species (Y_i's) vary with both position and time, and so does the average molar mass of the gas. The density of N_2 is calculated by completing the balance as

$$\rho_{N_2} = \rho - \rho_{O_2} - \rho_{CO_2} - \rho_{CO} - \rho_{CH4} - \rho_{H2O} \tag{2.16}$$

The temperature of the gas mixture (T_g) is determined from the total energy density e which is given as

$$e = e_{int} + e_{kin} \tag{2.17}$$

where

$$e_{kin} = \frac{1}{2}\rho u_i u_i \tag{2.18}$$

$$e_{int} = \sum_{i}^{N_g} \rho_i c_{vi} T_g \tag{2.19}$$

The internal energy density is calculated from equations (2.17) and (2.18). This is then used to calculate the temperature T_g from equation (2.19). The specific heat capacity of the gas species at constant volume is calculated using the relation $c_{vi} = c_{pi} - R_i$, where c_{pi} is the specific heat capacity at constant pressure, and R_i is the specific gas constant for the gas species. Gas species heat capacities at constant pressure, c_{pi}, are calculated as a linear function of temperature using correlations derived from NIST data [49]. Similar temperature dependent correlations [12] are used to calculate the thermal conductivity (λ_i) and the viscosity (μ_i) of the gas species. The properties of the gas mixture are determined as the mass weighted average of the individual gas species properties. Once the temperature and density of the gas species are known, the pressure of the gas mixture is determined using ideal gas equation (2.14).

To determine the fluxes in equation (2.13), we require models for calculating the stress tensor (τ), the heat-flux vector ($\boldsymbol{q}$), and the diffusive fluxes of the gas species (j_{gi}). The stress tensor of the gas mixture is calculated as the stress tensor for a single-component Newtonian fluid using Stokes' assumption and is expressed as:

$$\tau = -\mu(\nabla \mathbf{u} + (\nabla \mathbf{u})^T - \frac{2}{3}(\nabla . \mathbf{u})\mathbf{I}) \tag{2.20}$$

where μ is the gas mixture viscosity and $\mathbf{I}$ is the unit tensor.

In the present model we only include heat transport due to thermal conduction and neglect the transport due to mass diffusion. The effects due to pressure and concentration gradients are usually negligible [50]. For the heat flux $\boldsymbol{q}$ we adopt the often used Fourier expression for thermal conduction [51]:

$$\mathbf{q} = -\lambda \nabla T \tag{2.21}$$

with λ the thermal conductivity of the gas mixture.

The gas species conservation involves the calculation of species mass diffusive fluxes, $j_{g,i}$. The diffusion of the gas species can be caused by concentration gradients, pressure gradients, and temperature gradients in the gas mixture [52]. The effects of temperature and pressure gradients on the diffusion of gas species are negligible [50]. The diffusion caused by concentration gradients is described by the Stefan-Maxwell equation [53]. However, in this equation the diffusion rate of one species depends on the concentration gradients of all other species, which makes the use of this equation computationally very expensive. So, the calculation of the diffusive flux in the current model is treated in a simplified manner by using an expression which is similar to Fick's law of binary diffusion. The species mass diffusive fluxes, $j_{g,i}$ are calculated as

$$j_{gi} = D_{gi,m} \nabla \rho_i \tag{2.22}$$

where $D_{gi,m}$ is an effective diffusion coefficient of the gas species in the gas mixture given by:

$$D_{gi,m} = \frac{1 - X_{gi}}{\sum_{i \neq j} \frac{X_{gj}}{D_{gi,gj}}} \tag{2.23}$$

where X_{gj} is the mole fraction of the gas species and $D_{gi,gj}$ is the binary diffusion coefficient of the gas pair available as a function of temperature [12].

2.3.1 Two-way coupling

The two-way coupling terms (L_{2way}) in the governing equations for the gas phase (eq. (2.13)) account for the transfer of mass, momentum and energy between the gas and the particles. It should be noted, that these terms do not change the total mass, total momentum and total energy of the system but rather account for the transfer between the discrete and the continuous parts of the model. The assumption is that all these two-way coupling terms act as point sources in the conservation laws for the gas phase. The control volume in which a particle is located can be identified from the coordinates of the centre of the particle. The coupling terms stemming from this particle will be included only in the gas equations of this control volume.

The two-way coupling term in eq. (2.13) can be written as:

$$\int_V L_{2way}\, dV = -\sum_i \frac{d}{dt} \begin{bmatrix} m_i u_i \\ m_i v_i \\ m_i w_i \\ m_i \\ e_i \\ m_{O2,i} \\ m_{CO2,i} \\ m_{CO,i} \\ m_{H2O,i} \end{bmatrix} \tag{2.24}$$

where the sum is taken over all particles within the volume V. The first three components represent the momentum exchange between the two phases and are calculated using Eq. (2.10). The fourth component in equation (2.24) is the total mass exchange between particles and gas phase due to pyrolysis and combustion reactions. The mass exchange term, $\frac{dm_i}{dt}$, for the various stages of conversion of particles - pyrolysis and combustion - is calculated based on the change in particle density during the pyrolysis stage or corresponding reaction rates during the combustion stage. For pyrolysis:

$$\left(\frac{dm_i}{dt}\right)_{pyro} = 4\pi r_c^2(\rho_B - \rho_c)v_c \tag{2.25}$$

For combustion:

$$\left(\frac{dm_i}{dt}\right)_{comb} = 4\pi R_{core}^2 \sum_i r_i \tag{2.26}$$

where r_c and v_c are the radius and velocity of the char front and ρ_B and ρ_c are the mass densities of the solid biomass and char respectively.

The fifth component in eq. (2.24) is the two-way coupling term for the energy exchange between the particles and the gas. It includes convective heat exchange between the gas and the particle surface, heat released or consumed during the particle conversion, and the change in kinetic energy of the particles:

$$\frac{de_i}{dt} = h_m A_{p,i}(T_g - T_i) + c_{v,g}T_p\left(\frac{dm_i}{dt}\right)_{pyro} + c_{v,g}(T_i - T_g)\left(\frac{dm_i}{dt}\right)_{comb} - \frac{d}{dt}(\frac{1}{2}m_i v_i^2) \tag{2.27}$$

The first term in the above equation is the convective exchange between the gas and the particles which depends on the particle surface area A_p, relative temperature difference between the particle and the gas $(T_g - T_i)$, and the heat transfer coefficient h_m which is calculated using the following well established correlation for a spherical particle:

$$h_m = \frac{\lambda}{d_p}(2 + 0.6Re^{1/2}Pr^{1/3}) \tag{2.28}$$

The second term in eq. (2.27) is the energy associated with the release of volatile gases from the biomass during pyrolysis. The volatiles are released at the char front at the pyrolysis temperature, T_p. The specific heat capacity of the volatiles is calculated for methane. The third term in eq. (2.27) is energy exchange associated with the combustion stage. Gases (O_2 and CO_2) at bulk gas temperature, T_g, travel to the particle surface where they react with the solid char and the gaseous products of the reactions are formed at the particle surface temperature, T_i. The last term in eq. (2.27) is the change in kinetic energy of the particle due to their motion within the gas flow.

Apart from the total mass, momentum, and energy exchange terms between the gas and the particles, eq. (2.24) also contains the species exchange terms. These species mass exchange terms are calculated based on the rates of char-gas reactions (1) and (2):

$$\frac{dm_{g,i}}{dt} = A_{p,i} \sum_i a_{g,i} r_i \tag{2.29}$$

where $a_{g,i}$ is the stoichiometric coefficient of the corresponding gas species in the char-gas reactions.

The properties of the gas at the particle position need to be computed because they appear in the particle equations and in the two-way coupling terms. To this end a trilinear interpolation is employed that uses the values of gas properties in the control volume where the particle is located and in the neighbouring control volumes.

2.4 Numerical Method

All equations for the gas and the particles are non-dimensionalized using appropriate reference values. The particle equations are in the form of ordinary differential equations. The gas equations assume this form after the spatial discretization based on a second-order accurate finite volume method. To this effect, the domain is divided into small rectangular cells, closely following Russo et al. [28]. All the dependent variables are stored in cell centers. All convective and viscous fluxes in eq. (2.13) are calculated at the cell faces. The values of the dependent variables at cell faces are determined by averaging over the values of the two nearest neighbouring cell centers. The spatial derivatives of velocity components, temperature, and gas species concentrations at the cell faces, which are required in the calculation of viscous fluxes, are calculated using the smallest stencil possible. The two-way coupling terms in eq. (2.24) account for all particles present in the cell.

Boundary conditions in the streamwise and spanwise directions are periodic. In the wall-normal direction the walls of the channel coincide with the boundaries of the cells neighbouring the walls. No-slip boundary conditions are applied at the walls for all three velocity components. An isothermal wall condition is applied to the energy conservation equation with a constant temperature set for both the upper and the lower wall. A zero-flux condition is applied to the species conservation equations with the gradients of gas species concentrations set to zero at the walls. The wall is also considered to be inert and all the solid-gas reactions take place only at the biomass particle surface.

In the wall normal direction, the faces of the cells adjacent to the wall coincide with these walls. For the convective flux the only non-zero flux is then due to the pressure. The temperature at the wall is given by the constant temperature wall boundary condition. The three velocity components at the cell faces at the wall are given by no-slip boundary conditions. The mass density and the energy density at the cell faces are the average of the values at the first cell inside the geometry and the dummy cell outiside the geometry. The value of the energy density in the dummy cell is set equal to the energy density in the first cell.

2.4.1 Time Integration

Due to the coupling between the gas and the particles, it is important that the particle and the gas equations are evaluated at the same time level. Russo et al. [28] used a low-storage second-order explicit Runge-Kutta scheme to simulate the process of biomass pyrolysis. We extend their model by including the combustion stage in the particle conversion model. The results of a single-particle model for particle surface temperature vs. time during the pyrolysis and combustion stages are shown in Figure 2.3. In figure 2.3 different stages of the particle conversion process can be identified, and are marked, in the particle temperature profile. The first stage is the initial heating-up of the virgin biomass which continues until the particle surface temperature reaches the pyrolysis temperature (I). We use a value of pyrolysis temperature equal to 600 K in this work. Once the particle surface temperature reaches this value, pyrolysis of the biomass starts. This continues until all the virgin biomass in the particle is converted into char. During this period, volatile gases are released (II). Afterwards the combustion of the particle starts where oxygen diffuses from the bulk gas to the particle surface. The highly exothermic and fast char combustion reaction at the particle surface results in a rapid rise of particle surface temperature (III). Once the particle radius becomes very small, we stop the combustion reaction and the remaining particle cools down to the surrounding gas temperature. We stop the combustion reaction when the reaction core radius shrinks down to 1% of the initial particle size.

It can be seen in figure 2.3 that the rate at which the particle temperature rises in the combustion stage is much faster than during the pyrolysis stage. The

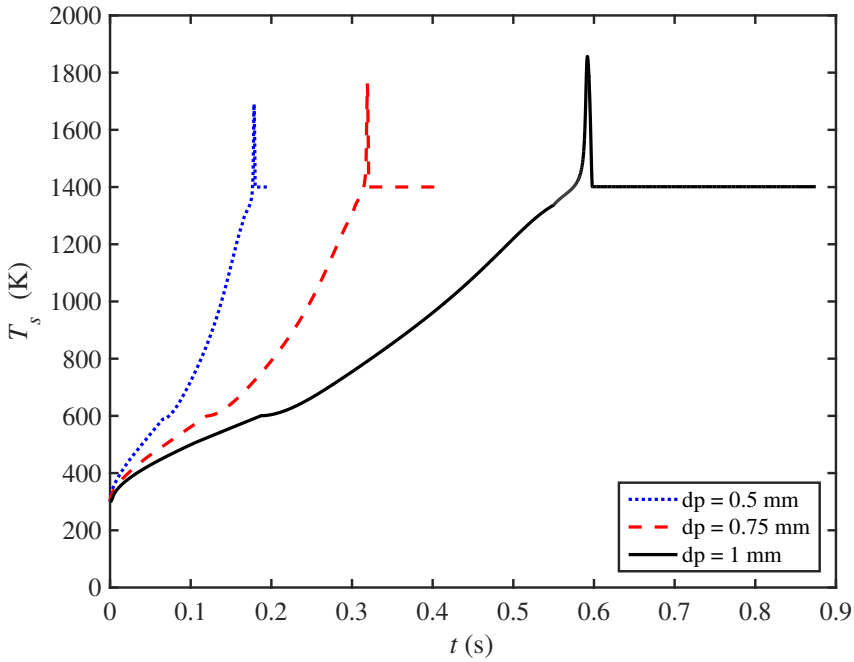

Figure 2.3: Single-particle model results for particle surface temperature (T_s) vs. time (t) during the pyrolysis and combustion stages for various values of the particle diameter as indicated in the legend. The initial particle temperature is 300 K and the temperature of the channel walls is 1400 K.

fast nature of the combustion process presents itself in the form of stiffness of the system of equations. This renders the explicit Runge-Kutta scheme (as used during pyrolysis) inefficient for solving the particle model equations, as a large number of time steps is required to achieve stability. To resolve this problem, a hybrid implicit-explicit method [54] is used. The system of ordinary differential equations for gas (after spatial discretization) and particle phases can be represented as follows:

$$\frac{dw}{dt} = L(w) + N(w) \tag{2.30}$$

where L comprises the stiff terms and N is the non-stiff part of the equations. A three sub-step hybrid explicit-implicit scheme to advance from $w^{(0)}$, at time t, to $w^{(3)}$, at time $t + \Delta t$, is as follows:

$$w^{(1)} = w^{(0)} + \Delta t[L(\alpha_1 w^{(0)} + \beta_1 w^{(1)}) + \gamma_1 N^{(0)}] \tag{2.31}$$

$$w^{(2)} = w^{(1)} + \Delta t[L(\alpha_2 w^{(1)} + \beta_2 w^{(2)}) + \gamma_2 N^{(1)} + \zeta_1 N^{(0)}] \tag{2.32}$$

$$w^{(3)} = w^{(2)} + \Delta t[L(\alpha_3 w^{(2)} + \beta_3 w^{(3)}) + \gamma_3 N^{(2)} + \zeta_2 N^{(1)}] \tag{2.33}$$

The coefficients α_i, β_i, γ_i and ζ_i are taken from Spalart et al [54] . To solve the non-linear algebraic equations arising from the implicit scheme in the combustion stage, a Newton-Raphson scheme is used. As the stiffness is due to the combustion model, the implicit scheme is used only during this stage of the particle conversion. The explicit part of the hybrid scheme is used for the non-stiff gas phase equations, particle pyrolysis and particle tracking.

2.5 Setup of simulations

We consider the gas-particle system inside a channel, bounded by two parallel horizontal plates (Figure 2.4). The domain size is $4\pi H$ in streamwise direction (denoted by x) and $2\pi H$ in spanwise direction (denoted by y), where H is half the channel height. Simulations are performed with frictional Reynolds number approximately equal to $Re_\tau = 150$, which is based on friction velocity $u_\tau = \sqrt{\tau_w/\rho_g}$ and half the channel height. Here, τ_w is the wall shear stress based on the mean streamwise velocity component, averaged over the two homogeneous directions and time.

The domain is divided into 128^3 control volumes. The grid spacing is uniform in streamwise and spanwise directions, whereas it is non-uniform in the wall-normal direction with clustering of grid points near the walls. This choice for the grid resolution is motivated in detail in Marchioli et al. [35] where simulation results obtained with various numerical methods were compared. They present simulation of a particle-laden turbulent channel flow at $Re_\tau = 150$ using second-order central differences, similar to the method used in this work, for the same grid resolution of 128^3. Their results show a good agreement in gas and particle statistics with other studies based on pseudo spectral methods. Bukhvostova et al. [56] report that this grid resolution is fine enough to capture the flow characteristics without the need for any turbulence model in the DNS of droplet-laden turbulent channel flow for the same Re_τ values.

The properties of virgin biomass and char formed after pyrolysis are presented in Table 2.2. The difference between biomass and char mass density is important as it is an indicator of mass loss in the form of volatile gases from the particle during pyrolysis.

In all simulations the flow is initialized with a turbulent velocity field in the statistically steady state as obtained from a simulation without particles. For the base case, the initial oxygen mole fraction is $X_{O2} = 0.21$ with nitrogen the remainder. The initial gas temperature is set equal to 1400 K, and the particles are initialized with a temperature of 300 K which is constant within the particle. The walls of the channel are maintained at a temperature of 1400 K [28]. We select a temperature of 1400 K for the walls as this is the typical temperature of furnace walls in co-firing power plants [3]. Above 1400 K the ash present in the solid fuels starts to melt and causes operational problems.

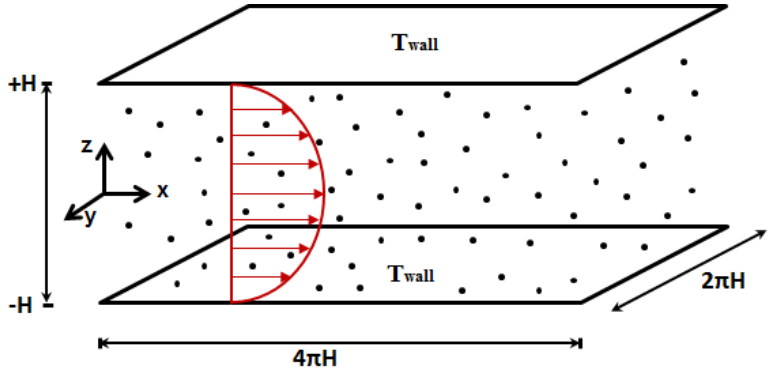

Figure 2.4: Geometry of the channel with randomly distributed particles, z is the wall-normal direction

Table 2.2: Virgin biomass and char properties used in the simulations [28]

	Mass density (kg/m^3)	Thermal conductivity (W/m/K)	Specific heat capacity (J/kg/K)
Biomass	650	0.25	2500
Char	190	0.1	1100

Initially, the particles are randomly, and uniformly, distributed throughout the channel and the particle velocity is initialized with the gas velocity at the position of particle. With these initial conditions we simulate the pyrolysis and combustion of biomass particles in a turbulent channel flow.

2.6 Analysis of model results

We present the results of the DNS model for biomass pyrolysis and combustion in a turbulent channel flow. One of the key parameters in designing a combustor is the conversion time of the fuel particles. For biomass particles, the total conversion time (t_{conv}) is the sum of the time required for the virgin biomass to get converted into char during the pyrolysis stage (t_{pyro}) and the time required by the char particle to burn in the combustion stage (t_{comb}). The pyrolysis time includes the time required to heat the particles from their initial temperature (300 K) to the cut-off pyrolysis temperature. The combustion time (t_{comb}) includes the time taken for the char conversion via the gasification reactions and the time taken by the char particles to cool down to the wall temperature.

In a single run of the simulation, the conversion time of different particles with

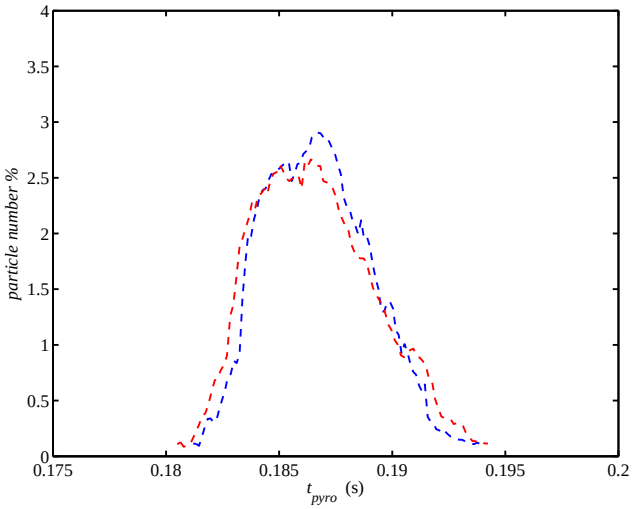

(a)

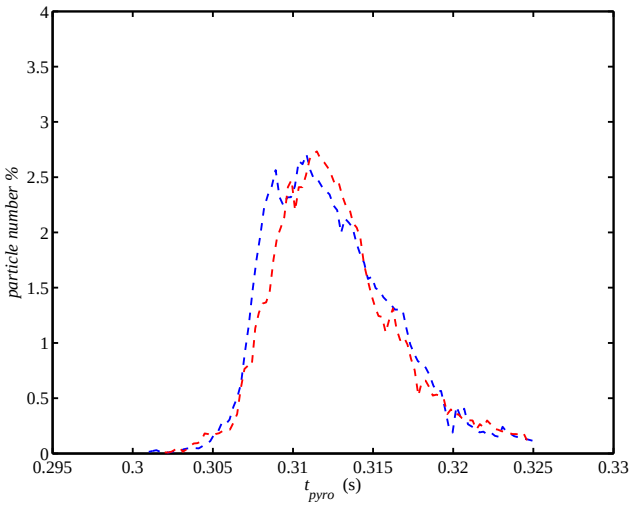

(b)

Figure 2.5: Probabilty density function for the particle pyrolysis time for different initial particle sizes and two different initial spatial distributions of the particles, a: 0.5 mm, b: 0.7 mm

the same initial size varies significantly. Different particles have different conversion time dependent on their initial spatial location in the domain. Initially, the particles are randomly, and uniformly, distributed inside the domain. As particles travel inside the domain they encounter varying gas phase temperature and gas species concentrations which result in variations in the conversion time of the particles. We observe a probability density function for the particle conversion time. Figure 2.5 presents the PDFs for particle pyrolysis time for two different particle sizes. We observe a variation of about 6.6% between the minimum and maximum conversion time for the particle size $d_p = 0.5$ mm. The difference is around 7.4% for the larger particle of size $d_p = 0.7$ mm. It can be seen that for the same initial particle size there is a slight variation in the PDF of conversion time for a different initial spatial distribution of the particles in the domain. This indicates that these PDFs are case specific. For all the analysis that follows, we use the values of the maximum conversion time for the particles.

Temperature profiles for the gas and the particles are shown in Figure 2.6. The gas and the particle temperatures are averaged over the homogeneous directions and plotted as functions of the wall normal co-ordinate at different instants of time. The particle diameter is 0.7 mm and the initial volume fraction $\phi = 2 \times 10^{-4}$. The gas is initialized at a much higher temperature than the particles, so early on the particles start extracting energy from the gas by convection. This is the initial heating up of the particles till they reach the pyrolysis temperature when the virgin biomass starts converting into char. As the process of pyrolysis continues, particles keep on extracting heat from the gas. In effect, the pyrolysis of a particle is an endothermic process which cools down the gas. Particles are also heated up through the radiation from the hot walls. After a certain time ($t = 0.315s$), the particles become warmer than the gas due to the radiative flux from these walls and the direction of the convective heat flux changes.

Once the process of pyrolysis is finished (at around $t = 0.325s$), i.e., when all the biomass is converted into char, the combustion of char begins. This process is highly exothermic - and fast - as compared to the slow endothermic pyrolysis process, and generates heat on the particle surface. It results in a sharp rise in the particle temperature ($t = 0.36s$). During the same time, the heat is transferred by convection, resulting in a temperature rise of the gas. The rate and magnitude of the temperature increase of the gas are dependent on the interphase convective heat transfer coefficient and the volume fractions of the particles. In Figure 2.6, we observe that the temperature rise of the gas during combustion is much slower than that of the particles, in accordance with the low convective heat transfer coefficient (which in turn depends on Re_p) and the volume fraction of particles ($\phi = 2 \times 10^{-4}$) used in the simulation.

The particle combustion model is based on a shrinking core approximation where the radius of the reactive core keeps on shrinking as the combustion continues. During the combustion stage, the fast char-oxidation reaction with O_2 is always

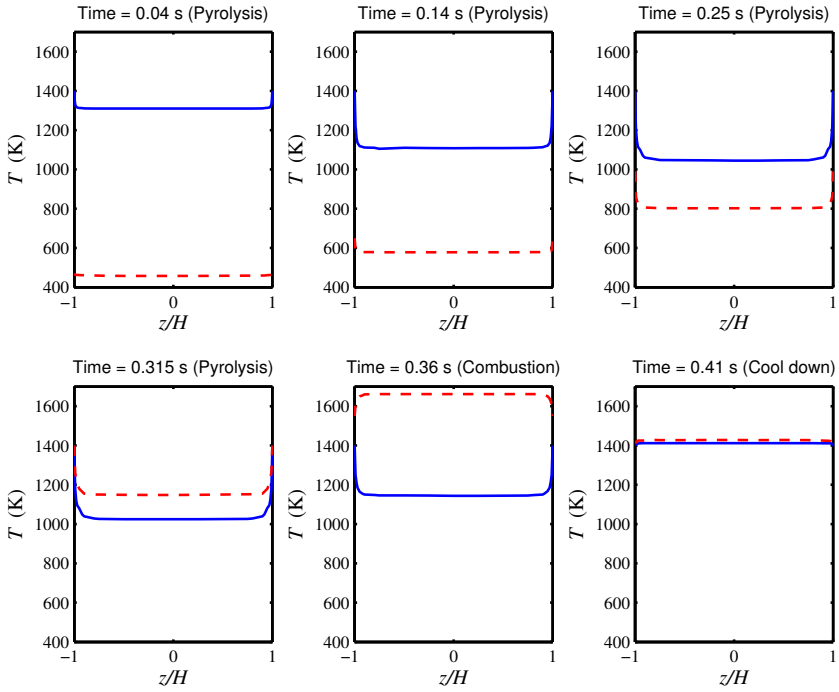

Figure 2.6: Averaged gas temperature(—) and particle temperature(- - -) at different instants of time during pyrolysis and combustion; the pyrolysis is finished around $t = 0.315$ s, z is the wall normal co-ordinate

coupled to the slow endothermic char-gasification with CO_2. Both these reactions consume the char particle. We stop the surface reactions when the reactive core radius becomes very small (less than 1% of its initial value). At this point almost all the char in the particle has reacted and only the inert ash inside the particle remains. The inert particles then start cooling down until the particle temperature reaches the wall temperature.

The sections that follow present the effects of variations in different model parameters on the conversion time of biomass particles. In subsection 2.6.1, we analyze the effects of two-way coupling on the conversion of the biomass particles. We only consider two-way coupling in this work and no four-way coupling. We limit our investigations to $\phi < 10^{-3}$, as according to Elghobashi [27], four-way coupling of momentum, i.e. particle-particle collisions, needs to be considered at $\phi > 10^{-3}$. It has recently been shown [39] that particle-particle collisions can become important even at lower particle volume fractions due to preferential concentration of particles. However, the duration of the simulations in this work is so small that preferential concentration does not have the time to develop.

We analyze the local particle volume fraction of the particles by dividing the

domain into 40 blocks in each Cartesian direction. The maximum local particle volume fraction is observed at the end of the pyrolysis stage and close to the wall due to turbophoresis effects. After the pyrolysis is finished, the particle volume fraction decreases rapidly during combustion as the particle size decreases due to reactions at the particle surface. The observed maximum local volume fraction of particles during the particle conversion process is about 3 times the initial particle volume fraction. For all the cases presented in this chapter, except for the case where the initial particle volume fraction $\phi = 5 \times 10^{-4}$, the maximum local particle volume fraction is less than 10^{-3}. Therefore, four-way coupling of momentum is neglected for all cases. Four-way coupling for the energy equation would include particle-particle radiative heat exchange that is neglected in the present model and will be a future extension of this study.

The particle size is also varied during the simulations, but it is always smaller than the Kolmogorov length, the smallest scale of turbulence, throughout the channel. This justifies the point particle assumption used in this work. In subsections 2.6.2-2.6.3, we vary different model parameters - namely particle size, and initial particle volume fraction - to study their effect on the conversion time of biomass particles using the DNS model.

2.6.1 Effect of two-way coupling

When simulating a large number of particles, the conversion times for particles are different from those obtained from a single-particle biomass conversion model. The two-way interaction of the particles with the gas affects the surrounding gas temperature and the gas species concentrations, which in turn affect the particle conversion process. In this section, we analyze the effect of two-way coupling on the biomass pyrolysis and combustion stages. Figure 2.7 presents the mean gas temperature and mean particle temperature as a function of time for two different initial particle volume fractions (ϕ) - in this subsection referred to as high and low.

The large variation in average gas temperature for the high particle volume fraction justifies the choice of two-way coupling in the model. For low particle volume fractions, it can be seen that there is almost no variation in the gas temperature. In Figure 2.7 the effect of two-way coupling can also be noticed on the particle temperature profiles. For sufficiently low ϕ, pyrolysis is finished earlier and the average particle temperature at the end of pyrolysis is higher. For higher ϕ, there is a delay in the pyrolysis, as also observed by Russo et al. [22].

Similarly, the combustion stage for the particles in the low particle volume fraction case is faster. This is because the oxygen present in the gas mixture is more than sufficient for the small number of particles. The particles are burnt quickly due to the fast char-oxidation reaction, and the maximum temperature attained by the particles is also higher than for the high ϕ case. For higher ϕ, the larger number of particles quickly consumes the oxygen in the surrounding gas mixture which slows

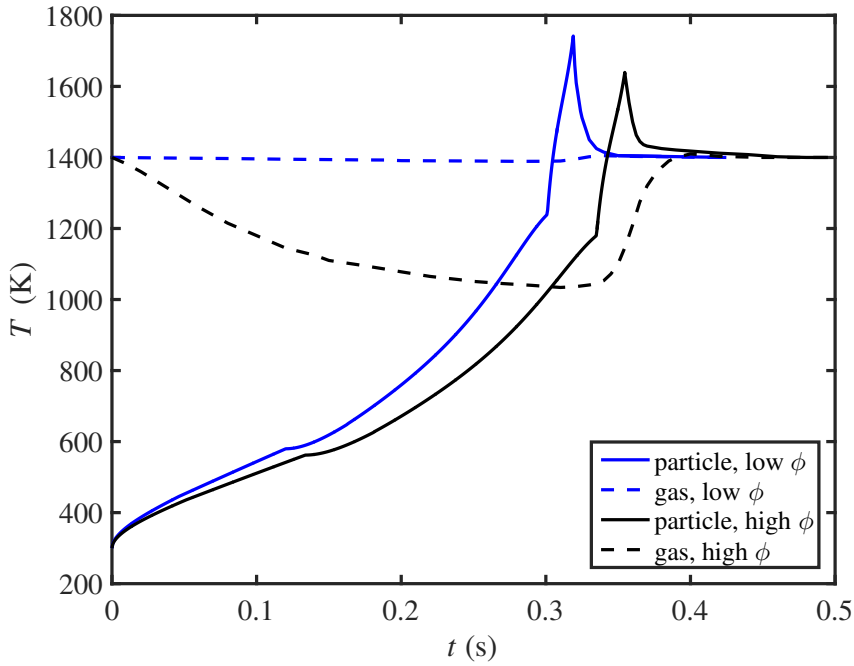

Figure 2.7: Averaged gas temperature (- - -) and particle temperature (—) at different instants of time during pyrolysis and combustion, low $\phi = 1 \times 10^{-7}$ (blue), high $\phi = 2 \times 10^{-4}$(black)

down the combustion process and also decreases the maximum temperature reached by the particles.

In Figure 2.8, we present a comparison between the time required in pyrolysis for two-way and one-way coupling between the gas and the particles. For one-way coupling, there is no feedback from the particles to the gas and the gas temperature remains constant during the particle conversion process. Thus, there is no change in the pyrolysis time either. On the other hand, with two-way coupling, the presence of particles affects the gas temperature. It can be seen that the effects of two-way coupling become significant for $\phi > 1 \times 10^{-5}$. For higher volume fraction $\phi = 5 \times 10^{-4}$, the inclusion of the two-way coupling increases the time required for pyrolysis by almost 100%. It can be concluded that for accurately predicting the conversion time of particles for $\phi > 1 \times 10^{-5}$, two-way coupling between the gas and the particles is essential. In contrast, for small particle volume fractions ($\phi < 1 \times 10^{-6}$) we can safely neglect the effects of gas-particle interactions and a constant temperature for the surrounding gas appears to be a good approximation for modeling the particle reactions.

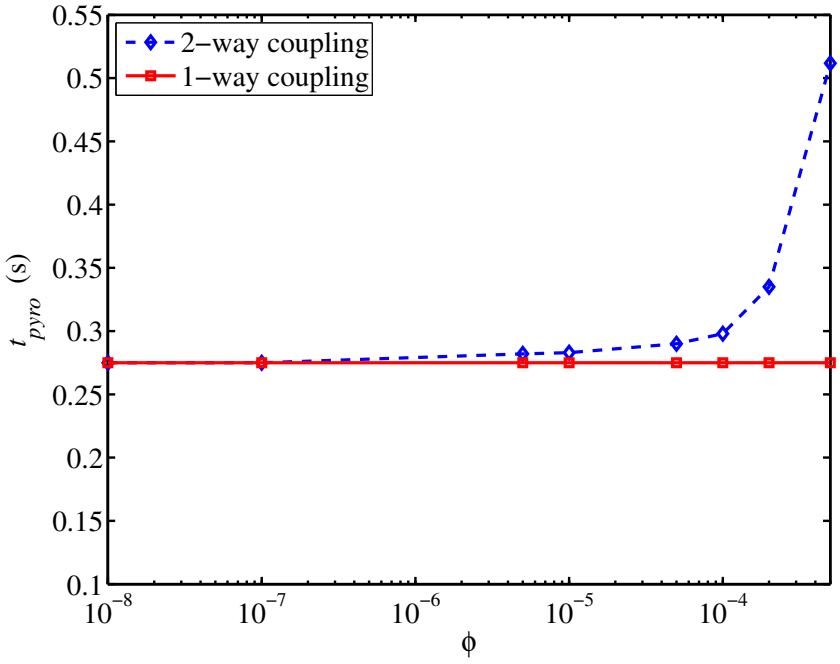

Figure 2.8: Pyrolysis time (t_{pyro}) for different initial particle volume fractions ϕ

2.6.2 Effect of particle size

To analyze the effects of particle size on conversion time, we performed simulations at constant initial particle volume fraction ($\phi = 2 \times 10^{-4}$) and contant initial oxygen mole fraction ($X_{O2} = 0.21$). Figure 2.9 shows the conversion time dependence on the particle diameter (d_p). Both the pyrolysis time (t_{pyro}) and combustion time (t_{comb}) increase with increasing particle diameter, although for different reasons. The process of pyrolysis is governed by the convective heat exchange between the hot surrounding gas and colder particles. Larger particles require more time for the heat flux at the surface to influence the particle centre, thus increasing the pyrolysis time. On the other hand, combustion is modelled using a shrinking core model where the particle radius decreases during the reactions as the char particle is consumed by the gas-particle surface reactions. Thus a larger particle would require more time as it takes longer for its reactive core to shrink.

From Figure 2.9, we can study the contributions of t_{pyro} and t_{comb} to the total conversion time ($t_{conv} = t_{pyro} + t_{comb}$). It can be seen that t_{pyro} is the major contributor in the particle conversion process, contributing between 60-75 % of t_{conv}, dependent on particle size. The mass lost from a solid fuel particle during pyrolysis depends on the proximate volatile matter content of the solid fuel. Biomass, with its high volatile content (about 70 %), loses most of its mass in the pyrolysis stage

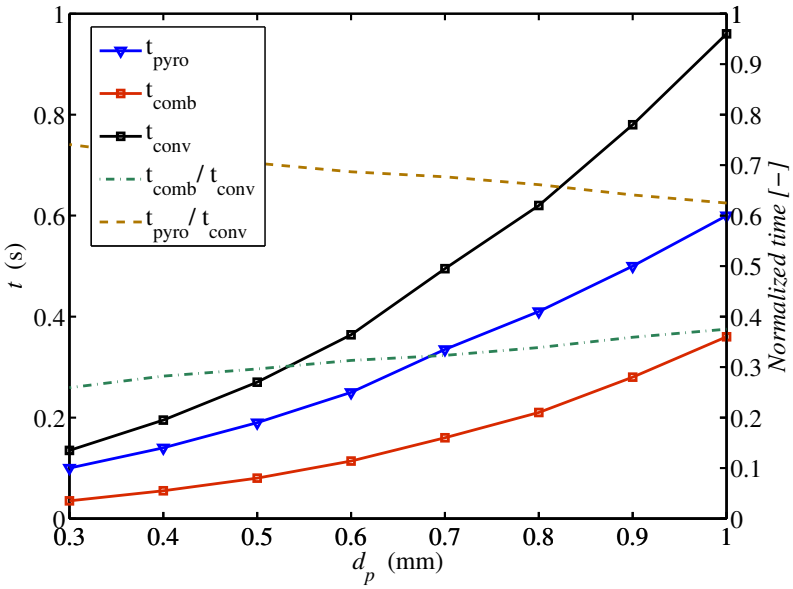

Figure 2.9: Total conversion time (t_{conv}), pyrolysis time (t_{pyro}) and combustion time (t_{comb}) vs particle diameter (d_p) at constant volume fraction (2×10^{-4})

and thus requires more time for pyrolysis. After the volatiles are released, the remaining solid, i.e., char - conversion is mainly due to fast combustion reactions. Note that these results are specific to the surrounding gas oxygen concentration and temperature used in the simulations.

Figure 2.9 also shows the relative contribution of t_{pyro} and t_{comb} to t_{conv}. The relative contribution of pyrolysis (t_{pyro}/t_{conv}) decreases with increasing particle size, whereas the contribution of combustion t_{comb}/t_{conv} increases by about 10% as the particle size is increased from 0.3 mm to 1 mm. This trend provides a qualitative validation to the model results as Yang et al. [58] obtained similar qualitative results in their experiments for wood pyrolysis and combustion.

Figure 2.10 presents the variation of t_{pyro} and t_{comb} with particle size (d_p) on a log-log scale along with their corresponding one-way coupling values. The one-way coupling is only applied to the energy equation, i.e., in case of one-way coupling there is no heat exchange between the particles and the gas. The coupling for the total mass, species mass, and momentum equations is always two-way. It can be seen in Figure 2.10 that both for the pyrolysis and for the combustion, the difference between two-way and one-way coupling is higher at smaller particle sizes. This is because as the particle size increases at constant volume fraction, the total surface area available for heat exchange between the gas and the particles decreases. This reduces the total interphase convective heat exchange for larger particles as

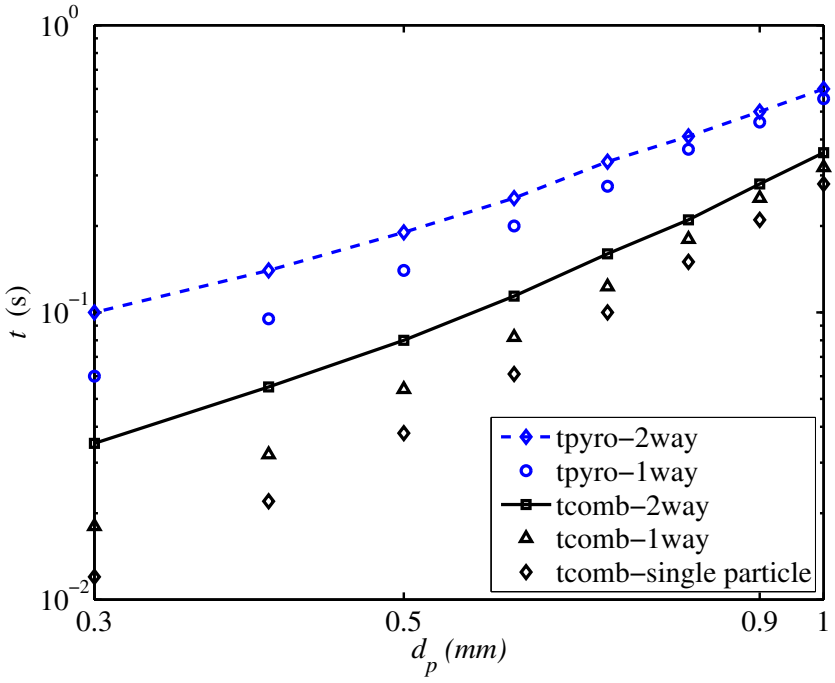

Figure 2.10: Pyrolysis time (t_{pyro}) and combustion time (t_{comb}) vs particle diameter (d_p) for one-way and two-way coupling

compared to the smaller particles and hence a closer agreement between one-way and two-way coupling is observed for larger particles.

During pyrolysis, for smaller particles, the higher convective heat exchange between the gas and the particles increases the pyrolysis time as particles withdraw more heat from the gas which decreases the temperature of the gas. In contrast, during the combustion stage more heat is transferred to the gas because of the larger interphase surface area thus reducing the particle temperature compared to larger particles. This reduced temperature decreases the kinetic rate of surface reactions, thereby increasing the combustion time. According to figure 2.10, we also present the corresponding values for the combustion time as calculated from a single-particle model. The single-particle model has a constant surrounding gas temperature and constant oxygen mass fraction. From figure 2.10, the conversion times from the single-particle model are the lowest. The relative difference in the combustion time results for the two-way coupling, one-way coupling and the single-particle model highlights the importance of two-way coupling for the combustion stage.

2.6.3 Effect of particle volume fraction

To investigate the effects of particle volume fraction we perform simulations by varying the initial particle volume fraction (ϕ) and keeping the particle size constant at $d_p = 0.7$ mm. The results in Figure 2.11 show that when two-way coupling is applied, the time required for pyrolysis increases with increasing ϕ. The convective heat exchange between the gas and the particles affects the gas temperature. During the pyrolysis stage, the gas heats up the particles as particles extract heat from the gas. More particles extract more heat from the gas which slows down the pyrolysis [22].

During combustion, a higher value of ϕ requires more oxygen according to the reaction stoichiometry. For all simulations shown in figure 2.11, the initial oxygen mass fraction in the surrounding gas is the same ($X_{O2} = 0.21$). The amount of oxygen is stoichiometrically sufficient for $\phi = 5 \times 10^{-4}$ and is in excess for all lower values of ϕ. In Figure 2.11 the combustion time increases with higher volume fraction because more particles consume the surrounding oxygen more quickly. At lower volume fractions there is enough oxygen and char particles lose most of their mass through the fast oxidation process. In contrast, at higher volume fractions, the concentration of oxygen in the gas phase decreases quickly which slows down the oxidation reaction rate. This also results in a higher share of the char particles being consumed by the slower gasification reaction with CO_2.

2.7 Conclusions

In this chapter, we have extended the DNS model of Russo et al. [22] for biomass pyrolysis by including Haseli's [16] single-particle model for biomass combustion, which is suitable for DNS with a large number of biomass particles. The model has been adopted for modeling gas-particle interactions with chemically reacting particles in a turbulent flow.

We observe that the heat exchange between the gas and the particles strongly influences the particle conversion during pyrolysis and combustion. From the results in this chapter, which are specific to initial conditions of gas velocity, temperature, and concentration used in the simulations, it is observed that the effect of two-way coupling in the energy equation is significant for particle volume fractions $\phi > 1 \times 10^{-5}$. At lower volume fractions $\phi < 10^{-6}$, the effect of particles on the gas is negligible and at such low volume fractions, particles can be modelled by just including the one-way coupling to reduce the computational costs. However, typical industrial furnaces have particle volume fractions on the higher side with $\phi > 1 \times 10^{-3}$ [44] and hence the effect of two-way coupling becomes important. The conversion time of biomass particles is also sensitive to their diameter and increases for larger particles. The effect of two-way coupling is higher for smaller particles due to the higher total heat exchange area in case of small particles.

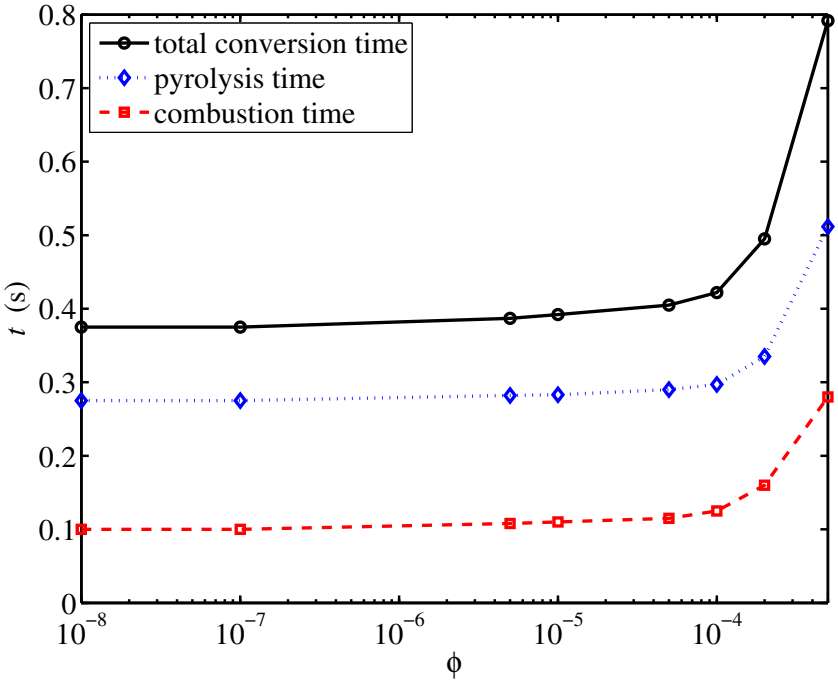

Figure 2.11: Total conversion time (t_{conv}), pyrolysis time (t_{pyro}) and combustion time (t_{comb}) vs initial particle volume fraction (ϕ)

In this chapter, we analyzed the results of the DNS model for biomass pyrolysis and combustion by only taking into account the heterogeneous solid-gas reactions. In the next chapter, we add homogeneous gas phase reactions to the DNS model and analyze the effect of adding these reactions on the biomass conversion process.

Appendix A

Biomass Pyrolysis Model

The biomass pyrolysis model of Haseli [12] consists of several phases for modeling the overall pyrolysis process. Here, we present the biomass pyrolysis model of Russo et al. [28] which is an extension of Haseli's work [12]. A summary of the biomass pyrolysis model is presented here and more details along with the derivations of equations can be found elsewhere [29].

The model considers a spherical biomass particle with uniform initial temperature. The particle is subjected to an inward heat flux ($\dot{q}$) at its surface due to the hot surrounding gas, and the surface temperature of the particle starts to rise. The temperature profile inside the particle starts to change due to thermal conduction. Theoretically, the velocity at which the thermal disturbance propogates through the particle is infinite [12, 28]. However, according to Haseli [27], immediately after the particle is subjected to heat flux at its surface, the particle is divided into two regions: the outer region closer to the surface where the temperature has changed from its initial value, and the inner region around the center of the particle where the temperature is still at its initial value. The boundary that separates these two regions is called the thermal front. The thermal front moves from the surface of the particle towards its center. Haseli [27] assumes that the thermal front moves with a finite velocity. This initial phase of biomass pyrolysis is called *heating of virgin biomass*.

At some point the thermal front reaches the particle centre and the second phase - *pre-pyrolysis heating* - starts. The only difference between the first two phases is in their mathematical formulation. Once the temperature of the particle surface reaches the pyrolysis temperature, volatiles are released and biomass is converted into char. This third phase of *pyrolysis* is marked by the movement of a char front from the particle surface towards the particle center. The thin layer which has reached the cut-off pyrolysis temperature is instantaneously converted into char and volatile gases. The char front separates the volume of the particle - which remains constant during the pyrolysis - into two regions: an outer region of char and an inner

region of virgin biomass.

Once the pyrolysis stage has finished completely, the biomass has been converted into char. The solid char then reacts with gases through heterogeneous solid gas reactions which were described earlier in chapter 2. This is different from the biomass pyrolysis model of Russo et al. [28] where the char combustion is not included in the model and a *post-pyrolysis heating* stage is added after the pyrolysis.

It should be noted that if the particle diameter exceeds a certain value, depending on the initial temperature, the pyrolysis temperature, and the heat flux, it may happen that pyrolysis starts before the thermal front has reached the particle center. Therefore, Haseli et al. [27] distinguish between thermally thin and thermally thick particles. Next, we present the pyrolysis model for a thermally thin particle. This is followed by the pyrolysis model for a thermally thick particle.

A.1 Pyrolysis model for thermally thin biomass particle

A.1.1 Heating of virgin biomass

The heat equation in spherical coordinates (assuming spherical symmetry) governing the temperature of the particle in the first stage is:

$$\frac{\partial T}{\partial t} = \alpha_B \frac{1}{r^2} \frac{\partial}{\partial r} \left(r^2 \frac{\partial T}{\partial r} \right) \tag{A.1}$$

where r is the radial coordinate, t the time, $T(r,t)$ the temperature, and α_B the thermal diffusivity of the virgin biomass. Haseli [27] assumes a parabolic temperature profile which transforms the above partial differential equation into an ordinary differential equation which is written as follows:

$$\frac{d}{dt}(\dot{q} f(r_t)) = 60 \alpha_B \dot{q} \tag{A.2}$$

with $f(r_t) = 6R^2 - \dot{q} R r_t + {r_t}^2 + {r_t}^3/R + {r_t}^4/R^2$, r_t the thermal front position, R the radius of the particle , and $\dot{q}$ the external heat flux. The external heat flux $\dot{q}$ is given as:

$$\dot{q} = h(T_g - T_s) + \sigma \epsilon (T_w^4 - T_s^4) \tag{A.3}$$

The external heat flux is the sum of convective heat flux and radiative heat flux. The convective heat flux is proportional to the temperature difference $(T_g - T_s)$ between the surrounding gas and the particle surface. The convective heat transfer coefficient h is computed using a correlation given as follows:

$$\frac{hR}{\lambda} = 1 + 0.3 {Re_p}^{1/2} Pr^{1/3} \tag{A.4}$$

where λ is the thermal conductivity, Re_p is the Reynolds number based on the particle diameter and the relative velocity between the particle and the carrier gas at the particle position, and Pr is the Prandtl number.

The radiative heat flux takes into account the heat flux received by the particle from the walls whose temperature is indicated by T_w and is constant. The Stefan-Boltzmann constant and the emissivity are indicated by σ and ϵ, respectively.

The temperature profile inside the particle is assumed to be parabolic. The thermal front position r_t is given as:

$$r_t = R - \frac{2k_B}{\dot{q}}(T_s - T_0) \tag{A.5}$$

where k_B is the thermal conductivity of the biomass and T_0 is the initial particle temperature.

The governing equation of the first phase (*heating of biomass*) is equation (A.2). The unknown T_s in this equation needs to be calculated. Equation (A.2) can be rewritten as:

$$\frac{dT_s}{dt} = \frac{60\alpha_B\dot{q} - f\frac{\partial\dot{q}}{\partial T_g}\frac{dT_g}{dt} - \dot{q}\frac{\partial f}{\partial r_t}\frac{\partial r_t}{\partial\dot{q}}\frac{\partial\dot{q}}{\partial T_g}\frac{dT_g}{dt}}{f\frac{\partial\dot{q}}{\partial T_s} + \dot{q}\frac{df}{dr_t}\left(\frac{\partial r_t}{\partial\dot{q}}\frac{\partial\dot{q}}{\partial T_s} + \frac{\partial r_t}{\partial T_s}\right)} \tag{A.6}$$

with dT_g/dt the time derivative of the gas temperature at the particle location.

For times close to the initial time, the solution of this equation is approximately proportional to $\sqrt{t}$. Hence, explicit time integration methods are not capable of solving this equation accurately. In order to avoid this problem, Russo et al. [28] analyzed the solution for small values of t in more detail. For small values of t, T_s will be close to T_0 and $\dot{q}$ can be assumed constant. A taylor expansion of $f(r_t)$ for T_s close to T_0 shows that $f(r_t)$ is proportional to $(T_s - T_0)^2$. It follows that $(T_s - T_0) \sim \sqrt{t}$. Therefore, Russo et al [28] solve a differential equation for $(T_s - T_0)^2$, which is written as:

$$\frac{d}{dt}(T_s - T_0)^2 = \frac{2(T_s - T_0)\left(60\alpha_B\dot{q}(T_s - T_0) - f\frac{\partial\dot{q}}{\partial T_g}\frac{dT_g}{dt} - \dot{q}\frac{\partial f}{\partial r_t}\frac{\partial r_t}{\partial\dot{q}}\frac{\partial\dot{q}}{\partial T_g}\frac{dT_g}{dt}\right)}{f\frac{\partial\dot{q}}{\partial T_s} + \dot{q}\frac{df}{dr_t}\left(\frac{\partial r_t}{\partial\dot{q}}\frac{\partial\dot{q}}{\partial T_s} + \frac{\partial r_t}{\partial T_s}\right)} \tag{A.7}$$

A.1.2 Pre-pyrolysis

The main difference between this phase and the previous phase is the absence of the moving thermal front. The governing equation for this phase following Haseli et al. [27] can be written as:

$$\frac{d}{dt}\left(T_s R - \frac{1}{5}\frac{R^2\dot{q}}{k_B}\right) = 3\frac{\alpha_B}{k_B}\dot{q} \tag{A.8}$$

The above equation can be solved for T_s by numerically integrating the following equation:

$$\frac{dT_s}{dt} = \frac{3\frac{\alpha_B}{k_B}\dot{q} + \frac{1}{5}\frac{R^2}{k_B}\frac{\partial \dot{q}}{\partial T_g}\frac{dT_g}{dt}}{R - \frac{1}{5}\frac{R^2}{k_B}\frac{\partial \dot{q}}{\partial T_s}} \tag{A.9}$$

A.1.3 Pyrolysis

In the pyrolysis phase, the particle is divided into two regions which are separated by a moving char front. The location of the char front (r_c) is the interface at which the temperature has reached the cut-off pyrolysis temperature. The pyrolysis is assumed to occur instantaneously. The temperature profiles in the two regions separated by the char front are assumed to be quadratic functions and are written as:

$$T(r) = \phi_2(r - r_c)^2 + \phi_1(r_c - r) + \phi_0, \quad \text{for } 0 \le r \le r_c \tag{A.10}$$

$$T(r) = \psi_2(r - r_c)^2 + \psi_1(r_c - r) + \psi_0, \quad \text{for } r_c \le r \le R \tag{A.11}$$

The heat equation for the inner region ($0 \le r \le r_c$) is equation (A.1). The heat equation for the outer region ($r_c \le r \le R$) is written as:

$$\frac{\partial T}{\partial t} = \alpha_C \frac{1}{r^2}\frac{\partial}{\partial r}\left(r^2 \frac{\partial T}{\partial r}\right) + (1 - \omega)\frac{\dot{m}}{4\pi r^2}\alpha_{vol}\frac{\partial T}{\partial r} \tag{A.12}$$

where, α_C is the thermal diffusivity of biomass char. The second terms on the R.H.S. of the above equation represents the heat transfer between the volatiles released at the char front and the char during their transport towards the partial surface. In the above equation, $\alpha_{vol} = C_{vol}/\rho_C C_C$ where C_{vol} and C_c are the specific heats of volatiles and char, respectively, and $\omega = \rho_C/\rho_B$ is the ratio of mass densities of char and biomass. This second term in the R.H.S. of equation (A.12) is an addition by Russo [29] to the model of Haseli [27].

The model of the pyrolysis phase consists of two heat diffusion problems which are connected to each other at the char front r_c. Because of the moving char front and the co-existence of two regions inside the particle during pyrolysis phase, there are 3 governing ordinary differential equations in this phase. The first governing equation is obtained from energy conservation in the char region and is written as:

$$\frac{d}{dt}f(r_c, \dot{q}, v_c, \phi_1) = 60\alpha_C\{R^2\dot{q} + k_B r_c^2\phi_1 - r_c^2 v_c \Delta h_p \rho_B + (1 - \omega)\rho_B v_c C_{vol} r_c^2 (T_s - T_p)\} \tag{A.13}$$

where $f(r_c, \dot{q}, v_c, \phi_1) = 9R^4 a + 6R^4\dot{q} - 11R^3 a r_c - 9R^3\dot{q}r_c + R^2\dot{q}r_c^2 - R^2 a r_c^2 + R\dot{q}r_c^3 - Rar_c^3 + 4ar_c^4 + \dot{q}r_c^4$, $a = v_c\rho_B\Delta h_p - k_B\phi_1$, with v_c the velocity of the char front, and Δh_p the heat of pyrolysis of biomass.

Similarly, the second governing equation for the pyrolysis phase is the energy conservation equation in the inner region (virgin biomass) and is given as:

$$\frac{d}{dt}\left(\frac{1}{15}\phi_1 r_c^4\right) = -\alpha_B r_c^2 \phi_1 \tag{A.14}$$

Finally, the third governing equation is the definition of char front velocity v_c:

$$\frac{d}{dt} r_c = v_c \tag{A.15}$$

In the pyrolysis phase, the three unknowns are T_s, v_c, and ϕ_1 which are calculated by solving the three governing equations.

After the pyrolysis is complete, Haseli [12] includes a post-pyrolysis heating phase that is excluded in our work. This is because as soon as the pyrolysis of biomass is finished, the combustion of char starts.

A.2 Pyrolysis model for thermally thick biomass particle

The temperature profile inside a thermally thick biomass particle consists of three regions.

$$T(r) = T_0, \quad \text{for } 0 \le r \le r_t \tag{A.16}$$

$$T(r) = \phi_2(r - r_c)^2 + \phi_1(r_c - r) + \phi_0, \quad \text{for } r_t \le r \le r_c \tag{A.17}$$

$$T(r) = \psi_2(r - r_c)^2 + \psi_1(r_c - r) + \psi_0, \quad \text{for } r_c \le r \le R \tag{A.18}$$

The coefficients in the above equations have to be determined using the boundary conditions. The governing equation for the virgin biomass region ($r_t \le r \le r_c$) is written based on the conservation of energy:

$$\frac{d}{dt} h(r_t, r_c) = -60\alpha_B \frac{r_c^2}{r_c - r_t} \tag{A.19}$$

where $h(r_t, r_c) = 4r_c^3 + 3r_c^2 r_t + 2r_c r_t^2 + r_t^3$. The energy conservation in the outer char region ($r_c \le r \le R$) leads to the second governing equation for this phase of pyrolysis of the thermally thick particle:

$$\frac{d}{dt} g(r_c, v_c, r_t) = 60\alpha_C \left\{ R^2 \dot{q} - r_c^2 \left(\rho_B v_c \Delta h_p + 2k_B \frac{T_p - T_0}{R_c - r_t} \right) \right\} \tag{A.20}$$

with $g(r_c, v_c, r_t) = \dot{q}(6R^4 - 9R^3 r_c + R^2 r_c^2 + R r_c^3 + r_c^4) + (2k_B(T_p - T_0)/(r_c - r_t) + \rho_B v_c \Delta h_p)(9R^4 - 11R^3 r_c - R^2 r_c^2 - R r_c^3 + r_c^4) + (1-\omega)\rho_B v_c C_{vol} r_c^2 (T_s - T_p)$. Apart from the above two governing equations, the third governing equation is the definition of char front velocity as given in equation (A.15).

A.3 Stiffness of the equation in pyrolysis model

Russo [29] found that in the early and the late phases of pyrolysis, the particle equations of the pyrolysis model are stiff, for both the thermally thin and the thermally thick particles. To overcome this problem, Russo [29] divided the pyrolysis phase into three sub-phases: early stiff pyrolysis, regular pyrolysis, and late stiff pyrolysis. The equations for the regular pyrolysis phase are the same as presented earlier in section A.1 and section A.2. The equations for the early stiff pyrolysis sub-phase can be derived in the same way by assuming a linear temperature profile in the char region (instead of a quadratic profile). The equations for the late stiff pyrolysis sub-phase are derived by assuming a constant temperature profile in the virgin biomass region.

Russo [29] provides more details about the biomass particle pyrolysis model including the derivation of equations. An scheme of routes of a biomass particle undergoing pyrolysis is presented in figure 2.2 of chapter 2.

Chapter 3

Effect of gas phase reactions on Biomass conversion

3.1 Introduction

In the previous chapter, we discussed DNS of biomass particle conversion in a channel flow by including solid-gas reactions. In this chapter, we extend the model by adding homogeneous gas phase reactions to the model and study the effect of these reactions on biomass conversion.

In the biomass conversion process there are two main mechanisms that produce reactive gases. One is the release of volatile gases during the process of solid particle pyrolysis, and the other is the heterogeneous solid-gas reactions between the biomass particle and surrounding gas. We included both of these processes in the model presented in chapter 2. During biomass pyrolysis, the volatile content of the solid fuel gets decomposed and is released in the form of volatile gases [13] which is a complex mixture of several gases. After the pyrolysis is complete, the solid char burns in the presence of oxygen to produce gaseous products. These gases, which are released as volatiles and produced during char combustion, can further react with the oxygen present in the gas phase. In this chapter, our aim is to model these additional reactions of combustible gases with oxygen.

There are several methods to model gaseous combustion reactions in finite volume simulations [39]. Various levels of detail in terms of kinetics [42, 48] can be chosen to model these reactions. Studies focussing only on the combustion of gases [22, 39, 59] employ detailed kinetics of gas phase reactions. In these studies the reaction kinetics of the gas phase are represented by a combination of several elementary reactions [59]. Such methods are suitable for modeling gas combustion and are frequently used to analyze flame structures. On the other hand, studies of solid particle combustion frequently employ simplified models for gas reactions [20, 21, 18]. It is computationally very expensive to model turbulent channel flow

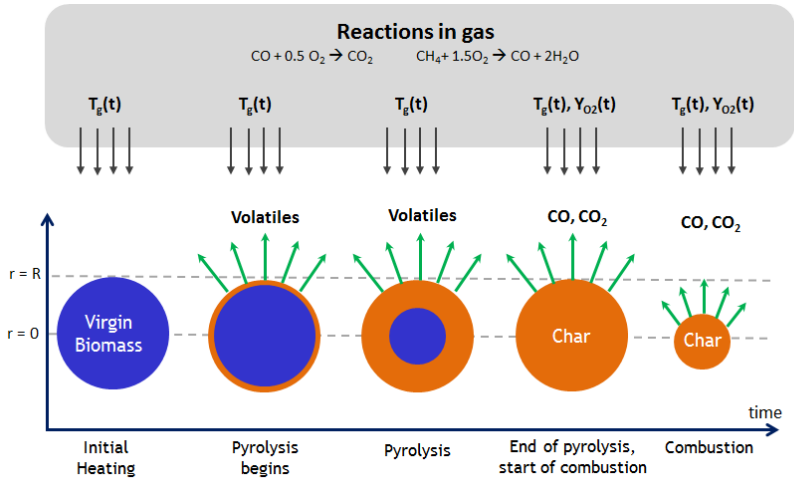

Figure 3.1: Stages of the biomass conversion process including the homogeneous gas phase reactions; T_g and Y_{O2} are the bulk gas temperature and bulk gas oxygen concentration respectively; R is the initial radius of the biomass particle.

with chemically reacting solid particles along with detailed reaction chemistry in the gas phase [23]. Since we focus on the biomass particle conversion process, we can limit ourselves to simplified, yet resonably accurate, kinetics [24] for the gas phase reactions and study this in interaction with the turbulent flow.

In this chapter we first outline in Section 3.2 the model for including the gas combustion reactions in the DNS. After this, in Section 3.3, we present and analyze the results of the DNS model particularly focussing on the effect of gas phase reactions on the biomass conversion process. We summarize our findings in Section 3.4.

3.2 Gas model

A schematic (a modified version of figure 2.1) to show the biomass conversion process by including the gas phase reactions is presented in figure 3.1. The models for biomass particle conversion as described in the previous chapter (section 2.2) remain the same here. The only addition is the incorporation of the gas phase reactions. Most of the equations used for modeling the gas phase in the DNS have already been described in section 2.3 of the previous chapter. Here, we describe the additional modifications introduced to the DNS model in order to capture the gas phase reactions of CO and CO2 released during pyrolysis and combustion.

Presently, the model includes 6 gas species - O_2, CO_2, CO, CH_4, H_2O, and N_2. The governing equations for gas, as presented in eq. 2.13, is repeated here with

Table 3.1: Kinetic data for gas phase oxidation reactions of methane and CO [60]

Reaction	Pre-exponential factor A_{ig} (m^3/kg/s)	Activation energy E_{ig} (J/mol)
CH4	1.6×10^7	1.08×10^5
CO	7×10^4	6.65×10^4

additional terms to account for the gas combustion reactions:

$$\int_V \frac{\partial \mathbf{w}}{\partial t} \mathrm{dV} + \int_{\partial V} \hat{n}.f_c \, dS = \int_{\partial V} \hat{n}.f_v \, dS + \int_V L_{2way} \, dV + \int_V F \, dV \tag{3.1}$$

with $\mathbf{w}(\mathbf{x}, t) = [\rho u, \rho v, \rho w, \rho, e, \rho_{O2}, \rho_{CO2}, \rho_{CO}, \rho_{CH4}, \rho_{H2O}]^T$ the vector of dependent variables. These governing equations express the rate of change of $\mathbf{w}$ in the volume V in terms of the convective fluxes (f_c), the diffusive fluxes (f_v), and the two-way coupling terms (L_{2way}) as before, accounting for the presence of the particles, as well as the contributions represented by F, the source terms in the gas phase. In this chapter we will extend F to capture the additional gas phase reactions

The two-way couling terms (L_{2way}) in the species balance equations account for the addition (or consumption) of gases due to solid particle conversion. During pyrolysis, volatiles released from the particle are added to the gas phase, whereas during combustion, solid char consumes O_2 from the gas phase and generates CO_2 and CO. The source term F in the gas species balance equations includes the rates of homogeneous gas phase reaction which are described later. For the energy equation the source term F includes the heats of reactions of the homogeneous gas phase reactions also described later in this chapter.

While calculating the internal energy (eq. 2.19), we did not include the heat of formation of the gas species. The heat of formation of gas species can be included in the model in two ways. We can either include the heats of formation while calculating the internal energy in which case it would not be required to include the heat of reaction separately in the source term F. The other way, which we follow in this work, is to not include the heats of formation in the calculation of internal energy and separately include the heats of reactions in the source term F.

3.2.1 Gas phase reaction chemistry

During pyrolysis, volatile gases are released from the solid particle. These volatile gases are a mixture of various gases - mainly CO, CO_2, CH_4, and tar - depending on the type of the solid fuel particle. Tar is a complex mixture of higher hydrocarbon gases including aromatics like benzene and toluene [13]. Tar is represented chemically as $C_xH_yO_z$, and the reaction chemistry is adjusted according to the stoichiometry. However, reliable thermochemical information (i.e., activation energy,

pre-exponential factor, and reduced chemical mechanism for a general volatile fuel of the form $C_xH_yO_z$) is absent in literature. In the absence of this information and for the sake of simplicity we assume that the volatile matter released from the biomass is solely methane. Similar assumptions have been adopted by other authors in literature [18, 24] with acceptable results.

The methane released during pyrolysis reacts with the oxygen present in the gas. During biomass combustion, CO_2 and CO are produced and are added to the gas phase. The CO produced in this process can further combust by reaction with oxygen. For the gas phase reactions, we consider two-step reaction chemistry which involves the oxidation reactions of CH_4 and CO:

$$CH_4 + 1.5O_2 \rightarrow CO + 2H_2O \tag{3.2}$$

$$CO + 0.5O_2 \rightarrow CO_2 \tag{3.3}$$

The reaction rates for the reacting gases - methane and CO - are calculated based on the follwing equation:

$$r_{ig} = A_{ig} \exp\left(-\frac{E_{ig}}{RT_g}\right) \rho_g^2 Y_g Y_{O2} \tag{3.4}$$

where the pre-exponential factors (A_{ig}) and the activation energies (E_{ig}) for the two reactions are given in table 3.1.

3.3 Numerical implementation

The details of the numerical method employed for the DNS of the coal conversion process are similar to the DNS of biomass conversion as outlined in chapter 2. The main difference is in the rates of biomass pyrolysis and combustion reactions due to the interaction with the additional gas phase reactions.

The exothermic nature of gas phase reactions, increases the temperature of the gas phase which then increases the heat transfer to the particle surface. Due to this the rate of pyrolysis of the biomass particles also increases. The gas reactions also consume the oxygen in the gas phase thereby reducing the oxygen available to the particles for the char combustion reaction. This slows down the char combustion process. The challenge in this chapter is to understand the interplay between these two counteracting mechanisms.

In chapter 2, we described the time integration scheme used in the DNS model. We adopted a hybrid implicit-explicit RK method [54] for the time integration of particle and gas equations. The implicit part of the scheme is used for the faster char combustion stage, while the explicit part is used for the char pyrolysis, particle tracking, and the gas equations. The details of the method have been presented earlier in chapter 2.

The properties of virgin biomass and char formed after pyrolysis are same as presented in Table 2.2 of chapter 2. In all simulations the flow is initialized with a turbulent velocity field in the statistically steady state as obtained from a simulation without particles. For the base case, the initial oxygen mole fraction is $X_{O2} = 0.21$ with nitrogen the remainder. The initial gas temperature is set equal to 1400 K, and the particles are initialized with a temperature of 300 K which is constant within the particle. The walls of the channel are maintained at a temperature of 1400 K [28]. Initially, the particles are randomly, and uniformly, distributed throughout the channel and the particle velocity is initialized with the gas velocity at the position of particle.

In the next section, we present the analysis of results of the DNS model after including gas phase reactions.

3.4 Analysis of results

We present the results of the DNS model for biomass pyrolysis and combustion in a turbulent channel flow. As in chapter 2, we observe that in a single run of the simulation, the conversion time of different particles with the same initial size varies significantly. We present the pdf of conversion time of particles in figure 3.2. For the results presented in figure 3.2, the initial solid volume fraction was 1×10^{-5}.

We observe a variation of about 11% between the minimum and maximum conversion time for an initial particle size $d_p = 0.5$ mm. It can be seen that for the same initial particle size there is a slight variation in the PDF of conversion time for a different initial spatial distribution of the particles in the domain. This indicates that these PDF's are slightly case specific. Figure 3.2 also shows multiple peaks in the PDF for different particle sizes. We observe one characteristic peak for the particle size of 1 mm, and two peaks for the smaller particle sizes. However, the detailed analysis of the characteristics of these PDF's is beyond the scope of this work. For the analysis that follows in this chapter, we concentrate on the maximum conversion time observed over all particles.

In the subsections that follow, we study the effect of two-way coupling, gas phase reactions, particle size, and particle size distribution on the biomass conversion process. For all the results presented, unless specified otherwise, the initial oxygen mole fraction is $X_{O2} = 0.21$ with nitrogen the remainder.

3.4.1 Effect of two-way coupling

In chapter 2 we determined that for accurately predicting the conversion time of particles for volume fractions larger than 1×10^{-5}, two-way coupling between the gas and the particles is essential. Similar to the previous chapter, we analyze the effect of two-way coupling on the biomass conversion process after including gas

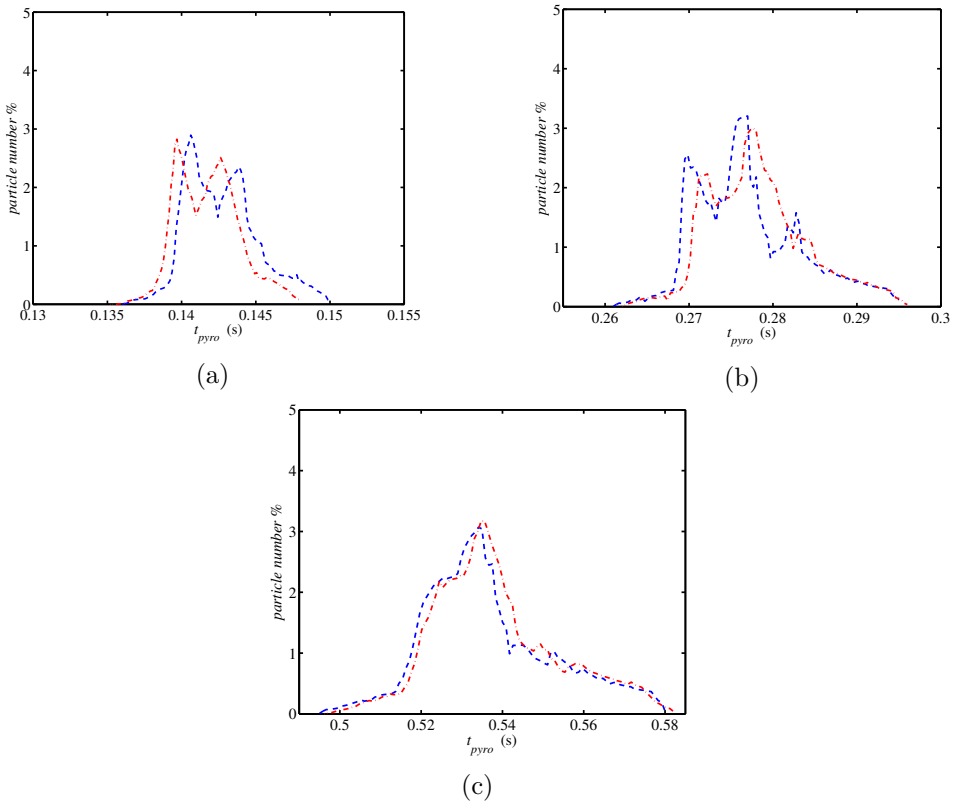

Figure 3.2: Probabilty density function for the particle pyrolysis time for different initial particle sizes and two different intial spatial distributions of the particles, a: particle size 0.5 mm, b: 0.7 mm, c: 1 mm.

phase reactions in figure 3.3. For the results presented in figure 3.3 the initial particle size (d_p) is 0.7 mm.

When the gas phase reactions are included in the model, the difference in the pyrolysis time between one-way and two-way coupling is reduced. This can be explained as the effect of the two competing phenomena mentioned above. In fact, during pyrolysis, the particles withdraw heat from the gas thus contributing to a lowering of the gas temperature. But during pyrolysis the particles also release volatile combustible gases which react with oxygen in the bulk gas to produce additional heat. Combined, these gas combustion reactions are seen to result in higher gas temperatures as compared to the case of two-way coupling without gas reactions. The higher gas temperatures thus result in a lower biomass pyrolysis time, as can be seen in figure 3.3.

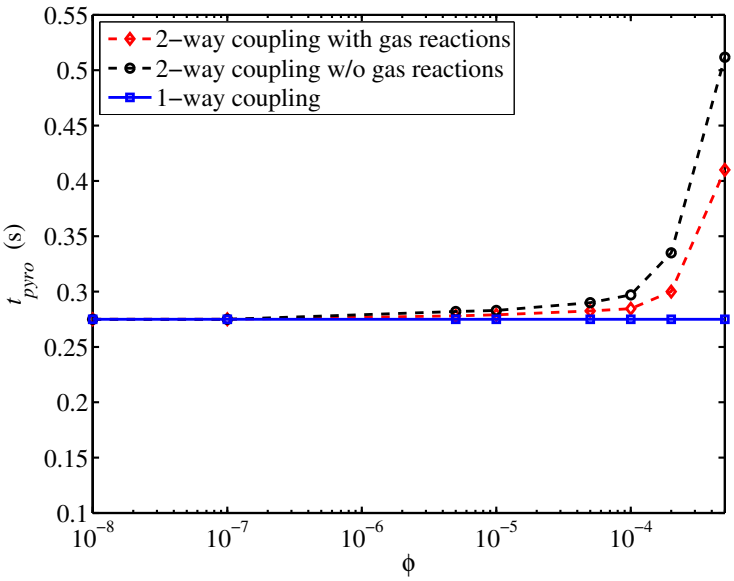

Figure 3.3: Pyrolysis time (t_{pyro}) for different initial particle volume fractions ϕ with one-way and two-way coupling illustrating the inclusion of gas phase reactions, lowering the pyrolysis time

3.4.2 Effect of gas phase reactions

Figure 3.4 presents the mean gas temperature and mean particle temperature for two cases - with and without gas phase reactions. The initial particle size is 0.7 mm and the initial particle volume fraction is 2×10^{-4}. It can be seen that during pyrolysis, the gas and particle temperatures are higher for the case which includes gas phase reactions. This is due to the combustion of volatile gases in the gas phase. This increased temperature results in a shorter pyrolysis time of the biomass particles. Conversely, during combustion, as can be seen in figure 3.4, the particle temperatures are lower for the case with gas phase reactions. This is because the volatile gases consume a part of the oxygen and hence decrease the availability of oxygen at the particle surface during the char combustion phase. This slows down the rate of char combustion reactions and hence we observe lower particle temperatures. We can also see a drop in the maximum particle surface temperature for the same reason.

In figure 3.4, we can also see that the particle temperature decreases more slowly during char combustion with gas reactions than without. The slow decrease of the particle temperature during combustion in the case with gas phase reactions is due to a higher mean gas temperature. This is because of the exothermic reactions in the gas phase which increase the mean gas phase temperature. It can be seen in the figure that at some point the mean gas temperature is equal to or even higher than the particle temperature. When this happens, the direction of convective heat

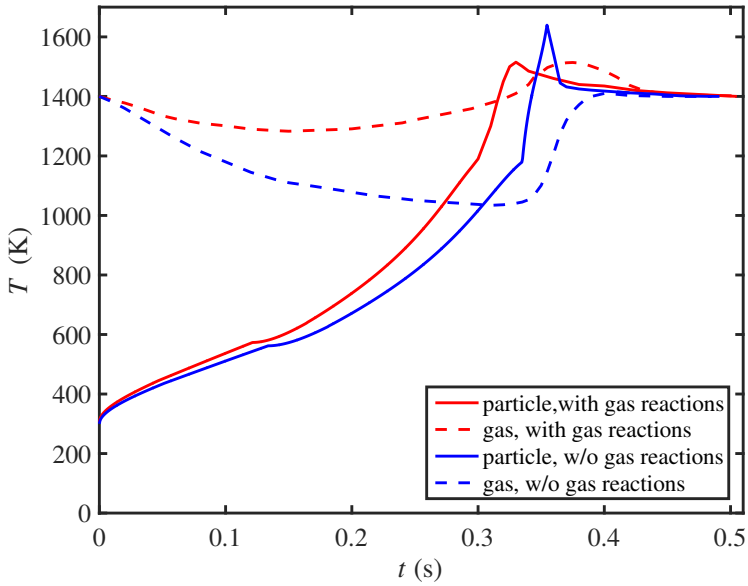

Figure 3.4: Averaged gas temperature(- - -) and particle temperature(—) during pyrolysis and combustion, with and without gas phase reactions.

exchange between the particles and gas is reversed, which in turn slows down the cooling of particles.

Figure 3.5 presents the pyrolysis time of biomass particles for varying initial particle sizes for cases with and without gas reactions. It can be seen that the effect of gas phase reactions on the pyrolysis time is stronger for smaller particles. This is because pyrolysis is governed by the heat transferred from the gas to the particles. For smaller particles the availability of a large total surface area for heat exchange implies that more heat can be transferred to the particles. This reduces the pyrolysis time. It can be seen that for larger particles, the effect of including gas phase reactions is very small.

In Figure 3.6, we present the combustion times for varying particle sizes. It can be seen that, unlike during pyrolysis, the effect of gas phase reactions is stronger for larger particles. This is because unlike pyrolysis, the combustion process is mainly governed by the kinetic rates of char-gas reactions which in turn depend on the availability of oxygen at the particle surface. For large particles, the duration of the combustion process is longer which causes a higher fraction of oxygen to be consumed in the gas phase reactions. Hence, during combustion, the effect of including gas phase reactions is stronger for larger particles.

In figures 3.5 and 3.6, the results are presented for two different values of the initial particle volume fraction - low (1×10^{-5}) and high (1×10^{-4}). It can be seen that the effects of including gas phase reactions, during both the pyrolysis and

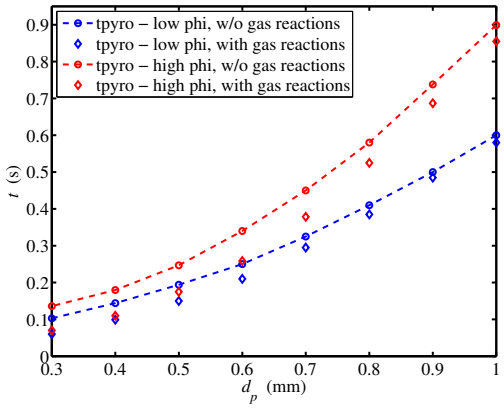

Figure 3.5: Pyrolysis time (t_{pyro}) vs. initial particle diameter (d_p) for cases with and without gas phase reactions at low (10^{-5}) and high (10^{-4}) volume fraction.

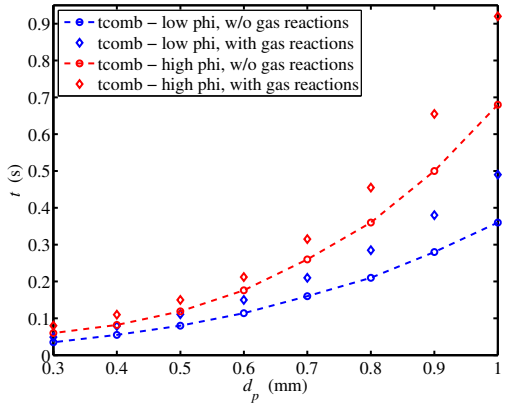

Figure 3.6: Combustion time (t_{comb}) vs. initial particle diameter (d_p) for cases with and without gas phase reactions at low (10^{-5}) and high (10^{-4}) volume fraction.

the combustion phases, are stronger for the higher initial volume fraction. This is mainly because of the larger amount of volatile gases released during pyrolysis at high particle volume fractions. Since the amount of reacting gases is higher, the effect of gas phase reactions on both pyrolysis and combustion is also stronger.

3.4.3 Effect of initial particle size

To analyze the effects of the initial particle size on conversion time, we performed simulations at constant initial particle volume fraction ($\phi = 2 \times 10^{-4}$) and constant initial oxygen mole fraction ($X_{O2} = 0.21$) while varying the initial particle size (and hence the number of particles). Figure 3.7 presents the variation of t_{pyro} and t_{comb} with particle size (d_p) on a log-log scale along with their corresponding one-way coupling values. Similar to the analysis in chapter 2, i.e., without gas phase reactions in the DNS model, it can be seen in Figure 3.7 that both for pyrolysis and combustion, the relative difference between two-way and one-way coupling is higher at smaller particle sizes. In fact, as the particle size increases at constant volume fraction, the total surface area available for heat exchange between the gas and the particles decreases. This reduces the total interphase convective heat exchange for larger particles as compared to the smaller particles and hence a closer agreement between one-way and two-way coupling is observed for larger particles.

The particle size also affects the local tempearture gradients in the domain. In Figure 3.8 and Figure 3.9, we present the RMS temperature of the gas, during pyrolysis and combustion stages respectively, for 3 different particle sizes. The RMS

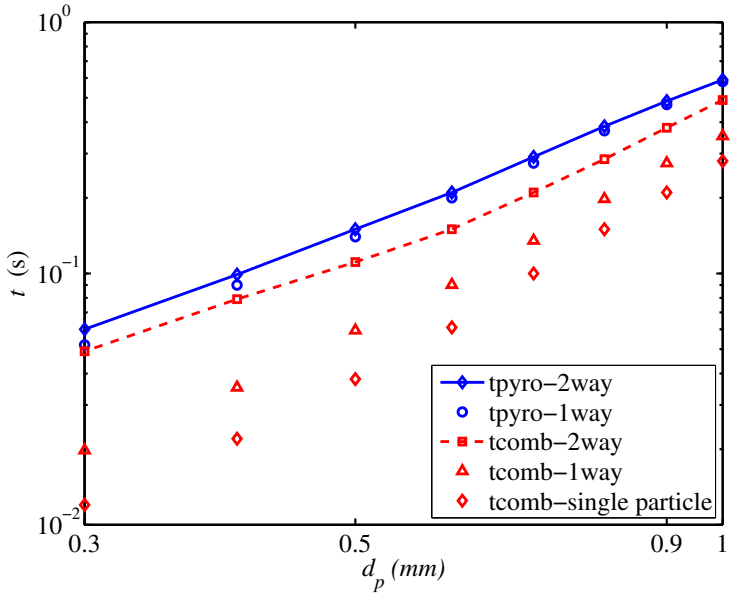

Figure 3.7: Pyrolysis time (t_{pyro}) and combustion time (t_{comb}) vs. initial particle diameter (d_p) for one-way and two-way coupling. The effect of multiple particles is clear from a comparison with the single particle combustion time prediction.

of the gas temperature is averaged over the homogeneous directions and presented as a function of the wall normal coordinate for time instants where the particles have undergone 50% conversion in both the pyrolysis and combustion stages.

It can be seen that T_{RMS} is higher for larger initial particle sizes in both the pyrolysis and combustion stages. We also see higher peaks for T_{RMS} in case of larger particles. For the same initial particle volume fraction, smaller particles have a more uniform distribution over the domain. During the simulation, solid particles act as heat sinks in the pyrolysis stage and heat sources in the combustion stage. For smaller particles, a more uniform distribution of solid paricles means a more uniform distribution of heat sources and sinks which results in lower local variations in temperature of the gas phase and hence a lower T_{RMS}.

From figure 3.8 and 3.9 it can also be seen that T_{RMS} is higher in the combustion stage than in the pyrolysis stage. This can be attributed to the relative rates of pyrolysis and char-combustion reactions. The char combustion reaction is much faster (about 2 orders of magnitude) than the pyrolysis reaction. Notice that these local fluctuations in temperature, which have an effect on the particles, can not be predicted in simulations based on single particle models.

In Figure 3.10 we present the effect of initial particle size on oxygen concentration in the gas phase. During pyrolysis the oxygen is consumed by the volatile gases released from the solid particles, whereas during combustion the oxygen is consumed

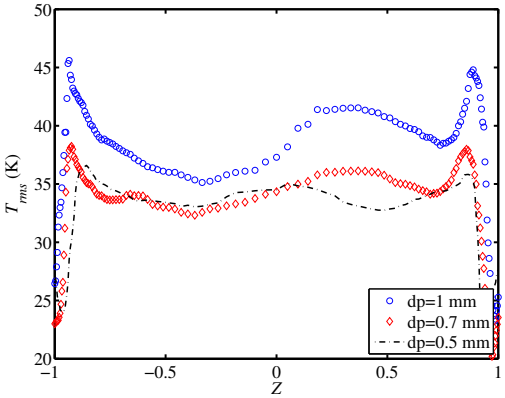

Figure 3.8: RMS of gas temperature during pyrolysis averaged over homogeneous directions for different particle sizes with gas phase reactions.

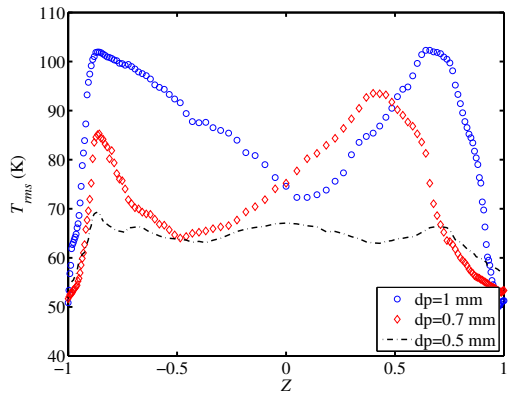

Figure 3.9: RMS of gas temperature during combustion averaged over homogeneous directions for different particle sizes with gas phase reactions.

at the solid particle surface by the char combustion reaction. In the figure, these two stages of oxygen - during pyrolysis and during combustion - can be seen distinctly. It can be seen in figure 3.10 that for the larger particles the rate of consumption of oxygen is slower in both pyrolysis and combustion stages. During pyrolysis, the intial heating up phase of the particles consumes no oxygen and this initial stage is relatively long for the bigger particles. During the combustion stage, the rate of combustion reactions determines the rate at which the oxygen is consumed in the domain. For larger particles, at fixed initial particle volume fraction, the total surface area available for char combustion is lower. This reduces the total rate of char combustion and so we see a slower rate of consumption of oxygen for larger particles.

3.4.4 Particle size distribution

In practical applications of burning biomass, the biomass particles are not monodispersed, i.e., they are not all of the same size, even initially. The biomass particle diameter usually follows a Rosin-Rammler distribution [57] as shown in figure 3.11. This Rosin-Rammler distribution is a good approximation for the small particles but it overpredicts the number of larger particles somewhat. Also, in reality, very few particles are larger than 3 mm. Therefore, we truncate the distribution at 3 mm. Moreover, for particles larger than 3 mm the point-particle assumption used in this study becomes questionable.

At the lower end of the distribution, the presence of smaller particles requires a very small time step because of the stability restrictions associated with the explicit time integration for the particle motion. Including very small particles would lead to

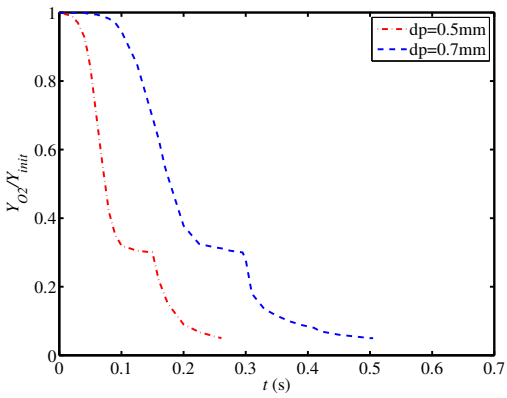

Figure 3.10: Evolution of mean oxygen mass fraction in the domain for two different particle sizes.

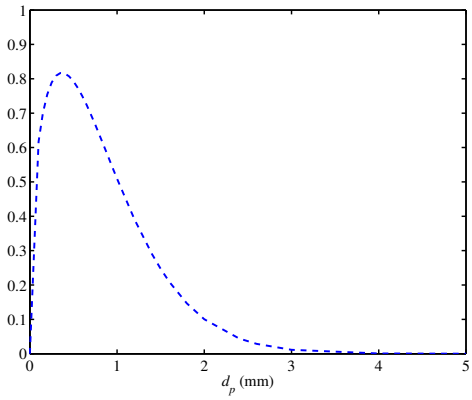

Figure 3.11: Rosin Rammler particle size distribution for biomass particles used in the simulation.

very long computational times. Therefore, we also truncate the distribution at the lower end at 0.3 mm. The lower bound for the particle diameter in the distribution implies that almost 13% of the particles present in the distribution are ignored. However, these small particles constitute a very small fraction (0.2%) of the total mass of biomass present. Hence, these smaller particles can be safely neglected in the simulation.

We compare the conversion time of particles in two cases: mono-dispersed (where all particles are of the same initial size) and PSD (where particle sizes follow a distribution) with the same initial solid volume fraction. We select a particular particle size in the PSD case and compare its conversion time with the mono-dispersed case with the same size. Figure 3.12 shows the total conversion time, pyrolysis time and combustion time of particles in the mono-dispersed and the PSD cases.

In a PSD case, at an instant in time, the particles of different sizes are in different reaction stages. This results in the interaction between these particles via the gas phase. It can be seen that for larger particles the total conversion time in the PSD case is considerably lower than in the mono-dispersed case. This holds true for both the pyrolysis and combustion and can be explained as follows. During a run in the PSD case, while the larger particles are undergoing pyrolysis, the smaller particles have already undergone their pyrolysis stage and are in the char combustion stage. The char combustion reaction of the smaller particles, and the gas phase reactions caused by the volatiles released during pyrolysis of the smaller particles, being highly exothermic, generate heat which speeds up the pyrolysis stage of larger particles thus decreasing the total conversion time. The heat which is generated by the combustion of smaller particles also helps in the combustion stage of larger particles by increasing the mean gas temperature and thus increasing the rate of char combustion reaction

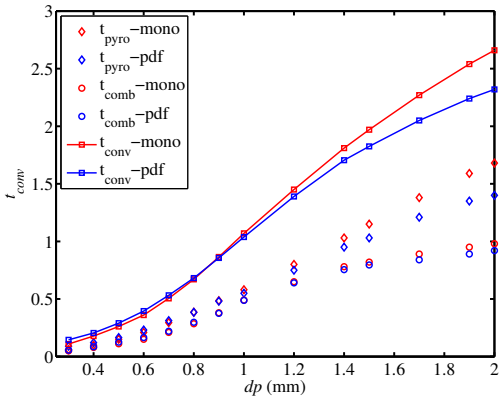

Figure 3.12: Total conversion time, pyrolysis time and combustion time of the particles for varying particle sizes in mono-dispersed and PSD cases.

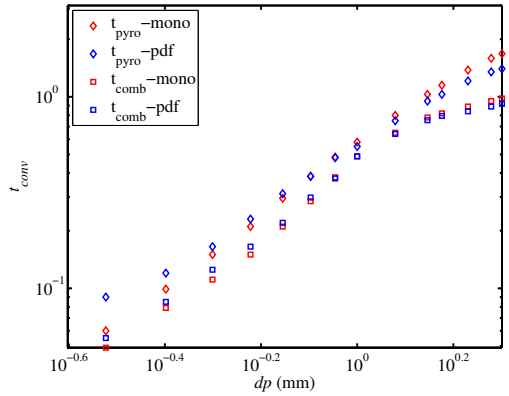

Figure 3.13: Comparison of pyrolysis time and combustion time on a log-log scale for varying particle sizes in mono-dispersed and PSD cases.

thereby decreasing the combustion time of larger particles as seen in figure 3.13. This effect is partially counteracted by the smaller available amount of oxygen, which is already consumed by the smaller particles.

The effect on the conversion time of smaller particles in the PSD case is opposite to that of the larger particles. The bigger particles being slow in the conversion process also slow down the conversion process of smaller particles. It can be seen in Figure 3.13 that for smaller particle sizes the combustion and pyrolysis times are higher for the PSD case than in the mono-dispersed case. It can also be seen in the figure that at a certain particle diameter these effects - speed up by the small particles and slow down due to the large particles in the distribution - are balanced and we see little difference between the mono-dispersed and PSD cases for these particle sizes. This happens for particles with a size around 0.9 mm.

3.5 Conclusions

In this chapter, we have extended the DNS model for biomass particle conversion by including homogeneous gas phase reactions.

We observe that the inclusion of gas phase reactions in the DNS model decreases the biomass pyrolysis time due to higher gas temperatures. In contrast, including gas phase reactions increases the combustion time of biomass due to the lower availability of oxygen at the particle surface. We also find that the effect of gas phase reactions on pyrolysis is higher for smaller particles due to the higher heat exchange area. However, for combustion the effect is higher for larger particles due to the longer duration of the combustion process which results in more oxygen getting consumed in

the gas phase reactions, thereby decreasing the oxygen available for char combustion.

The model is also used to perform simulations of realistic biomass particle size distributions (PSD) to compare the particle conversion times for both monodispersed and PSD cases. We analyze the interactions between particles of different sizes in the PSD case and find that the presence of smaller particles in the distribution speeds up the conversion process of larger particles and conversely slows down the conversion of the smaller particles.

The DNS model for biomass pyrolysis and combustion as presented in this chapter now includes models for almost all major chemical phenomena (although some in a much simplified form). Our aim in this work is to study the co-firing process of biomass with coal. Keeping this in mind, we describe the developement of a model for coal particle conversion in the next chapter.

Chapter 4

Coal particle pyrolysis and combustion

4.1 Introduction

Coal has occupied the position of a major primary energy source for a long time. However, coal-fired power plants produce large amounts of pollutants. The efficient and clean utilization of coal is a big problem in combustion processes. Researchers have been working towards improving the efficiency of the coal conversion process and the development of different ways to reduce the burden of coal conversion technologies on the environment [61, 62, 63]. Burning coal together with a cleaner, and more sustainable, fuel - like biomass - is one of the many ways in which coal-fired processes can be made more environmentally friendly.

Biomass co-firing with coal is still not well understood [39]. Our aim in this work is to develop a model for biomass and coal co-firing that can be used to improve our understanding of the co-firing process. In the previous two chapters, we described the models for biomass combustion and pyrolysis along with the scheme for gas phase combustion of reactive gases. In this chapter, we present the model for the conversion of solid coal particles.

Unlike biomass, coal combustion and pyrolysis has been the area of interest for many researchers [65, 66, 67, 68]. A small summary of this was presented earlier in section 2.1 of chapter 2. Here we present a more comprehensive literature survey of coal combustion CFD modeling studies.

A number of analyses have used Reynolds Averaged Navier Stokes (RANS) and Large Eddy Simulations (LES) for the analysis of coal combustion [65, 66, 67, 68]. A tubular oxygen-coal blast furnace was investigated by Guo et al. [65] using RANS simulations where they used a two-fluid model to describe coal particles. They studied the effect of residence time on the mixing of coal particles and oxygen. Another such sudy using RANS is by Gu et al. [66] where they study the flow

pattern inside a coal fired blast furnace using RANS simulations.

A number of coal combustion studies use Lagrangian tracking of coal particles. Maldonadao et al. [67] studied the combustion of pulverized coal in a blast furnace using RANS simulations. Shen et al. [68] carried out a similar study for pulverized coal combustion focussing on the effect of the injection location of coal particles inside the furnace. They used a mixture of hydrocarbons to represent the volatile gases released during coal pyrolysis. Bermudez et al. [69] studied NOx formation inside coal combustion furnaces using RANS simulations. Other studies [70, 71, 72] for RANS simulations of pulverized coal combustion include more detailed devolatilization models for coal pyrolysis which give better agreement with experiments.

Several studies using LES to investigate the coal conversion process inside a furnace exist in the literature [73, 74, 75]. Jovanovic et al. [73] numerically studied a system that uses oxygen and flue gas for the combustion of coal. They analyzed the ignition properties and flame stability near the injector inside the furnace. They also compared their results with RANS simulations of the same system and demonstrated that the predictions of the LES model provide better agreement with the experimental data. Franchetti et al. [74] conducted LES simulations of the coal combustion process of a pulverized coal jet flame. Stein et al. [75] used both Lagrangian and Eulerian representations of the particles for LES simulation of a laboratory scale burner and obtained satisfactory agreement between experimental data and the predictions of LES simulations. They compared conversion time and maximum gas phase temperature values from the experimental data with the simulation results.

In comparision to the RANS and LES studies for the coal conversion process, fewer studies exist that use DNS to analyze the coal conversion process. Luo et al. [18] carried out Direct Numerical Simulation for the carrier phase of a turbulent jet involving coal particle-laden flow. They used a simplification by representing the volatile gases as methane. They employed Lagrangian tracking of coal particles and treated the particles as point sources. A similar approach has been adopted by Brosch et al. [24] to study the localised forced ignition of coal particles in a turbulent flow. Hara et al. [23] carried out DNS of a jet flame with pulverized coal particles mainly focussing on the pyrolysis of coal particles. They used a global volatile matter reaction scheme based on the detailed reaction mechanism of various volatile gases.

In this chapter, we present our DNS model for coal pyrolysis and combustion. We use models from literature for various coal conversion processes and adapt them to be used in the DNS model. In the next section of this chapter, we present the kinetic models for the conversion of coal particles. The information about the numerical method used for the DNS and its implementation is presentated in section 4.3. This is followed by the analysis of some results in section 4.4.

Table 4.1: Proximate and ultimate analysis of bituminous coal [76]

Proximate	%	Ultimate (DAF)	%
Fixed Carbon	68.9	C	81.2
Volatiles	26.3	H	8.9
Moisture	3.9	O	6.9
Ash	15.5	N	2.1
		S	0.9

4.2 Coal conversion models

The general scheme for the coal particle conversion is similar to that of biomass particles as shown in figure 3.1 of the previous chapter. The main difference lies in the composition of coal particles and the kinetics of the coal conversion processes. A typical coal particle has relatively less volatile matter as compared to the biomass. The composition of a coal particle is given in terms of its proximate and ultimate analysis [76]. In this study, the type of coal we use is bitumious coal whose composition is given in table 4.1. The reason for choosing this type of coal is because it has been used in many experimental and numerical investigations [72, 73, 74, 76]. The proximate analysis of the coal consists of the fraction of fixed carbon, volatile matter, moisture, and ash in the coal. The ultimate analysis describes the elemental composition of the coal on a dry-ash-free (DAF) basis.

The process of coal conversion results in mass loss from the coal particles during pyrolysis and combustion. The total mass change of the coal particle can be written as:

$$\frac{dm_p}{dt} = \dot{m}_v + \dot{m}_c \tag{4.1}$$

where $\dot{m}_v$ is the volatile release rate i.e. the pyrolysis rate, and $\dot{m}_c$ is the mass loss rate due to the combustion of the coal particle. Similar to the biomass particles, we assume the pyrolysis and combustion stages to be sequential, i.e. pyrolysis followed by combustion. This assumption is justified as the release of volatile gases from the coal particle during pyrolysis prevents oxygen from reaching the particle surface, thus preventing the combustion of char [12].

4.2.1 Coal pyrolysis

There are several models for coal pyrolysis available in literature [23, 71, 72]. These models are specific to the type of coal used in the study. In this study, we use a more widely used pyrolysis model for the bituminous type of coal.

The coal pyrolysis reaction is simulated by a two competing reaction kinetic model as suggested by Kobayashi et al. [77]. In this model, the pyrolysis process

Table 4.2: Kinetic data for coal pyrolysis reactions[77]

Reaction	Pre-exponential factor $A_{v,i}$ (1/s)	Activation energy $E_{v,i}$ (J/mol)	Enthalpy $H_{v,i}$ (J/kg)
$\dot{m_{v,1}}$	3.7×10^4	7.37×10^4	1.67×10^6
$\dot{m_{v,2}}$	1.46×11^{10}	2.51×10^5	8.37×10^6

consists of two competing first order reactions to account for the effect of heating rates on coal pyrolysis. Each of these reactions describes the degradation of coal to residual chars (R_1 and R_2) and volatiles (V_1 and V_2) as given below

$$\begin{aligned} coal = (1-\alpha_1)R_1 + \alpha_1 V_1 \\ (1-\alpha_2)R_2 + \alpha_2 V_2 \end{aligned} \tag{4.2}$$

The mechanism involving R_1 and V_1 is dominant at low particle temperatures, whereas the mechanism involving R_2 and V_2 takes precedence at higher particle temperatures. The coefficient α_1 is the proximate volatile fraction of the coal (dry-ash-free basis) and the coefficient α_2 is determined experimentally [18]. Based on equation 4.2, the pyrolysis rate $\dot{m}_v$ can be expressed as [23, 18, 24]

$$\dot{m}_{v,i} = \dot{m}_{v,1} + \dot{m}_{v,2} \tag{4.3}$$

where, $\dot{m}_{v,i}$ is the mass loss rate which is calculated for the two elementary reactions as

$$\dot{m}_{v,i} = -\alpha_i m_{daf,p} A_{v,i} \exp\left(-\frac{Ea_{v,i}}{RT_p}\right) \tag{4.4}$$

where $m_{daf,p}$ is the mass of the dry-ash-free content of the particle and T_p is the temperature of the particle. The pre-exponential factors ($A_{v,i}$), the activation energies ($Ea_{v,i}$), and the enthalpies of devolatilization for the two reactions are listed in table 4.2 [77, 18, 24]. Moreover, similar to other DNS studies of coal conversion in literature, the volatiles released during the pyrolysis are assumed to be methane. This greatly reduces the kinetic reaction mechanism of the gas phase as it limits the number of gas species in the model [18].

4.2.2 Coal combustion

The coal combustion model is similar to the biomass particle combustion model as described in section 2.2 of chapter 2. We consider the following heterogeneous reactions of solid char with the gases.

$$C + \nu O_2 \rightarrow 2(1-\nu)CO + (2\nu - 1)CO_2 \tag{4.5}$$

Table 4.3: Kinetic data for coal char oxidation and gasification used in this study [18]

Reaction	Pre-exponential factor ($kg/m^2/s/atm^n$)	Activation energy (kJ/kmol)
Oxidation	280	78652
Gasification	312	172350

$$C + CO_2 \rightarrow 2CO \tag{4.6}$$

As described earlier, in the above equations the stoichiometric coefficient, ν, of oxygen in the char oxidation reaction (4.5) determines the molar ratio of CO and CO_2 in the reaction products. This coefficient, which satisfies $0.5 < \nu < 1$, depends on the temperature and is given by an Arrhenius type equation (equation 2.3). The reaction rates for the above two reactions are described by an Arrhenius law in the following way:

$$r_i = A_i \exp\left(-\frac{E_i}{RT_s}\right) P_{i,s}^{ni} \tag{4.7}$$

The kinetic data, i.e., pre-exponential factors (A_i), activation energies (E_i), and the order of reaction (n_i), are selected from a wide range of experimental data [77, 18] and are given in Table 4.3. To calculate the surface reaction rates, the partial pressures of various gases at the particle surface ($P_{i,s}$) need to be determined using a quasi steady-state assumption for the conservation of mass of O_2 and CO_2. The relevant equations (eq. 2.6 and eq. 2.7) for the calculation of partial pressures of gas species at the particle surface were described before in chapter 2 of this thesis.

The pyrolysis of a coal particle is an endothermic process, i.e, it consumes energy, whereas the combustion is mainly an exothermic process. Various enthalpies of reactions are associated with these processes and they result in energy loss/gain from the solid particle surface. The coal particle energy balance equation can be written as

$$m_p c_{pc} \frac{dT_p}{dt} = h_m A_p (T_g - T_p) + \sigma \epsilon A_p (T_w^4 - T_p^4) - \dot{m_{v,1}} H_{v,1} - \dot{m_{v,2}} H_{v,2} + \sum_i r_i A_p \Delta H_i \tag{4.8}$$

where m_p is the mass of the particle and A_p is its surface area, c_{pc} is the specific heat capacity of the particle, σ is the Stefan-Boltzmann constant, ϵ is the emissivity, $H_{v,1}$ and $H_{v,2}$ are the enthalpies of the pyrolysis reactions, ΔH_i is the heat of reaction for the char-gas reactions during the combustion stage, and T_w is the reactor wall temperature. In this study, the enthalpies of the high and low temperature pyrolysis reactions are considered constant [18, 24].

In equation 4.8, the specific heat capacity of a coal particle c_{pc} is calculated as follows

$$c_{pc} = 836.0 + 1.53(T_p - 273.0) - 5.4 \times 10^{-4}(T_p - 273.0)^2 \tag{4.9}$$

Unlike the larger biomass particles, where we considered a non-uniform temperature inside the particle during the pyrolysis stage, the temperature of the coal particle both during the pyrolysis and the combustion is assumed to be uniform. This assumption is reasonable due the much smaller size of the coal particles (d_p = 0.025-0.1 mm) as compared to the biomass particles (d_p = 0.25-1 mm).

The coupling between the mass, momentum, energy, and species conservation equations between the dispersed phase (i.e. coal particles) and continuous phase is obtained by means of two-way coupling terms as described before in chapter 2 and chapter 3. For momentum exchange, the particle tracking equations are based on the drag force on a spherical particle (section 2.2.3). Moreover, like biomass particles, we limit ourselves to lower solid volume fractions so that particle-particle collisions can be safely neglected.

4.3 Numerical Implementation

The details of the numerical method employed for the DNS of the coal conversion process are similar to the DNS of biomass conversion as outlined in chapter 2. All equations for the gas and for the particles are non-dimensionalized using appropriate reference values. The particle equations are in the form of ordinary differential equations. The gas equations assume this form after spatial discretization based on a second-order accurate finite volume method. To this effect, the domain is divided into small rectangular cells. The domain is divided into 128^3 control volumes. The grid spacing is uniform in streamwise and spanwise directions, whereas it is non-uniform in the wall-normal direction with clustering of grid points near the walls.

Despite the many similarities between the numerical implementation of the DNS of coal and biomass particles, there are some significant differences. These diferences are described in the next few subsections.

4.3.1 Grouping of coal particles

Initially, the particles are randomly, and uniformly, distributed throughout the channel. The smaller size of coal particles (0.025-0.1 mm) as compared to the larger biomass particles (0.25-1 mm) presents itself in the form of a computational problem. For a simulation with the same volume fraction, the number of coal particles is orders of magnitude higher than the number of biomass particles. This greatly increases the computational time of the model as the number of particle equations to be solved in the simulation increases. The number of coal particles for different solid volume fractions and particle sizes is given in table 4.4. As can be seen in table

Table 4.4: Number of coal particles (N_p) for different solid volume fractions ϕ, and particle sizes d_p (in mm)

ϕ	d_p [mm]	N_p
1×10^{-6}	0.025	1.54×10^{8}
	0.05	1.93×10^{7}
	0.1	2.41×10^{6}
1×10^{-5}	0.025	1.54×10^{9}
	0.05	1.93×10^{8}
	0.1	2.41×10^{7}
1×10^{-4}	0.025	1.54×10^{10}
	0.05	1.93×10^{9}
	0.1	2.41×10^{8}

4.4, for higher solid volume fractions and smaller particles, the number of particles can easily be more than 1 billion. This results in very long computational time and memory requirements.

In order to circumvent this problem, we investigated whether it is possible to solve the particle equations only for a reduced number of particles, which would be representing the entire set of particles in much the same way as members of a parliament represent a much larger population. To do this, we adopt a particle grouping model. In this approach, a number of real coal particles is represented by a single virtual coal particle. The virtual particle has the same properties like velocity, temperature, location etc. as the real particles it represents. In this way we avoid solving solid particle equations for all the particles, and the equations are only solved for the virtual particles. We define the number of real particles represented by the virtual particles as the particle grouping factor, ζ. The two-way coupling terms for the mass, momentum, energy, and species exchange between the particles and gas are multiplied by ζ. The scheme can easily be implemented as we assume the solid coal particles to be point sources, and do not resolve the velocity field of the gas around the particles.

We investigate the accuracy of this particle grouping scheme by simulations with different values of ζ for varying particle volume fraction (ϕ) and particle size (d_p). The results will be discussed below in section 4.5.

4.3.2 Time integration

The results of a single-particle model for solid particle surface temperature vs. time during the pyrolysis and combustion stages of coal particle conversion are shown in Figure 4.1. The results are shown for two different particle sizes of 0.025 mm and 0.05 mm. These sizes are much smaller than the minimum size of the biomass

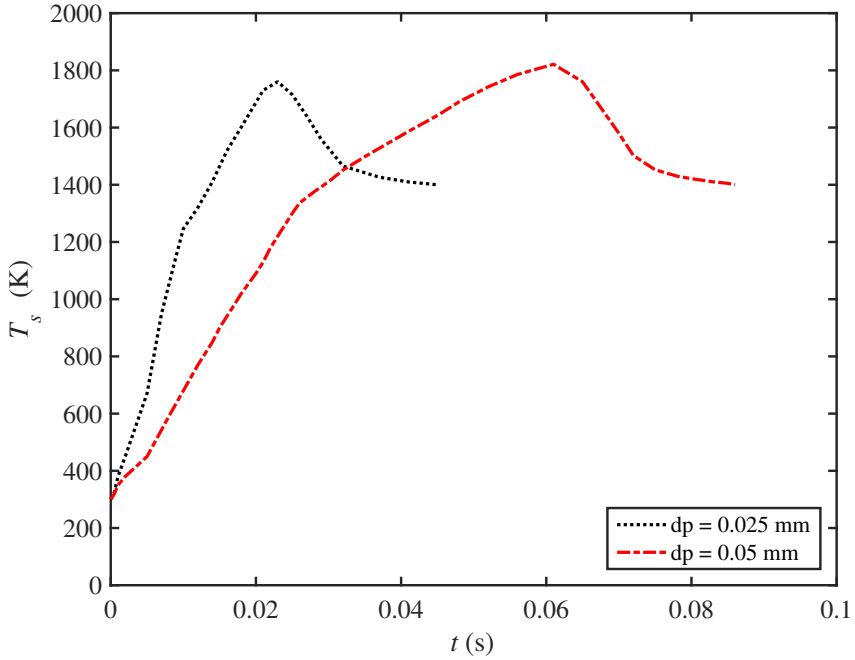

Figure 4.1: Single-particle model results for coal particle surface temperature (T_s) vs. time (t) during the pyrolysis and combustion stages for two different values of the particle diameter as indicated in the legend. The initial particle temperature is 300 K and the temperature of the channel walls is 1400 K.

particles that we investigated in chapter 3. The main difference between the single particle model results for the biomass and coal particles is in the relative rates of the pyrolysis and combustion stages. In chapter 2, figure 2.3 presents the single particle model results for the biomass conversion model. It can be seen by comparing figure 2.3 with figure 4.1, that the rate of pyrolysis reaction for the coal particle is much faster than that of the biomass particles. On the other hand, the rate of combustion reaction for the coal particles is slower when compared to that of biomass particles.

The difference in rates of reaction during the pyrolysis stage can be explained by the different formulation of pyrolysis models for the coal and biomass. For biomass, the pyrolysis model is based on the heat transfer inside the particle from the surface of the particle and is limited by the rate of heat conduction inside the particle. This formulation of the pyrolysis model was applied for the biomass particles due to their much larger size. In contrast, for the smaller coal particles, the pyrolysis model is based on kinetics. The reaction rate kinetics for coal pyrolysis are quite fast.

The char combustion models for the biomass and coal are similar in their formulation, although the kinetic rates of the combustion reactions are different. This difference in rates is due to the difference in properties of char formed after the

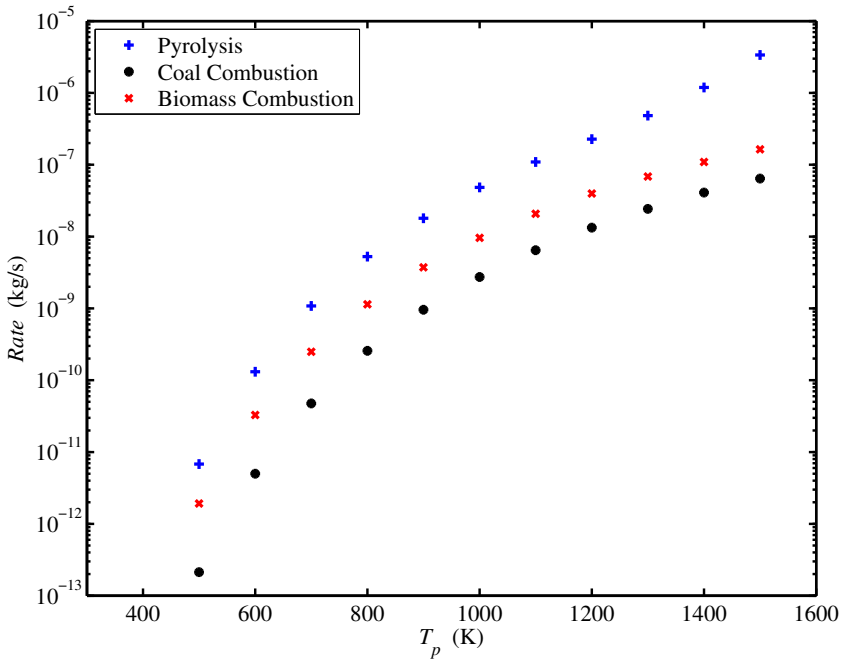

Figure 4.2: Relative rates of coal pyrolysis, coal combustion, and biomass combustion reactions for a solid particle of size (d_p) 0.1 mm for different particle surface temperatures. The coal particle density is 2200 kg/m^3.

volatiles are released from coal and biomass. The different pore structure of the char formed after the pyrolysis of coal and biomass results in different kinetics of combustion and gasification reactions of the solid char with the gases.

Figure 4.2 shows the relative initial rates of pyrolysis and combustion for the coal particle of size (d_p) 0.1 mm at different temperatures. The figure also shows the corresponding rates of biomass combustion reaction for the same particle size. It can be seen from figure 4.2 that coal pyrolysis is the fastest when compared to coal combustion and biomass combustion. Coal pyrolysis is approximately an order of magnitude faster than the biomass combustion and about 2 order of magnitudes faster than the coal combustion at higher temperatures.

In chapter 2, we presented the time integration scheme used in the DNS for the biomass conversion process. A hybrid implicit-explicit Runge-Kutta method [54] was used. For the faster biomass combustion process, we used the implicit part of the method, whereas for the non-stiff gas equations, particle tracking, and biomass pyrolysis we used the explicit part of the time integration scheme. In this chapter, for coal conversion, we use the implicit part of the method for both the coal pyrolysis and combustion reactions. Moreover, we also use a variable time step with smaller time steps during the pyrolysis stage of the coal conversion process. This does not

result in a significant increase in time required for the simulation as the total time required for coal conversion is much shorter than that required for the biomass conversion process. For the gas phase equations, the explicit part of the method is used.

4.4 Setup of simulations

We consider the gas-particle system inside a channel, bounded by two parallel horizontal plates. The domain size is $4\pi H$ in streamwise direction and $2\pi H$ in spanwise direction, where H is half the channel height. Simulations are performed with frictional Reynolds number approximately equal to $Re_\tau = 150$, which is based on friction velocity $u_\tau = \sqrt{\tau_w/\rho_g}$ and half the channel height. Here, τ_w is the wall shear stress based on the mean streamwise velocity component, averaged over the two homogeneous directions and time.

In all simulations the flow is initialized with a turbulent velocity field in the statistically steady state as obtained from a simulation without particles. For the base case, the initial oxygen mole fraction is $X_{O2} = 0.21$ with nitrogen the remainder. In all the simulations presented in this chapter the amount of oxygen is stoichiometrically sufficient. The initial gas temperature is set equal to 1400 K, and the particles are initialized with a temperature of 300 K which is constant within the particle. The walls of the channel are maintained at a temperature of 1400 K [28]. Initially, the particles are randomly, and uniformly, distributed throughout the channel and the particle velocity is initialized with the gas velocity at the position of particle. With these initial conditions we simulate the pyrolysis and combustion of coal particles in a turbulent channel flow.

Initially, simulations are carried out without any particle grouping at particle volume fractions (ϕ) of 1×10^{-6}, 1×10^{-5} and 1×10^{-4} with a particle size of 0.1 mm. The results of these simulation are used to determine a suitable particle grouping factor. In the next section, an analysis of the results is presented for the DNS of the coal conversion process.

4.5 Analysis of results

Similar to biomass particles, we observe that in a single run of the simulation, the conversion time of different coal particles with the same initial size varies significantly. We present the pdf of the conversion time of particles in figure 4.3. For the results presented in figure 4.3, the initial solid volume fraction was 1×10^{-5}.

As observed in the figure, there is a variation of about about 9% for the larger particle of size 0.05 mm and a variation of about 11% for the smaller particles with size 0.025 mm. It can also be seen that for the same initial particle size there is a slight variation in the PDF of the conversion time for a different initial spatial

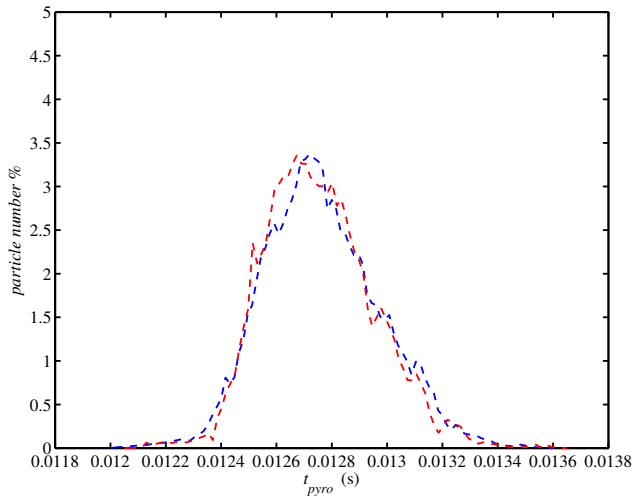

(a)

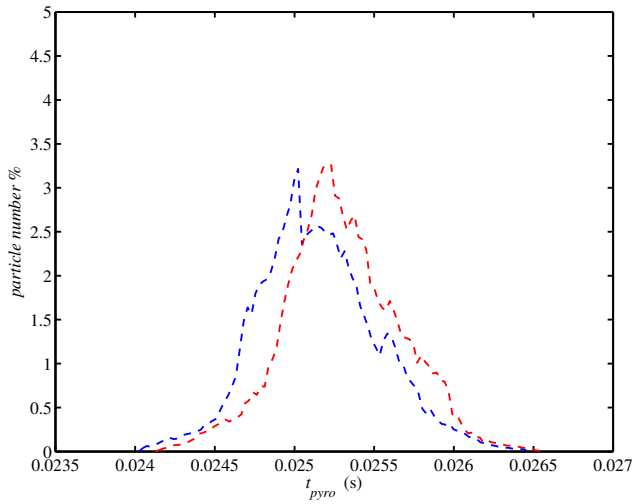

(b)

Figure 4.3: Probabilty density function for the coal particle pyrolysis time for different initial particle sizes and two different initial spatial distributions of the particles, particle size a: 0.025 mm, b: 0.05 mm

distribution of the particles in the domain. This indicates that these PDF's are case specific. We also observe a relatively big tail towards the end of the distribution of conversion time. This is especially true for smaller particles. In the earlier chapters on biomass conversion, we based our analysis of biomass conversion times on the maximum conversion time of the distribution, i.e., the time at which the last particle was converted. This would be less appropriate in case of the smaller coal particles because of the big tail towards the end of the distribution of conversion time. To solve this problem we perform the analysis of coal particle conversion times based on the time at which 90% of the particle have completed the converison ($t_{90\%}$). For the analysis that follows, we use the value of $t_{90\%}$.

As given in table 4.4, due the small size of coal particles, the number of coal particles in the DNS is very large. This makes it computationally expensive to run different simulations to study the effect of different model parameters on model results. We adopt a particle grouping approach to reduce the computational time of the simulations.

Figure 4.4 presents the pyrolysis time of coal particles for different particle grouping factors (ζ) and for three different solid volume fractions. The coal particle size is 0.1 mm. The solid volume fractions (ϕ) are 1×10^{-6}, 1×10^{-5}, and 1×10^{-4}. In figure 4.5 we present the combustion time of coal particles for different particle grouping factors. It can be seen from figures 4.4 and 4.5 that the pyrolysis time increases with increasing particle grouping factor while the combustion time slightly decreases. This can be explained on the basis of the endothermic nature of the pyrolysis reaction and the exothermic nature of the combustion reaction. As the grouping factor increases, it creates larger heat sinks by two-way coupling between the particles and the gas, thus decreasing the local temperature of the gas at the particle position. This in turn decreases the rate of the pyrolysis reaction. The opposite is true for the exothermic combustion reaction. In case of combustion, which releases heat, larger particle grouping factors result in higher temperatures around the particles, thus increasing the rate of the combustion reaction.

The reduction in combustion time is largest for the smallest particle volume fraction. This can be understood from the oxygen present near a coal particle. For larger particle volume fraction the reduction in local oxygen concentration near the particle is larger than for smaller particle volume fractions and therefore has a larger negative effect on the speed of combustion.

4.5.1 Effect of particle grouping

Intuitively, the accuracy of this particle grouping scheme will be dependent on the number of particles present per finite volume cell of the numerical method used for the gas phase. If the number of particles present per computational cell is high, the local differences in variables of the gas phase will be small. We postulate that the particle grouping scheme would be accurate if the number of virtual particles does

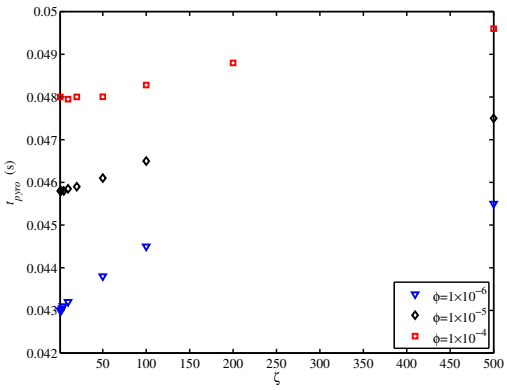

Figure 4.4: Pyrolysis time of coal particles for different particle grouping factors and different solid volume fractions. Particle size is 0.1 mm.

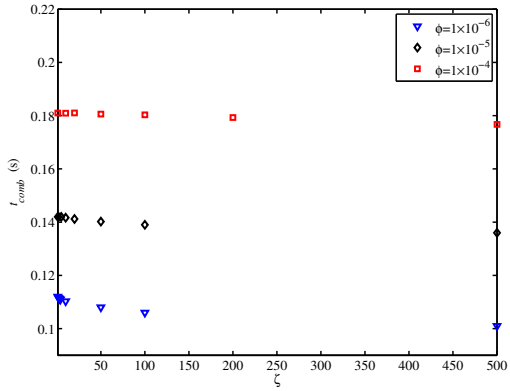

Figure 4.5: Combustion time of coal particles for different particle grouping factors and different solid volume fractions. Particle size is 0.1 mm.

Table 4.5: Different particle volume fractions (ϕ) and particle sizes (d_p) used in the simulations

ϕ	d_p	N_p	N_p/N_{cell}
1×10^{-6}	0.1	2.41×10^6	1.1
1×10^{-5}	0.05	1.93×10^8	92
	0.07	7.13×10^7	35
	0.08	4.82×10^7	23
	0.1	2.41×10^7	11
1×10^{-4}	0.1	2.41×10^8	110

not differ much from the number of computational cells in the numerical method for the gas. Indeed, mathematically, the two-way coupling terms between the gas and the particles would be equal if there are N similar particles present in a cell, or if one effective particle with the same properties and ζ = N is present in the cell.

We investigate this by running simulations for a particle size of 0.1 mm for different particle grouping factors and for different initial solid volume fractions. Table 4.5 lists the different cases with corresponding values of number of particles (N_p). The table also shows the ratio of number of particles and number of computational cells in the domain ($N_p/Ncell$).

We study the relative error in pyrolysis and combustion times for different particle grouping factors. Figure 4.6 presents the relative error in values of pyrolysis and combustion times of coal particles for different particle grouping factors at an initial solid volume fraction of 1×10^{-6}. At this solid volume fraction, the N_p/N_{cell}

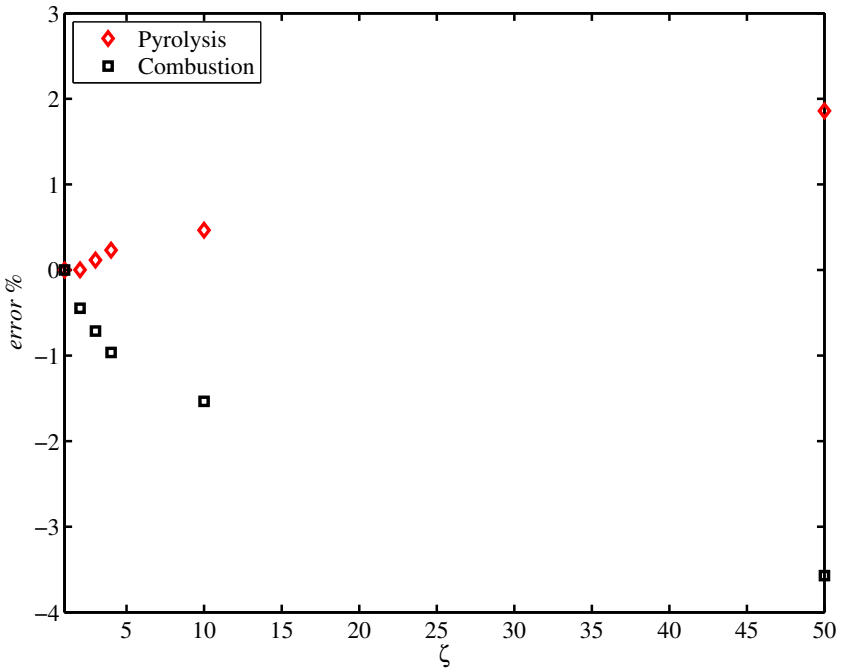

Figure 4.6: Relative error in pyrolysis and combustion time of coal particle for different particle grouping factors (ζ). Particle size is 0.1 mm and initial solid volume fraction is $\phi = 1 \times 10^{-6}$

is 1.1. The values of particle grouping factors that we investigate for this case are $\zeta = [1, 2, 3, 4, 10, 50]$.

In figure 4.6 we observe that the error in the conversion times starts increasing as we increase the value of ζ from 1 to higher values. This is expected as N_p/N_{cell} is equal to 1.1 and so a value of ζ greater than 1 should result in higher errors. However, we see that relative error in both the pyrolysis and combustion time is less than 1% for $\zeta < 4$. At higher values of the particle grouping factor ($\zeta = 50$), we observe higher errors of 2% and 3.5% in the pyrolysis time and the combustion time respectively.

We perform a similar analysis for a higher value of the particle volume fraction ($\phi = 1 \times 10^{-5}$). At this ϕ, N_p/N_{cell} is 11. Figure 4.7 presents the relative errors in the conversion times for this case. As can be seen from the figure, the error in the conversion times is negligible for $\zeta < 10$. The error starts increasing for higher values of ζ. For $\zeta > 50$, we observe that the relative errors in the conversion times are larger than 1%.

Figure 4.8 shows the relative errors in the conversion times for an even higher value of the particle volume fraction ($\phi = 1 \times 10^{-4}$). This is the highest particle volume fraction we use in case of coal particle conversion. In this case, N_p/N_{cell}

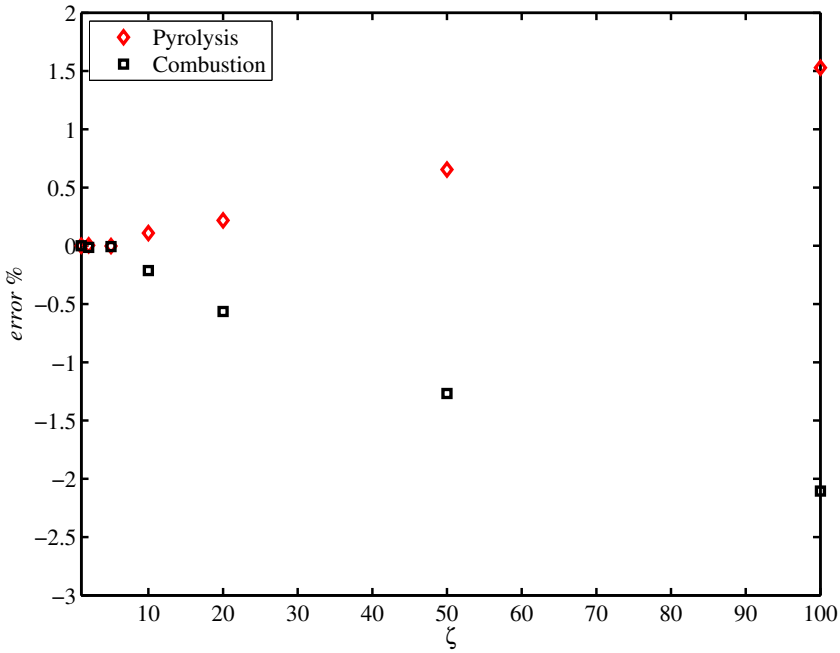

Figure 4.7: Error in pyrolysis and combustion time of coal particle for different particle grouping factors (ζ). Particle size is 0.1 mm and initial solid volume fraction is $\phi = 1 \times 10^{-5}$

is 110. We observe that for this value of particle volume fraction, the errors in conversion times are insignificant for $\zeta < 100$.

From the above three cases, we conclude that the relative errors in conversion times for varying values of particle grouping factor (ζ) are dependent on the initial particle volume fraction. At higher particle volume fractions (ϕ) we can use larger values of ζ without compromising the accuracy of the results. It should be noted that the pyrolysis and combustion times are mean quantities in the simulation. To further validate the above conclusion, we study the effect of particle grouping on the RMS of the gas temperature for the three particle volume fractions.

In figure 4.9, we present the RMS of the gas temperature during the pyrolysis stage averaged over the homogeneous directions for different particle grouping factors. The particle size is 0.1 mm. We present results of T_{RMS} for three different initial particle volume fractions. It can be seen that just like particle conversion times, the difference in T_{RMS} for varying values of ζ is dependent on the initial particle volume fraction. From figure 4.9a we see that T_{RMS} for $\zeta = 1$, and $\zeta = 2$ is very close, whereas T_{RMS} starts showing noticeable variations at higher particle grouping factors. This is in accordance with N_p/N_{cell}=1.1 for this case.

Similarly, from figures 4.9b and 4.9c we observe that also at higher particle

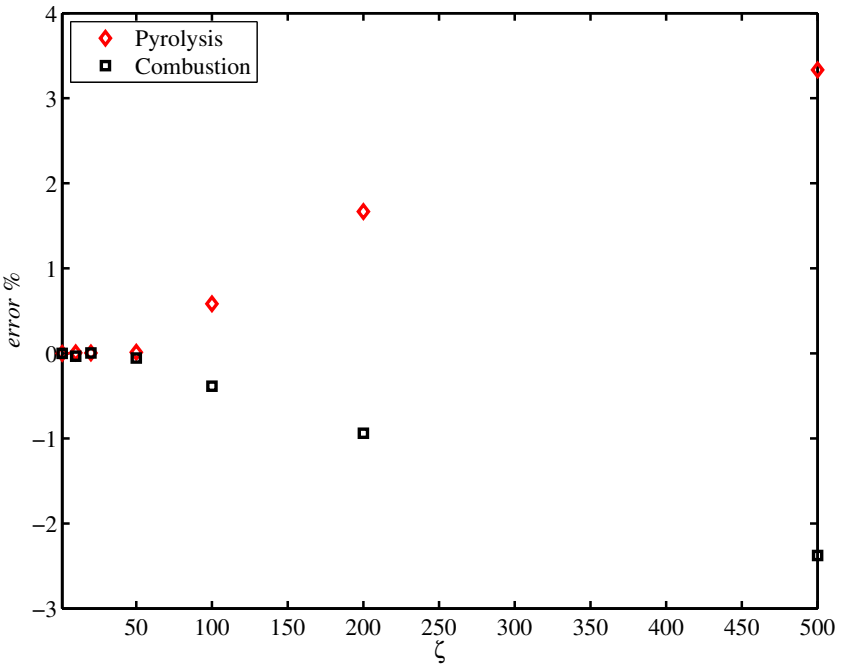

Figure 4.8: Error in pyrolysis and combustion time of coal particle for different particle grouping factors (ζ). Particle size is 0.1 mm and initial solid volume fraction is $\phi = 1 \times 10^{-4}$

volume fractions, the differences in T_{RMS} are insignificant for $\zeta < N_p/N_{cell}$. These observations are similar to those observed in the case of pyrolysis and combustion times of coal particles. Hence, we conclude that for a given initial particle volume fraction (ϕ), using a value of $\zeta < N_p/N_{cell}$ results in insignificant errors in coal particle conversion times and gas temperatures. This result can be used to perform simulations of coal particles at higher values of the particle grouping factors for higher particle volume fractions. This keeps our simulation time limited as we no longer need to solve the particle equations for all the solid particles.

4.5.2 Effect of particle volume fraction

In figures 4.10 and 4.11 we present the relative errors in pyrolysis time and combustion time of coal particles for different particle grouping factors (ζ) and initial particle volume fractions (ϕ). For all the cases, the conversion time value at $\zeta = 1$ is used as the base case value. It can be seen from the figures that the relative errors in conversion time are higher at lower particle volume fractions. Moreover, the rate at which these errors increase are also higher for lower particle volume fractions. This means that the effect of particle grouping is larger at lower particle volume

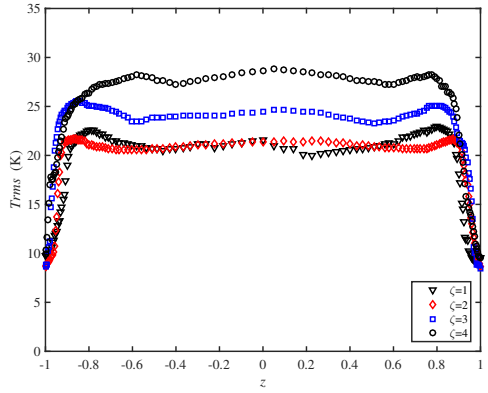

(a)

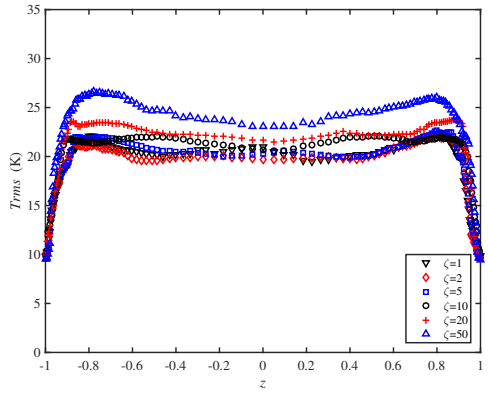

(b)

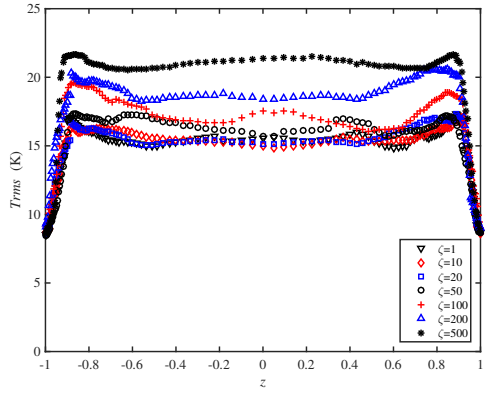

(c)

Figure 4.9: RMS of gas temperature for different values of particle grouping factors and different initial particle volume fraction(ϕ). a) $\phi = 1 \times 10^{-6}$; b) $\phi = 1 \times 10^{-5}$; c) $\phi = 1 \times 10^{-4}$. The particle size is 0.1 mm.

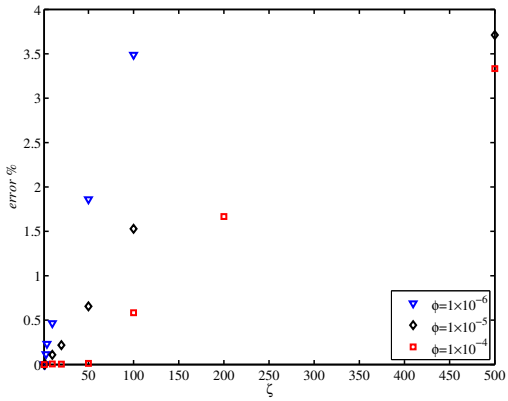

Figure 4.10: Relative error in pyrolysis time for coal particle of size 0.1 mm as a function of particle grouping factor (ζ) for different initial particle volume fraction (ϕ) values as shown in legend.

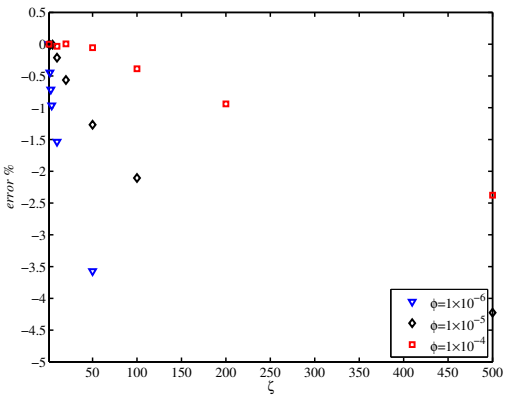

Figure 4.11: Relative error in combustion time for coal particle of size 0.1 mm as a function of particle grouping factor (ζ) for different initial particle volume fraction (ϕ) values as shown in legend.

fractions. We observe that the smaller the number of particles in the domain, the higher is the effect of particle grouping method.

4.5.3 Effect of particle size

Next, we analyze the effect of particle grouping for different values of the particle size on coal particle conversion. Figure 4.12 presents the pyrolysis time and the combustion time of coal particles of different particle sizes at a particle volume fraction of $\phi = 1 \times 10^{-5}$. In figure 4.12 no particle grouping is applied so that $\zeta = 1$. It can be seen in the figure that both the pyrolysis time and the combustion time increase with increasing particle size. This is because for coal particles both these processes are modelled as shrinking core kinetic models. Hence, larger particles take more time for conversion. Also, the combustion times are higher than the pyrolysis times as the process of combustion of coal particles is slower than pyrolysis. This is in contrast to the conversion of biomass particles where the process of pyrolysis is much slower than combustion. This is because coal particles have relatively lower volatile content as compared to biomass particles. A typical sub-bituminous coal has about 30% volatile content whereas the volatile content of biomass is around 70%.

To study the effect of particle grouping for varying particle diameter, we run simulation for 4 different particle sizes (d_p) while keeping the initial particle volume fraction (ϕ) constant at 1×10^{-5}. At different particle size the number of coal particles in the domain is different. This results in the values of N_p/N_{cell} as shown in table 4.5. Based on the results of the previous sections, that indicate the importance

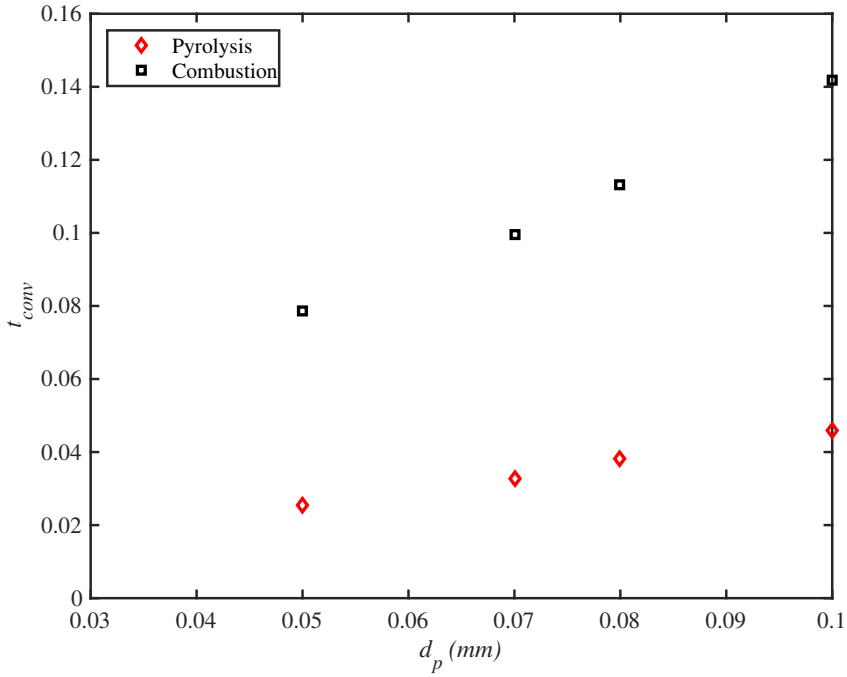

Figure 4.12: Pyrolysis and combustion time of coal particle for different particle sizes (d_p). The initial solid volume fraction is $\phi = 1 \times 10^{-5}$

of the value of N_p/N_{cell}, we use different values of the particle grouping factor for different particle sizes. From the results we observe that our previous obervation that the relative error in the conversion times is insignificant for $\zeta < N_p/N_{cell}$ holds true also at smaller particle sizes.

Figure 4.13 shows the pyrolysis time of coal particles of different sizes for varying values of the particle grouping factor. In these simulations the particle volume fraction is kept constant. It can be seen from the figure that the relative errors in the pyrolysis time are negligible for lower particle grouping factors. We also observe that the rate at which the errors due to particle grouping increase is higher for larger particles. For a given particle volume fraction, larger particles imply a smaller number of particles in the domain. Thus the effect of particle grouping is larger for larger particles.

Figure 4.14 shows the corresponding results for the combustion time of coal particles. Similar to the pyrolysis time, the effect of particle grouping is higher for larger particles. From these observations we can conclude that the effect of particle grouping is relatively lower for cases with a larger number of particles in the domain.

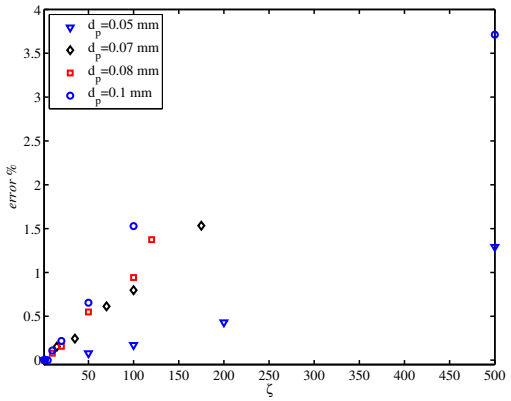

Figure 4.13: Relative error in pyrolysis time of coal particles for different particle grouping factor (ζ) and different particle sizes(d_p).

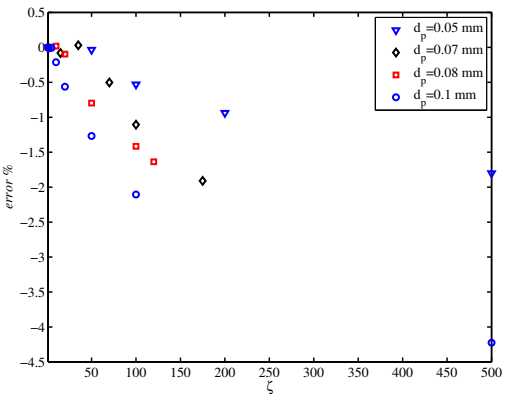

Figure 4.14: Relative error in combustion time of coal particles for different particle grouping factor (ζ) and different particle sizes(d_p).

4.5.4 Scaling the particle grouping factor

In the previous three subsections, we analyzed the effect of the particle grouping factor (ζ) on coal conversion by varying either the particle volume fraction or the particle size. To study the combined effect of particle size and volume fraction, we define a parameter that represents the average distance between the coal particles.

If $N_{p,v}$ is the number of virtual particles, V_p is the volume of one particle, and V_D is the volume of the domain, then, $\zeta N_{p,v}$ is the number of real particles. It follows that solid particle volume fraction (ϕ) can be expressed in these variables as:

$$\phi = \frac{\zeta N_{p,v} V_p}{V_D} \tag{4.10}$$

The average volume per computational particle is then equal to:

$$V_D / N_{p,v} = \frac{\zeta V_p}{\phi} \tag{4.11}$$

The average distance between the particles in the domain (δ) is a measure of the size of this volume and equals:

$$\delta = \left(\frac{\zeta V_p}{\phi} \right)^{1/3} \tag{4.12}$$

We use this parameter to study the effect of particle grouping for different particle sizes and particle volume fractions. Figure 4.15 presents the relative error in the pyrolysis time for different particle sizes and volume fractions as a function of the average distance between the particles in the domain. We observe that the relative

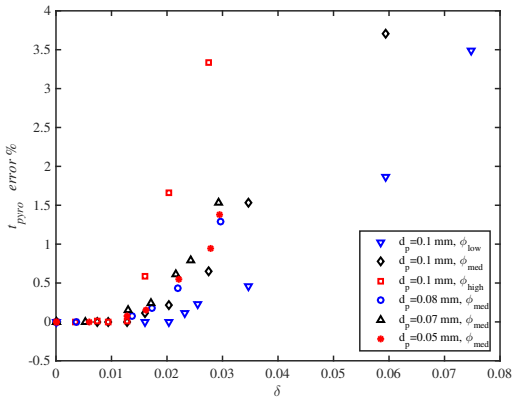

Figure 4.15: Relative error in pyrolysis time as a function of average distance between the particles (δ). The particle sizes and volume fractions are as shown in legend.

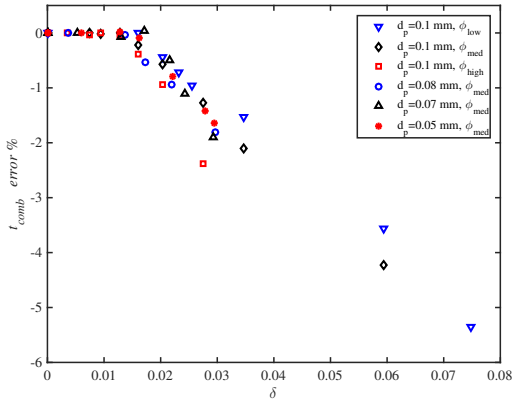

Figure 4.16: Relative error in combustion time as a function of average distance between the particles (δ). The particle sizes and volume fractions are as shown in legend.

errors for different cases are negligible below some threshold value of δ, irrespective of the particle volume fraction and diameter. From the figure we can see that this threshold value of δ is around 0.015. For values of δ higher than 0.015, we start seeing some differences in pyrolysis time. As expected, the relative error increase as the value of δ increases. We also observe that the rate at which the error increases after the threshold value of δ is different for different combinations of particle size and particle volume fraction.

Figure 4.16 shows the corresponding results for the combustion time. We observe similar behavior as for the pyrolysis time. Again, below the threshold value of $\delta = 0.015$, we observe negligible differences. As explained earlier, the combustion time decreases for higher particle grouping factors. Hence, the deviations in the combustion time are negative.

Apart from the pyrolysis time and combustion time, we also study the error in T_{RMS} of the gas phase as a function of δ. To do this, we define the relative error in T_{RMS} as follows:

$$T_{RMS,error} = \frac{\int_{-H/2}^{H/2}(T_{RMS,\zeta} - T_{RMS,1})^2 dz}{\int_{-H/2}^{H/2}(T_{RMS,1})^2 dz} \tag{4.13}$$

where the integral is between the two walls of the channel. Figure 4.17 shows the relative error in T_{RMS} as a function of δ. Similar to the results of pyrolysis time and comsbution time, we observe that the error in T_{RMS} is negligible for all values of δ below a threshold value. This threshold value is again close to 0.015. From the observations from figures 4.15, 4.16, and 4.17, we conclude that for the

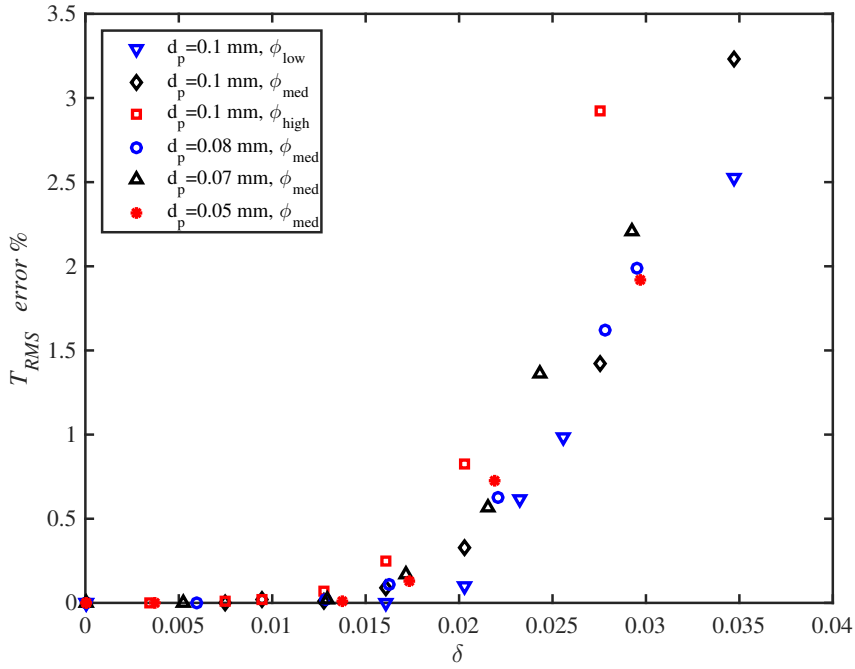

Figure 4.17: Relative error in T_{RMS} as a function of average distance between the particles (δ). The particle sizes and volume fractions are as shown in legend.

coal conversion simulations presented in this chapter, the errors in quantities due to particle grouping are negligible for an avarage distance between the particles δ equal to 0.015.

4.6 Conclusions

In this chapter we presented the model for DNS of coal pyrolysis and combustion. We use single particle coal conversion models from literature and use them for the DNS of coal particles in a turbulent channel flow.

As the size of coal particles is very small compared to the biomass particles, the number of coal particles in our simulations is very large. Solving the equations for all the coal particles during the simulation is computationally very expensive and takes a large amount of memory. To overcome this problem we adopt a particle grouping method where a virtual particle represents a number of real coal particles with the same properties. In order to model the interaction between the two phases, we multiply the two way coupling terms between the gas and particles with the particle grouping factor.

We analyze the accuracy of this particle grouping scheme by running simulations at varying values of the particle grouping factor (ζ). We observe that a value of

$\zeta = N_p/N_{cell}$ results in a good approximation for the simulation with no particle grouping. This is true for all the particle sizes and solid volume fractions used in our study. We also observe that the errors due to larger values of ζ are low for simulations with high solid volume fractions. This is also true for simulations with smaller particles.

We observed that the threshold for ζ below which the relative error in the results is negligible corresponds to an average distance between two particles approximately equal to $0.015H$, where H is half the channel height. This distance can be compared to the size of a computational cell. The length of a grid cell in the streamwise direction equals $0.098H$ and in the spanwise direction $0.049H$, both significantly larger than this threshold value. The average length of a grid cell in the wall-normal direction, however, is $0.016H$, which is very close to the threshold value. We hypothesize that this threshold value of δ is linked to grid resolution and not to the actual physics of the problem. More research into the origin of threshold value of δ is required.

In the next chapter, we will use the models developed in chapter 3 and chapter 4 to analyze the co-firing process of biomass and coal.

Chapter 5

Co-firing of biomass and coal

5.1 Introduction

In the earlier chapters of this thesis, we presented models for biomass conversion in chapter 3 and for coal conversion in chapter 4. In this chapter, we study the process of co-firing of biomass with coal.

Co-firing coal with biomass is considered environmentally friendly for multiple reasons. First, burning biomass causes no net increase in CO_2. Biomass consumes the same amount of CO_2 from the atmosphere during its growth as is released during its burning. So, blending coal with biomass can effectively reduce the CO_2 emissions. In some cases, co-firing of biomass residues also reduces the amount of CH_4 by avoiding the CH_4 release from the otherwise land-filled biomass [78]. This is an important benefit, because it is believed that CH_4 is 21 times more harmful than CO_2 in terms of its global warming impact. Furthermore, co-firing of coal with biomass also results in reduced NOx and SOx emmissions [79]. Finally, from an economical point of view, co-firing biomass with coal can also result in the utilization of less expensive fuel with a possible reduction in fuel costs [80].

Blending of coal with biomass also improves some major operational problems in systems which rely on biomass as the sole fuel. The high moisture and ash content in biomass is the cause of ignition and combustion problems inside a furnace [81]. The highly variable properties of biomass are also a major source of problems. Furthermore, the lower heating value of biomass (as compared to coal) results in lower temperatures inside the furnace. This could result in slagging and fouling problems due to deposition of ash [81]. Coal has relatively lower ash and moisture content. It also has a higher heating value thus resulting in higher temperatures inside the furnace. Co-firing of coal with biomass can therefore prevent some of the problems in a sole biomass firing system.

Based on the above factors, co-firing holds more appeal than both sole fuel firing options. In this chapter we will present the model for biomass-coal co-firing and

analyze the results. In the next section we present a summary of models used for biomass and coal conversion along with the assumptions we make in the modeling. Section 5.3 describes the numerical implementation of the model. Next, we describe the setup of simulations in section 5.4. This is followed by an analysis of results in section 5.5, where we study the effect of blending ratio on biomass and coal co-firing process.

5.2 Modeling of biomass-coal co-firing

Modeling of conversion of a biomass-coal blend is a complex problem that involves modeling conversion of two chemically different solid fuels. Several studies for coal combustion exist in the literature (as presented in Chapter 4). However, there are fewer studies on biomass-coal co-firing in the literature. This is probably due to the fact that co-firing is still a developing technology. We present a summary of CFD modeling studies of biomass-coal co-firing in the literature.

A mathematical model for biomass-coal blend conversion using the k–ϵ turbulence model is presented by Abbas et al. [83]. They used a single step model for both coal and biomass devolatilization, and a kinetic shrinking core model for char combustion. They used a Eulerian-Lagrangian approach to model the gas and particle phases. The gas phase equations were based on a Eulerian reference frame while the particle phase equations were modeled using particle tracking in a Lagrangian reference frame. To account for the variations in the properties of coal and biomass, they track the volatile gases released from both fuels separately. The authors also compared the results with experiments on co-firing coal and biomass (sawdust) in an industrial furnace and found good agreement between the experiments and the model results.

A similar model was presented by Dhanaplan et al. [84] who used the same model to study coal-only and coal-biomass blend conversion. They predicted an early devolatilization of large biomass particles due to the presence of smaller coal particles. Their model also included chemistry for NOx formation and predicted lower NOx formation in biomass-coal co-firing as compared to sole coal firing.

A full-scale coal and straw–fired utility boiler was modeled by Kaer et al. [85]. They developed an extended particle conversion model and used a commercial CFD code (CFX 4.2) to model the gas phase. They used a k–ϵ turbulence model and incorporated a two-step homogeneous gas phase reaction model. They analyzed the combustion behavior of blend fuel near the burner mouth and found that the devolatilization and burnout of biomass (straw) occurred further away from the burner mouth than the devolatilization and burnout of coal. This was in strong contrast to sole coal converion models where most of the devolatiliation occurred very close to the burner. In addition, they observed significant variations in trajectories of biomass particles inside the furnace as compared to coal particles i.e. biomass

Table 5.1: Properties of the biomass (torrified wood) and coal used in the simulations

	Mass density (kg/m^3)	Thermal conductivity (W/m/K)	Heating Value (MJ/kg)
Torrified Wood	650	0.25	17.8
Coal	850	0.3	25.4

particles disperse more as compared to the coal particles.

Apart from the modeling studies of the co-firing process, there are several experimental studies on the co-firing of biomass-coal blends. A detailed review of literature on experimental studies of co-firing process is presented by Sami et al. [86]. In their review, they mention several types of biomass including agricultural wastes, municipal wastes, and organic material. They present experimental results of a large variety of coal and biomass blends, and also identify some critical operational issues in co-firing of biomass-coal blends.

In CFD modeling studies of co-firing, the k–ϵ model has been used extensively. This is mainly due to the relatively lower computational complexity of a Reynolds-averaged Navier-Stokes model and easier implementation. More detailed CFD studies on co-firing that use LES and DNS approaches are relatively few. In this section, we outline the major difference in conversion of coal and biomass. We also summarize the models for conversion of biomass and coal as presented in earlier chapters of this thesis.

In chapter 1, table 1.1 presents the typical composition of coal and biomass fuels. The properties of coal and biomass which are used in the simulation are presented in table 5.1. From the tables, the main differences between coal and biomass that are important for modelling of co-firing are summarized as follows:

- Coal has a much lower volatile content than biomass. A typical sub-bituminous coal has around 30% volatile matter, while biomass generally has more than 70% volatile matter.

- The heating value of coal is higher than that of biomass.

- The total carbon content of coal is higher than that of biomass. Biomass has a much higher oxygen content.

These factors result in differences in conversion behavior of coal and biomass particles. A CFD model should be able to capture these differences to analyze the interactions between the different solid fuel particles.

5.2.1 Biomass pyrolysis and combustion

As presented in chapter 2, we adopt the model developed by Haseli [27] for the pyrolysis of biomass particles. The model consists of several phases during which the biomass particle evolves from virgin biomass to char. Although we adopt a point particle assumption which usually implies a uniform temperature inside the particle, the pyrolysis model developed by Haseli [27] is based on thermal diffusion inside the particle which results in temperature variations within the particle. We also assume a fixed pyrolysis temperature, i.e., the temperature at which the virgin biomass is converted into char with the release of volatile gases. As soon as the temperature of a layer of virgin biomass inside the particle reaches this pyrolysis temperature, biomass breaks down into volatile gases and char.

The char produced after the pyrolysis of biomass further enters the combustion stage. The biomass combustion model is formulated based on the traditional shrinking core approximation. We consider reactions of char with O_2 and CO_2. The shrinking core approach implies that the char-gas reaction front starts at the surface of the particle and progresses towards the center as the reactions take place. This results in a decreasing particle size with continuing reactions. However, the mass density of the shrinking reactive core remains unchanged throughout the combustion process. The details of the models for biomass pyrolysis and combustion are presented in chapter 2.

5.2.2 Coal pyrolysis and combustion

In contrast to the biomass pyrolysis model that is based on heat transfer inside the solid particles, the coal pyrolysis model is based on reaction kinetics. The coal pyrolysis reaction is simulated by a two competing reactions kinetic model as suggested by Kobayashi et al. [77]. In this model, the pyrolysis process consists of two competing first order reactions to account for the effect of heating rates on coal pyrolysis. Each of these reactions describes the degradation of coal to their respective residual chars and volatiles.

The coal combustion model is similar to the biomass combustion model in its formulation. It also adopts a shrinking core approach to model the combustion of a coal particle. However, the kinetics of coal combustion are very different than biomass combustion. The details of the coal conversion model used in this chapter are presented in chapter 4.

In this thesis, our aim is to present a framework for DNS of biomass and coal co-firing. This is perhaps one of the first studies to do so. Our aim here is to demonstrate that such simulations are possible, without the ambition of comprehensive and fully quantitative modeling. We use biomass and coal conversion models from literature that can be adapted for use in DNS. We choose these models because they offer a good combination of level of detail and computational complexity.

5.2.3 Co-firing model assumptions

Apart from using different models for coal and biomass conversion, we make the following assumptions in our co-firing model:

- The volatile gases released from both the biomass and coal are considered to be methane. There is no difference in the methane released from biomass and coal. This assumption has been made in several CFD studies of coal conversion [23, 18, 19]. This assumption greatly simplifies the homogeneous gas combustion model without compromising too much on the accuracy of the results [18].
- All the differences in physical structure of chars formed after the pyrolysis of coal and biomass are accounted for by using different kinetic parameters for coal and biomass combustion.

We study the co-pyrolysis process by varying the blending ratio (θ). As stated earlier in chapter 1 of this thesis, the blending ratio is defined as the ratio between the amount of coal which is substituted by biomass and the original amount of coal. This blending ratio can be mass-based, if the coal is replaced by the same amount of biomass, or energy-based, if the total heating value of the fuel is kept the same. In this thesis, we study the effects of mass-based blending ratio on the co-firing process, as in most of the industrial settings the mass flow rate of solid fuel is a more relevant and controlled parameter [13].

5.3 Numerical Implementation

The details of the numerical method employed for the DNS of the co-firing process are similar to the DNS of biomass conversion as outlined in chapter 2. All equations for the gas and for the particles are non-dimensionalized using appropriate reference values. The particle equations are in the form of ordinary differential equations. The gas equations assume this form after spatial discretization based on a second-order accurate finite volume method. To this effect, the domain is divided into small rectangular cells. The domain is divided into 128^3 control volumes. The grid spacing is uniform in streamwise and spanwise directions, whereas it is non-uniform in the wall-normal direction with clustering of grid points near the walls.

Initially, the particles are randomly, and uniformly, distributed throughout the channel. The distribution is done separately for biomass and coal particles. In the co-firing process, the typical size of coal particles is very small as compared to biomass particles. This is a result of different grinding properties of biomass and coal particles.

Therefore, a similar mass of coal and biomass particles would result in very different numbers of solid particles. As we observed in chapter 4, for a similar solid

Table 5.2: Number of coal and biomass particles for different blending ratios (based on mass flow). The coal particle size (d_p) is 0.1 mm and the biomass particle size (d_p) is 0.5 mm. The base case mass flow rate is calculated for 100% coal particle feed with initial solid volume fraction of $\phi = 1 \times 10^{-4}$.

Blending ratio	$N_{p,coal}$	$N_{p,bio}$	$N_{p,coal}/N_{cell}$
0	2.41×10^8	0	115
0.1	2.17×10^8	2.52×10^5	103
0.2	1.93×10^8	5.05×10^5	92
0.3	1.69×10^8	7.57×10^5	80
0.4	1.45×10^8	1.01×10^6	69

volume fraction as used in chapter 2 for biomass particles, the total number of coal particles can be more than 1 billion. To solve this problem, we analyzed a particle grouping scheme for coal particles in chapter 4.

5.3.1 Grouping of coal particles

Table 5.3 present the number of biomass and coal particles for different blending ratios. As can be seen from the table, the number of coal particles can be very large which results in excessive computational costs. In chapter 4, we analyzed a particle grouping approach. In this approach, a number of real coal particles is represented by a single virtual coal particle. The virtual particle has the same properties like velocity, temperature, location etc. as the real particles it represents. In this way we avoid solving solid particle equations for all the particles by solving the equations only for the virtual particles. In chapter 4, we defined the number of real particles represented by one virtual particle as the particle grouping factor, ζ. In this approach of particle grouping, the two-way coupling terms for the mass, momentum, energy, and species exchange between the particles and gas are multiplied by ζ.

We analyzed the accuracy of this particle grouping scheme by running simulations at varying values of the particle grouping factor (ζ) and observed that a value of $\zeta = N_p/N_{cell}$ results in a good approximation for the simulation with no particle grouping. Here, N_p is the total number of real particles in the simulation, and N_{cell} is the number of grid cells in the DNS. We found that this conclusion holds true for all the particle sizes and solid volume fractions used in our study.

Based on these results, we use different particle grouping factors for different blending ratio in our study. The value of the particle grouping factor (ζ) for a particular blending ratio corresponds to the $\zeta = N_p/N_{cell}$. Here, N_p is the total number of real coal particles in the simulation.

5.3.2 Time integration

The main difference between the single particle model results for the biomass and coal particles is in the relative rates of the pyrolysis and combustion stages. In figure 4.2 of chapter 4, we presented the relative initial rates of pyrolysis and combustion for coal particles of size (d_p) 0.1 mm at different temperatures. The figure also showed the corresponding rates of the biomass combustion reaction for the same particle size. We observed that coal pyrolysis is the fastest when compared to coal combustion and biomass combustion. Coal pyrolysis is approximately an order of magnitude faster than biomass combustion.

The difference in rates of reaction during the pyrolysis stage can be explained by the different formulation of the pyrolysis models for the coal and biomass. For biomass, the pyrolysis model is based on the heat transfer inside the particle from the surface of the particle to its center and is limited by the rate of heat conduction inside the particle. This formulation of the pyrolysis model was applied to the biomass particles due to their much larger size. In contrast, for the smaller coal particles, the pyrolysis model is based on kinetics. The reaction rate kinetics for coal pyrolysis are quite fast.

The char combustion models for biomass and coal are similar in their formulation, although the kinetic rates of the combustion reactions are different. This difference in rates is due to the difference in properties of char formed after the volatiles are released from coal and biomass. The different pore structure of the char formed after the pyrolysis of coal and biomass results in different kinetics of combustion and gasification reactions of the solid char with the gases.

In chapter 2, we presented the time integration scheme used in the DNS for the biomass conversion process. A hybrid implicit-explicit Runge-Kutta method [54] was used. For the faster biomass combustion process, we used the implicit part of the method, whereas for the non-stiff gas equations, particle tracking, and biomass pyrolysis we used the explicit part of the time integration scheme. We use the same method for solving the biomass particle equations during the co-firing. For coal conversion, we use the implicit part of the method for both the coal pyrolysis and the coal combustion reactions. Moreover, we also use a variable time step with smaller time steps during the pyrolysis stage of the coal conversion process. This does not result in a significant increase in time required for the simulation as the total time required for coal conversion is much shorter than that required for the biomass conversion process. For the gas phase equations, the explicit part of the method is used.

5.4 Setup of simulations

We consider the gas-particle system inside a channel, bounded by two parallel horizontal plates. The domain size is $4\pi H$ in streamwise direction and $2\pi H$ in span-

wise direction, where H is half the channel height. Simulations are performed with frictional Reynolds number approximately equal to $Re_\tau = 150$, which is based on friction velocity $u_\tau = \sqrt{\tau_w/\rho_g}$ and half the channel height. Here, τ_w is the wall shear stress based on the mean streamwise velocity component, averaged over the two homogeneous directions and time.

In all simulations the flow is initialized with a turbulent velocity field in the statistically steady state as obtained from a simulation without particles. The initial gas temperature is set equal to 1400 K. For the base case, the initial oxygen mole fraction is $X_{O2} = 0.21$ with nitrogen the remainder. During the simulations we limit ourselves to low particle volume fractions $\phi \leq 1 \times 10^{-4}$. This is done to ensure that the amount of oxygen is stoichiometrically sufficient for all the simulations presented in the chapter.

The coal and biomass particles are treated as two separate solids and their equations are solved separately. We do not include collisions and heat transfer by radiation between the coal and biomass particles. All interactions between coal and biomass particles occur through the gas phase. The particles (coal and biomass) are initialized with a temperature of 300 K which is constant within the particle. The walls of the channel are maintained at a temperature of 1400 K [28]. Initially, the particles are randomly, and uniformly, distributed throughout the channel and the particle velocity is initialized with the gas velocity at the position of the particle.

In addition to the different kinetic rates of reaction for coal and biomass particles, the sizes of coal and biomass particles used in the simulation are also different. In this chapter, we study only mono-dispersed cases for coal and biomass particles. This means that all the biomass particles in the simulation have the same initial size. This is also true for coal particles, but the initial sizes of coal and biomass particles in the simulation are different.

With these initial conditions we simulate the co-firing of biomass and coal particles in a turbulent channel flow. In the next section, an analysis of the results is presented for the DNS of the biomass and coal co-firing.

5.5 Co-firing results

As stated earlier, coal and biomass are chemically two quite different fuels. In this section, our primary aim is to study the effect of one fuel on the conversion of the other during co-firing. We do this by varying the blending ratio (θ). As defined earlier, θ is the ratio between the amount (in kg) of coal which is substituted by biomass and the original amount of coal.

We keep the total mass of solids constant while varying the blending ratio. The total mass of solids is the sum of the mass of coal particles and the mass of biomass particles. We first select an initial solid volume fraction for a case with sole coal firing and calculate the mass of solids for this case. As we vary the blending ratio,

more biomass particles are added and the initial solid volume fraction changes (due to the difference in size of coal and biomass particles). However, since the blending ratio is defined in terms of mass, the total mass of solids remains constant.

In coal fired power plants, biomass blending in solid fuel is done in order to mitigate the harmful effects of coal burning on the environment. Generally, the biomass blending is between 5-15% of the solid feed by mass [9]. A higher blending ratio means more biomass in the solid feed. Since most of the furnaces are designed for a coal only operation, a higher blending ratio can lead to severe operational problems. Co-firing is still a developing technology and futher efforts are being made to increase the blending ratio in industrial furnaces.

In this study, we limit ourselves to blending ratios (θ) of less than 0.4. The θ values that we study are: [0, 0.1, 0.2, 0.3, 0.4, 1]. Here, $\theta = 0$ corresponds to the sole coal firing case, whereas $\theta = 1$ is for the sole biomass firing case.

Table 5.4 shows the different cases we analyze in this chapter. For all the cases presented in table 5.4, we vary the blending ratio as mentioned above. In our simulations, coal and biomass particles are of different sizes with coal particle size being smaller than biomass particle size. This is done in order to better represent the situation inside an industrial furnace where coal particles are much smaller than biomass particles.

As shown in table 5.4, we run simulations for two different solid mass loadings M1 and M2. These mass loadings correspond to solid volume fractions (ϕ) of 1×10^{-4} and 1×10^{-5} respectively, where ϕ is calculated for the sole coal firing case.

In this chapter, we focus our attention only on the cases with mono-dispersed particles i.e. we do not apply any PDF to the particle size. This is done to simplify our analysis. In cases with a particle size distribution, the simultaneous effect of different particle sizes along with other variables like blending ratio would be hard to quantify. In such cases, it would be hard to assign the effect to a specific parameter.

In the next subsection, we analyze the effect of blending ratio on the biomass and coal conversion during co-firing.

5.5.1 Effect of blending ratio

We first analyze the effect of the blending ratio on biomass conversion process. The effect of the presence of coal on biomass pyrolysis and biomass conbustion is analyzed separately. In figure 5.1, we present the pyrolysis time of biomass particles for different blending ratios (θ) during co-firing. Here, $\theta = 1$ is the case of sole biomass firing. As θ is reduced from its maximum value of 1, the amount of coal in the solid feed increases.

It can be seen in figure 5.1 that the pyrolysis time of biomass particles decreases as the blending ratio is decreased, i.e., as more coal is added. This can be explained from the different conversion times of coal and biomass particles. The conversion of coal is a much faster process than biomass conversion. This is because of the smaller

Table 5.3: Different cases studied to analyze the effect of blending ratio on co-firing of coal and biomass. The coal particle diameter ($d_{p,coal}$) is kept constant at 0.1 mm. The two mass loadings M1 and M2 correspond to solid volume fractions (ϕ) of 1×10^{-4} and 1×10^{-5} respectively, where ϕ is calculated for the sole coal firing case

Case	Solid mass loading kg	$d_{p,biomass}$ mm
A	1.07×10^{-1} (M1)	0.5
B	1.07×10^{-2} (M2)	0.5
C	1.07×10^{-1} (M1)	1
D	1.07×10^{-2} (M2)	1

size of coal particles and faster reaction kinetics of coal pyrolysis and combustion reactions. In contrast, the larger biomass particles take longer time for pyrolysis.

For the case presented in figure 5.1, the biomass particle size is 0.5 mm and the coal particle size is 0.1 mm. For these sizes of solid particles, the coal particles finish their pyrolysis quickly and start the combustion stage while the biomass particles are still in their pyrolysis stage. The coal combustion being an exothermic process results in an increase in temperature of the gas phase. This in turn increases the rate of pyrolysis of biomass particles and reduces their pyrolysis time. Hence, as we increase the fraction of coal particles (i.e. decrease θ) in the solid feed during co-firing, the pyrolysis time of biomass particles decreases.

Figure 5.2 shows the combustion time of biomass particles for different blending ratios during co-firing. As can be seen in figure, the effect of θ on the combustion of biomass is opposite to what we observed in case of biomass pyrolysis. As we decrease θ, it is observed that the combsution time of biomass particles increases slightly. To explain this we need to take into account two factors: the temperature of the gas phase and the oxygen available for combustion of biomass particles.

As explained earlier, the combustion of coal particles starts much earlier than the combustion of biomass particles. This increases the temperature of the gas phase which should result in faster combustion rates for biomass particles. However, the combustion of coal particles consumes a part of the oxygen. This reduces the availability of oxygen for the biomass particle combustion which slows down the rate of combustion reactions. As we observed in Chapter 3, the biomass combustion rate is very sensitive to the amount of oxygen available to the particles. So, despite an increase in gas temperature, the reduction in oxygen availability for biomass particle results in longer combustion time. The figure 5.2 shows that this effect is largest at the largest mass loading, where the decrease in the amount of available oxygen is largest.

In figure 5.3, we present the mass loss of biomass particles as a function of time for different blending ratios. The mass loss for different blending ratios has been

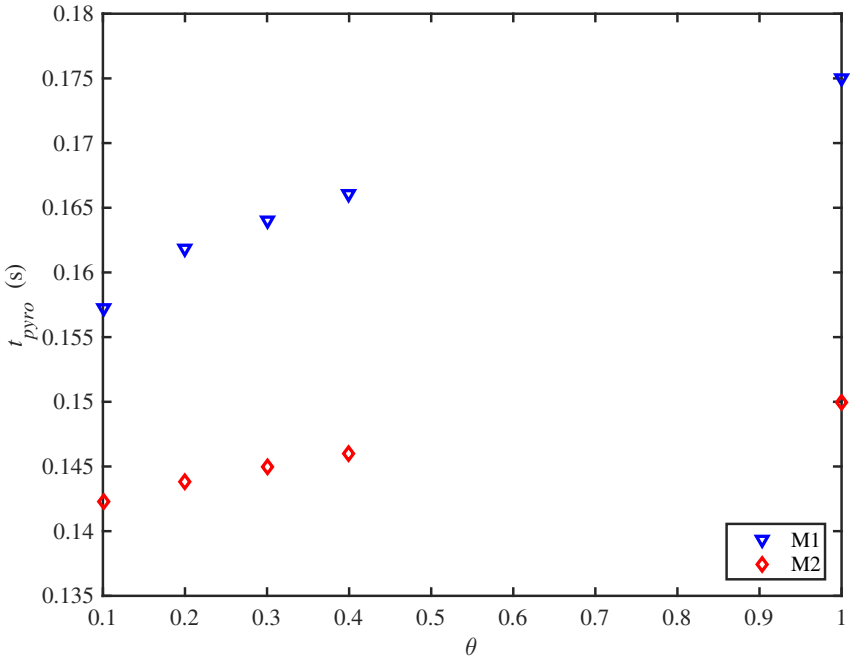

Figure 5.1: Pyrolysis time of biomass particles as a function of blending ratio (θ). The biomass particle diameter is 0.5 mm and the coal particle diameter is 0.1 mm. The results are for two different solid mass loadings M1 and M2 as given in table 5.4

normalized by the initial mass of biomass in each case. In figure 5.3, the two stages of biomass conversion - pyrolysis and combustion - can be identified separately. The combustion of biomass starts once all the volatiles in biomass are released i.e after about 70% of mass loss.

From figure 5.3, it can be seen that as the blending ratio is decreased, the biomass particles lose mass relatively faster, which results in a lower pyrolysis time. The effect of blending ratio on the combustion of biomass is also visible in the figure. At lower blending ratios the combustion stage starts earlier but the combustion time is also higher.

The total conversion time of biomass particles is the sum of their pyrolysis and combustion times. From figure 5.3 we can see that there is not much difference in the total conversion time of biomass particles for different blending ratios. This is because of the opposite effects of blending ratio in the pyrolysis and combustion stages of biomass particles. With decreasing blending ratio, the pyrolysis time decreases while the combustion time increases, and so the effect of blending ratio on total conversion time of biomass is small.

Next, we analyze the effect of blending ratio on coal conversion during co-firing.

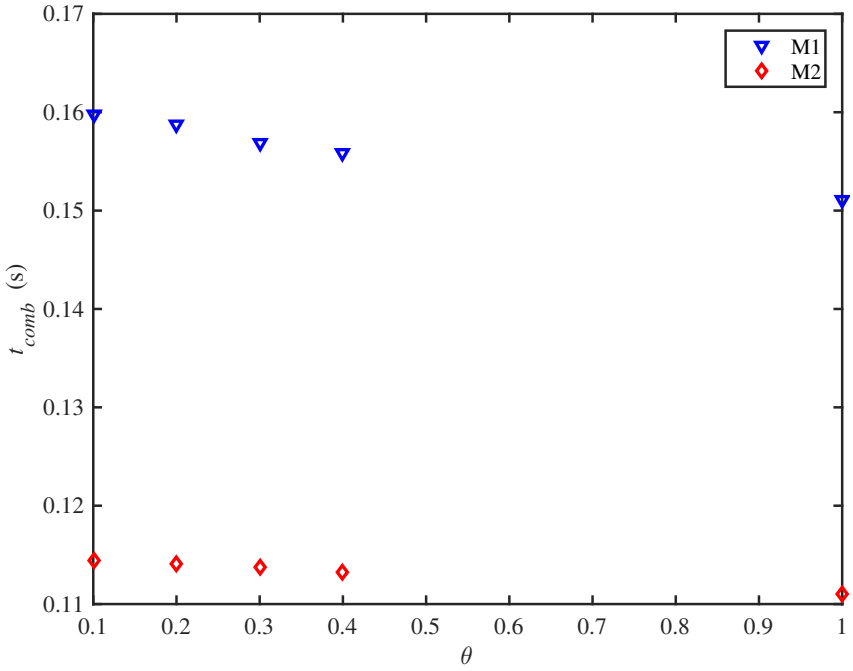

Figure 5.2: Combustion time for biomass particles as a function of blending ratio (θ). The biomass particle diameter is 0.5 mm and the coal particle diameter is 0.1 mm. The results are for two different solid mass loadings M1 and M2 as given in table 5.4

In figure 5.4, we present the pyrolysis time of coal particles for different blending ratios (θ) during co-firing. Here, $\theta = 0$ is the case of sole coal firing.

The effect of coal particles on biomass pyrolysis was to decrease the biomass pyrolysis time. In contrast, the effect of biomass particles on coal pyrolysis in just the opposite. We observe in figure 5.4, that as the blending ratio is increased i.e. as the fraction of biomass in the solid feed is increased, the pyrolysis time of coal particle also increases.

This increase in pyrolysis time of coal particles with increasing blending ratio can be attributed to the endothermic nature of the biomass pyrolysis stage. As the coal pyrolysis proceeds (at a rate much faster than biomass pyrolysis), the biomass particles are still in their pre-heating phase of the pyrolysis model (as explained in chapter 2 of this thesis). During this stage, the biomass particles consume a lot of heat which decreases the gas temperature. The rate of coal pyrolysis, being a kinetic process, depends on the gas temperature. So, a higher blending ratio (i.e. a higher fraction of biomass in feed) results in a higher coal pyrolysis time. This also explains the observation that the effect of blending ratio is larger at the larger mass loading.

Similarly, we observe an increase in coal combustion time with increasing blend-

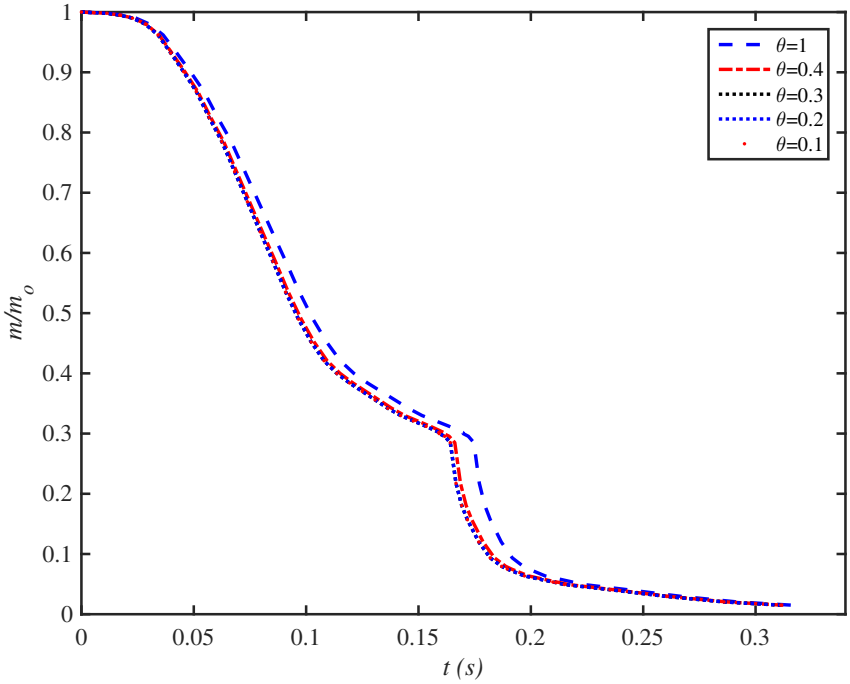

Figure 5.3: Mass loss for biomass particles for different blending ratios (θ). The mass loss has been normalized by the initial mass of biomass in each case. The biomass particle diameter is 0.5 mm and the coal particle diameter is 0.1 mm. The results correspond to solid mass loading M1

ing ratio. In figure 5.5, we present the coal combustion time for different blending ratios. As the coal particles start their combustion stage, the biomass particles are still undergoing pyrolysis. A higher number of biomass particles in the solid feed results in lower gas temperatures, which slows down the rate of combustion of coal particles. Also here we observe a relatively larger effect of the presence of biomass particles at the higher mass loading.

In figure 5.6, we present the relative changes in pyrolysis time for coal and biomass for varying blending ratio. The relative changes for each fuel are calculated with respect to the pyrolysis time of the sole fuel firing case. This means that relative changes in the pyrolysis time of coal are calculated based on the coal pyrolysis time at $\theta = 0$, while the relative change for biomass is calculated with respect on the biomass pyrolysis time at $\theta = 1$.

We observe that with varying blending ratio, the relative changes in pyrolysis time for biomass particles are larger than those of coal particles. This is due to the fact that the coal pyrolysis is a faster process than the biomass pyrolysis and so the biomass particles have less time to affect the coal pyrolysis process. In figure 5.6, we

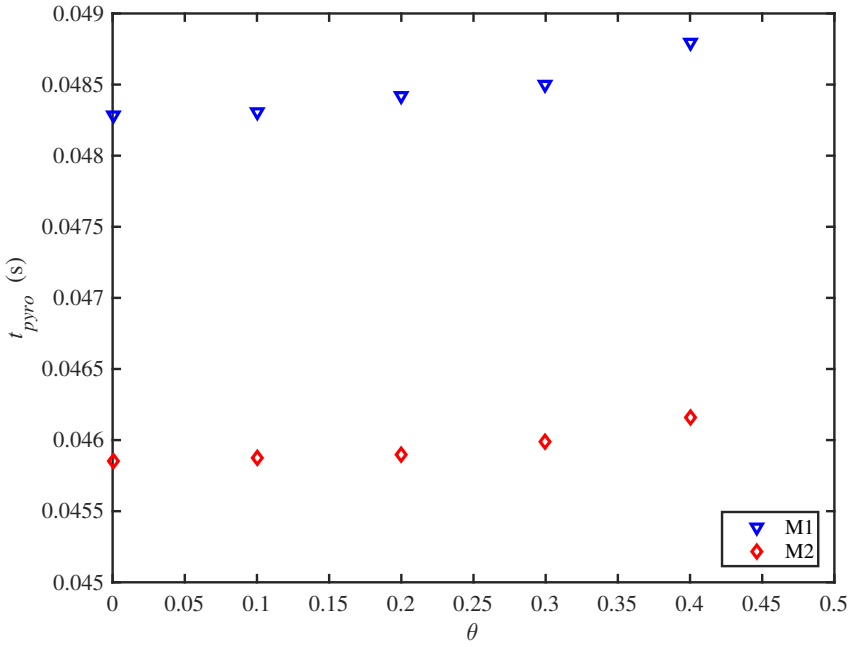

Figure 5.4: Pyrolysis time for coal particles as a function of blending ratio (θ). The biomass particle diameter is 0.5 mm and the coal particle diameter is 0.1 mm. The results are for two different solid mass loadings M1 and M2 as given in table 5.4

can also observe the opposite nature of the effect each fuel has on the pyrolysis of the other fuel, i.e., more coal decreases the pyrolysis time of biomass, whereas more biomass increases the pyrolysis time of coal.

Figure 5.7 presents the relative changes in combustion time for coal and biomass for varying blending ratio. We observe that, unlike pyrolysis, the relative effect of biomass on coal combustion and the relative effect of coal on biomass combustion are comparable. This is mainly due to the comparable combustion times of coal and biomass particles. The coal combustion is slower than the biomass combustion. This is dictated by the reaction kinetics of coal and biomass char. So, despite the much smaller size of coal particle for the cases presented in figure 5.7, its combustion time is comparable to the combustion time of a much larger biomass particle. Due to this we observe that the effect of blending ratio on coal combustion is significant.

In co-firing, the furnace has to be designed/operated to burn all the solid fuel, i.e., both coal and biomass. The residence time of solid particles inside a furnace is governed by the solid mass feed rate to the furnace and the size of the furnace. After the conversion of solid particles inside the furnace, the flue gas is collected at the exit of the furnace for processing. The inert ash from the solids is collected separately after it gets molten [3].

In our simulations, we observe that the biomass particles have a higher total

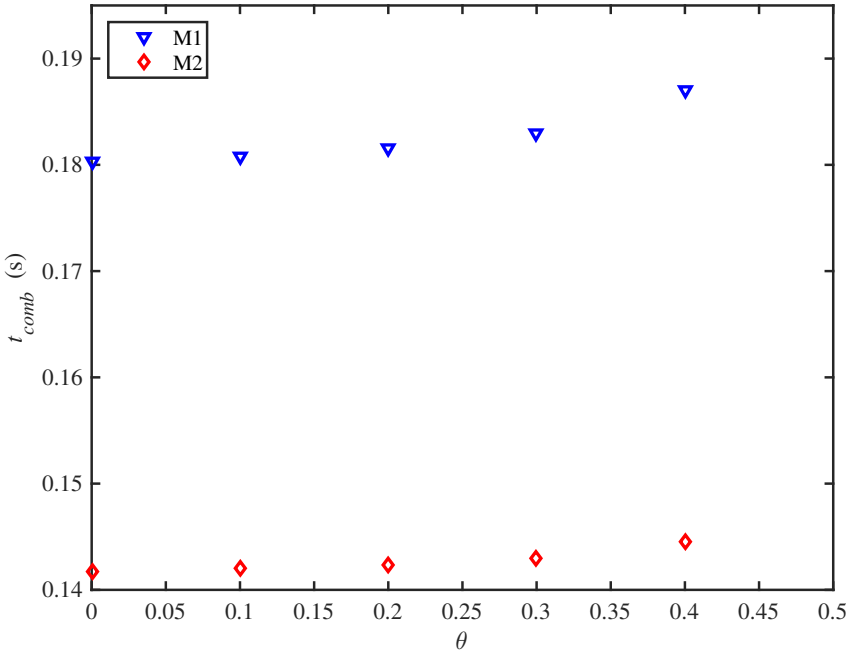

Figure 5.5: Combustion time for coal particles as a function of blending ratio (θ). The biomass particle diameter is 0.5 mm and the coal particle diameter is 0.1 mm. The results are for two different solid mass loadings M1 and M2 as given in table 5.4

conversion time than the coal particles. So the furnace should be operated such that all the biomass particles are burnt inside the furnance. During this time, all the coal particles will also be fully burnt as they have a shorter total conversion time than biomass particles.

From figures 5.6 and 5.7, we observe that as we increase the blending ratio, the total conversion time of both the biomass and the coal increases. This effect is quite small for coal particles and modest for biomass particles. During co-firing, the relative differences in biomass conversion time due to changes in blending ratio will govern the operation of the furnace. An increase in blending ratio will result in longer conversion time for biomass particles. Even a small increase in conversion time of the biomass particles inside the furnace can lead to unreacted solid particles being trapped in the flue gas and ash. The removal of solid particles from the flue gas requires additional equipments like cyclones [7]. Moreover, a high concentration of carbon containing solid particles in the molten ash makes it unusable for certain applications [9].

During co-firing, for a furnace designed to be operated at a particular blending ratio, the modest relative differences in conversion time of biomass that we observe

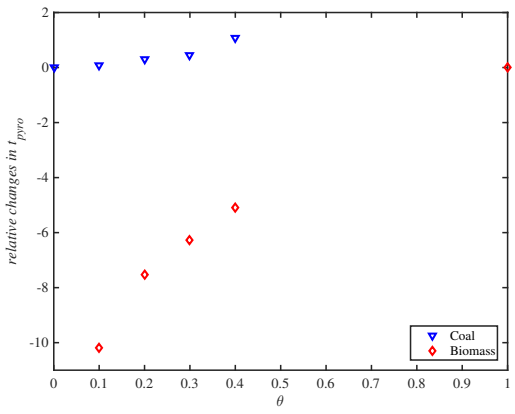

Figure 5.6: Relative changes in pyrolysis time of coal and biomass. The biomass particle diameter is 0.5 mm and coal particle diameter is 0.1 mm. The results correspond to the solid mass loading M1 as given in table 5.4

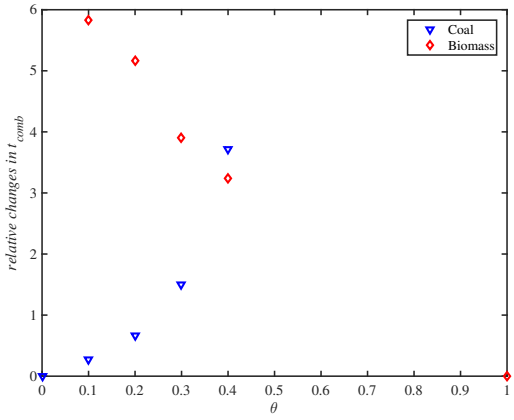

Figure 5.7: Relative changes in combustion time of coal and biomass. The biomass particle diameter is 0.5 mm and coal particle diameter is 0.1 mm. The results correspond to the solid mass loading M1

in figures 5.6 and 5.7 can lead to serious operational problems. To avoid these problems, the operating conditions (solid feed rate) should be changed accordingly.

5.5.2 Effect of varying biomass particle size and blending ratio

In this subsection, we analyze the effect of biomass particle size on the co-firing. As in the earlier analysis, we also vary the blending ratio.

Figure 5.8 presents the relative changes in the conversion time of biomass particles for two different sizes with varying blending ratio. From the figure it can be seen that the relative changes in both pyrolysis and combustion time of the biomass particles are somewhat higher for the larger particle size considered here. The absolute conversion time of larger biomass particles is higher and so coal particles have more time to affect the process of biomass conversion thus leading to higher relative changes in the conversion times.

In figure 5.9 we show the relative changes in the conversion time of coal particles for two different sizes of biomass particles with varying blending ratio. In this chapter, we do not change the size of the coal particles and only vary the size of biomass particle. As can be seen in the figure that when we vary the blending ratio, the effect of the biomass particles size on coal conversion is opposite to its effect on biomass conversion. In figure 5.9 we observe that the relative changes in coal combustion and pyrolysis are higher in case of smaller biomass particles.

This can be explained on the basis of number of biomass particles present in the

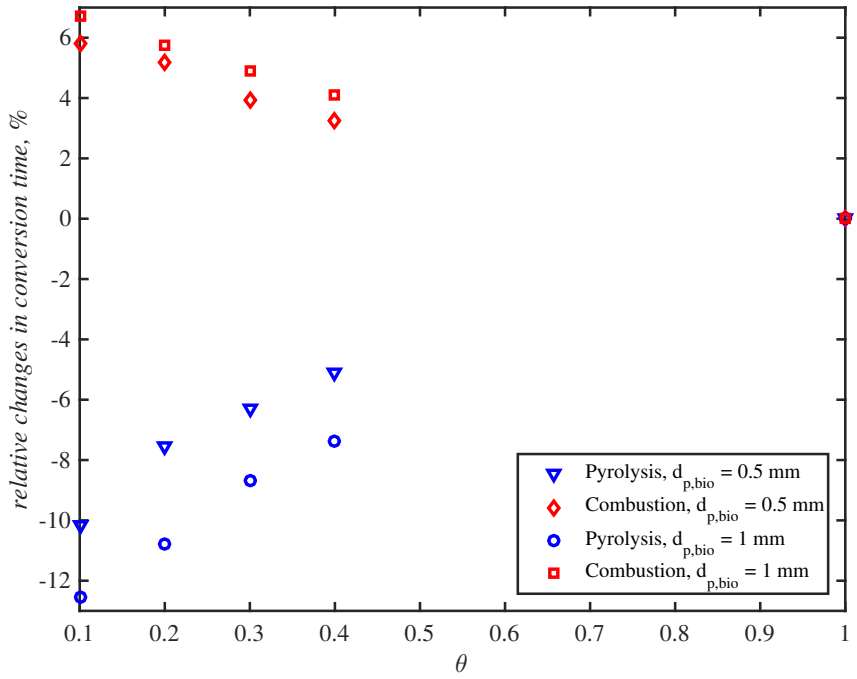

Figure 5.8: Relative changes in conversion time for biomass particles as a function of blending ratio (θ) and for two different sizes of biomass particles. The coal particle diameter is 0.1 mm and the results are for solid mass loading M1. The biomass particle diameter is as given in the legend.

domain. As we do not vary the size of the coal particles, for a given blending ratio and solid mass loading the number of coal particles remains constant. But as we increase the size of the biomass particles, the number of biomass particles decreases. In figure 5.9, we observe that the effect of blending ratio on coal conversion is larger at smaller biomass particle size. This is because a larger number of biomass particles is affecting the conversion process of coal.

5.5.3 Effect of varying solid mass loading and blending ratio

In this section we present results of varying the solid mass loading along with the blending ratio on the coal and biomass conversion. In figures 5.10 and 5.11 we show the relative changes in the conversion time of biomass particles and coal particles respectively. The results are presented for two different solid mass loadings with varying blending ratio. The two solid mass loadings - M1 and M2 - correspond to solid volume fractions (ϕ) of 1×10^{-4} and 1×10^{-5} respectively, where ϕ is calculated for the sole coal firing case.

From figures 5.10 and 5.11 we observe that the effect of blending ratio on the

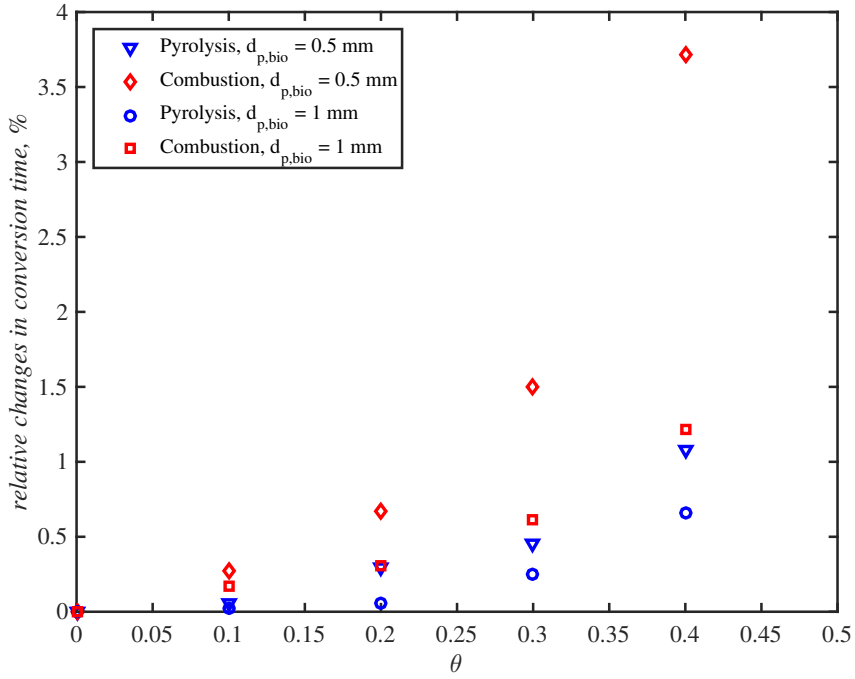

Figure 5.9: Relative changes in conversion time for coal particles as a function of blending ratio (θ) and for two different sizes of biomass particles. The coal particle diameter is 0.1 mm and the results are for solid mass loading M1. The biomass particle diameter is as given in the legend.

biomass and coal conversion is higher at mass loading M1. Mass loading M1 is 10 times the mass loading M2. This means that the total number of particles - both coal and biomass - for a given blending ratio will be higher at mass loading M1 as compared to mass loading M2.

The higher number of solid particles leads to more interaction between the two solid fuels through the gas phase. Hence, we observe higher relative changes in both the pyrolysis and combustion time of coal and biomass particles at mass loading M1.

5.5.4 Effect of blending ratio on the gas phase maximum temperature

In this subsection, we focus our attention on one of the important parameters in the design of a furnace for co-firing. As stated in the introduction of this chapter, the temperatures inside the furnace are critical for its operation. This is because the ash present in the solid fuels needs to melt, so that it can be taken out of the furnace without any problems. If the maximum temperature in the furnace becomes too low, then the ash might not melt which could lead to deposition and slagging

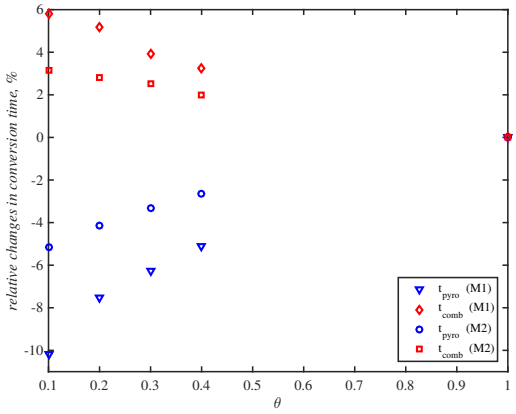

Figure 5.10: Relative changes in the conversion time of biomass as a function of blending ratio. The biomass particle diameter is 0.5 mm and the coal particle diameter is 0.1 mm. The results are for two different solid mass loadings M1 and M2 as shown in table 5.4.

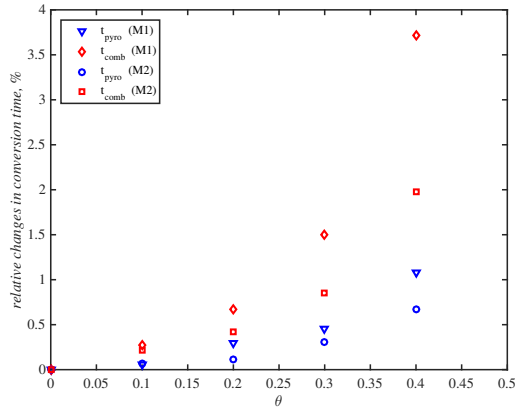

Figure 5.11: Relative changes in the conversion time of coal as a function of blending ratio. The biomass particle diameter is 0.5 mm and the coal particle diameter is 0.1 mm. The results are for two different solid mass loadings M1 and M2 as shown in table 5.4.

[81] inside the furnace.

We use the DNS model of co-firing to study the variation of maximum gas temperature with varying blending ratio. In figure 5.12 we present the maximum temperature of the gas phase for varying blending ratio for two different mass loadings.

It can be seen that as the blending ratio increases, the maximum temperature of the gas phase decreases. This is caused by the difference in heating values of coal and biomass. As given in table 5.1, coal has a higher heating value than biomass. As the blending ratio i.e, the fraction of biomass in the solid feed increases while keeping the mass loading constant, the total heating value of the solid fuel decreases. This casues the maximum temperature of the gas phase to decrease.

The blending ratio for co-firing should be chosen so that the maximum temperature of the gas phase does not go below the ash melting point. The ash melting temperature for wood-ash is typically around 1600 K. A higher blending ratio might lead to the maximum temperature falling below this value thus resulting in fouling inside the furnace. The results show that this can become especially critical at higher mass loadings, where the effect of the presence of biomass on the maximum gas temperature is highest.

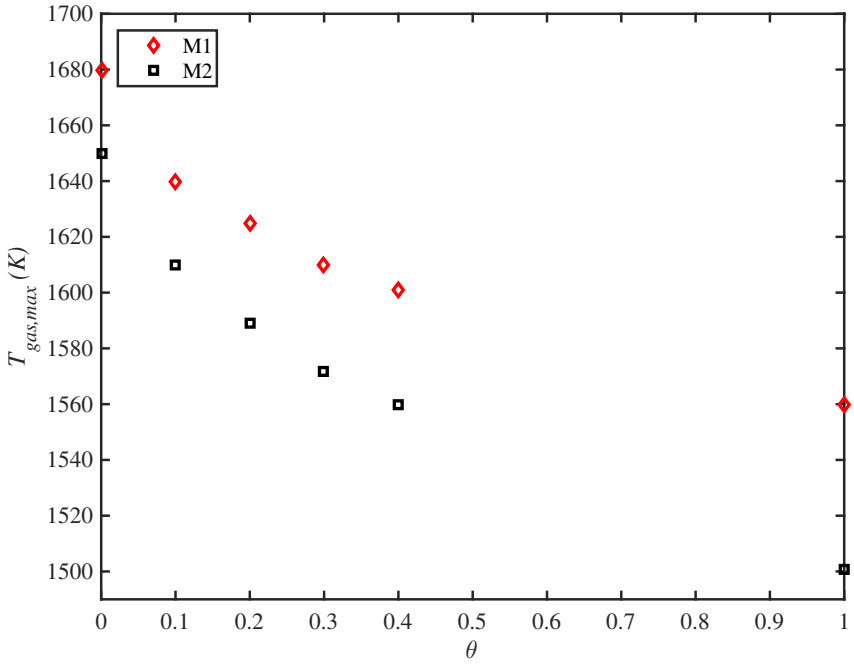

Figure 5.12: Maximum temperature of the gas phase as a function of blending ratio (θ). The biomass particle diameter is 0.5 mm and the coal particle diameter is 0.1 mm. The results are for two different solid mass loadings M1 and M2 as given in table 5.4

5.6 Conclusions

In this chapter we presented the model for DNS of co-firing of coal and biomass. We used the models developed for sole firing of coal and biomass for the DNS of co-firing.

We defined a mass based blending ratio as the ratio between the amount of coal which is substituted by biomass and the original amount of coal. We studied the effect of blending ratio on the conversion of coal and biomass in co-firing.

We found that the presence of coal particles decreases the pyrolysis time of biomass particles, whereas it increases the combustion time of biomass particles. In contrast, the presence of biomass particles increases both the pyrolysis and combustion time of coal particles.

We also found that the effect of blending ratio on coal conversion is higher in case of smaller biomass particles, which is caused by the higher number of biomass particles. The same effect was observed in case of higher solid mass loading where a larger number of solid particles in the domain increases the interaction between coal and biomass particles through the gas phase.

In our simulations, we observe that the biomass particles have a higher total conversion time than the coal particles. So the furnace should be operated such that all the biomass particles are burnt inside the furnance. In such a operation, all the coal particles will also be burnt as they have a smaller total conversion time. We observe that as we increase the blending ratio, the total conversion time of both the biomass and the coal increases. This effect is quite small for coal particles and modest for biomass particles. During co-firing, the relative differences in biomass conversion time due to changes in blending ratio will govern the operation of the furnace.

For a furnace designed to be operated at a particular blending ratio, even the modest relative differences in conversion time for biomass can lead to serious operational problems. To avoid these problems, the operating conditions should be changed accordingly.

Apart from the conversion time of solid fuel, the maximum temperature inside the furnace is one of the critical operating parameters for a furnace. This is because the ash present in the solid fuels needs to melt so that it can be taken out of the furnace without any problems. If the maximum temperature in the furnace becomes too low, then the ash might not melt which could lead to deposition and slagging inside the furnace. Even a small drop in temperature of the gas phase that leads to the temperature falling below the ash melting temperature could lead to severe fouling of the furnace.

In this chapter, we use the co-firing model to study the effect of blending ratio on the maximum temperature and observe that as the blending ratio increases the maximum temperature of the gas phase decreases. This is caused by the difference in heating values of the coal and biomass. Coal has a higher heating value than biomass so as the blending ratio, i.e., the fraction of biomass in the solid feed increases, the total heating value of the solid fuel decreases. This causes the maximum temperature of the gas phase to decrease.

Chapter 6

Conclusions and Recommendations

6.1 Conclusions

As described in the introductory chapter of this thesis, the main aim of this thesis was to develop a computational model for biomass and coal co-firing. To achieve this goal, we proceeded as follows:

- We studied the existing models for biomass particle conversion and adopted them for their use in a CFD code.
- We developed a DNS model for biomass conversion in a turbulent channel-flow and studied the effect of changing model parameters on the biomass conversion process.
- We developed a DNS model for coal conversion in a turbulent channel-flow and studied the effect of changing model parameters on the coal conversion process.
- We studied the coal-biomass co-firing process by varying the coal-biomass blending ratio.

In this thesis, we used the single particle models available for conversion of biomass and coal and adopted them for their use in the DNS model. The developed DNS model captures the main qualitative nature of the biomass and coal conversion processes. We used the DNS model to study the effect of various operating parameters like particle size and solid volume fraction on the solid conversion process. Next, we present the major conclusions of this thesis. We group these conclusions according to the chapters of the thesis.

In chapter 2 of the thesis, we have extended the DNS model of Russo et al. [22] for biomass pyrolysis by including Haseli's [16] single-particle model for biomass combustion, which is suitable for DNS with a large number of biomass particles. The model has been adopted for modeling gas-particle interactions with chemically reacting particles in a turbulent flow.

We observed that the heat exchange between the gas and the particles strongly influences the particle conversion during pyrolysis and combustion. From the results in chapter 2, it is observed that the effect of two-way coupling in the energy equation is significant for particle volume fractions $\phi > 1 \times 10^{-5}$. At lower volume fractions $\phi < 10^{-6}$, the effect of particles on the gas is negligible and at such low volume fractions, particles can be modelled by just including one-way coupling to reduce the computational costs. However, typical industrial furnaces have particle volume fractions on the higher side with $\phi > 1 \times 10^{-3}$ [44] and hence the effect of two-way coupling becomes important.

We also found that the conversion time of biomass particles is sensitive to their diameter and increases for larger particles. One of the main findings of chapter 2 is that at constant particle volume fraction the effect of two-way coupling is higher for smaller particles due to their higher total heat exchange area.

In chapter 2, we analyzed the results of the DNS model for biomass pyrolysis and combustion by only taking into account the heterogeneous solid-gas reactions. In chapter 3, we added homogeneous gas phase reactions to the DNS model to bring the model closer to reality. We used the model to study the effect of gas phase reactions on the biomass conversion process. We observed that the inclusion of gas phase reactions in the DNS model decreases the biomass pyrolysis time due to higher gas temperatures. In contrast, including gas phase reactions increases the combustion time of biomass due to the lower availability of oxygen at the particle surface.

We also found that the effect of gas phase reactions on pyrolysis is higher for smaller particles due to their higher heat exchange area. However, for combustion the effect is higher for larger particles due to the longer duration of the combustion process, which results in more oxygen getting consumed in the gas phase reactions, thereby decreasing the oxygen available for char combustion.

In chapter 3, the DNS model has also been used to perform simulations of realistic biomass particle size distributions (PSD) to compare the particle conversion times for mono-dispersed with PSD cases. We analyzed the interactions between particles of different sizes in the PSD case and found that the presence of smaller particles in the distribution speeds up the conversion process of larger particles.

In chapter 4, we presented the model for DNS of coal pyrolysis and combustion. We used single particle coal conversion models from literature for the DNS of coal particles in a turbulent channel flow.

As the size of coal particles is very small compared to the biomass particles, the number of coal particles in our simulations is very large. Solving the equations for all the coal particles during the simulation is computationally very expensive and

takes a large amount of memory. To overcome this problem we adopted a particle grouping method where a virtual particle represents a number of real coal particles with the same properties. In order to model the interaction between the two phases, we multiplied the two way coupling terms between the gas and particles with the particle grouping factor.

We analyzed the accuracy of this particle grouping method by running simulations at varying values of the particle grouping factor (ζ). We observe that a value of $\zeta = N_p/N_{cell}$, where N_p is the number of virtual particles and N_{cell} the number of grid cells, results in a good approximation for the simulation with no particle grouping. This is true for all the particle sizes and solid volume fractions used in our study. We also observed that the errors due to larger values of ζ are low for simulations with high solid volume fractions, irrespective of the size of the particles.

We observed that the threshold for ζ below which the relative error in the results is negligible corresponds to an average distance between two particles approximately equal to $0.015H$, where H is half the channel height. This distance can be compared to the size of a computational cell. The length of a grid cell in the streamwise direction equals $0.098H$ and in the spanwise direction $0.049H$, both significantly larger than this threshold value. The average length of a grid cell in the wall-normal direction, however, is $0.016H$, which is very close to the threshold value.

Finally, in chapter 5, we presented the model for DNS of co-firing of coal and biomass. We used the models developed for sole firing of coal and biomass for the DNS of co-firing. A mass based blending ratio is defined as the ratio between the amount of coal which is substituted by biomass and the original amount of coal. In chapter 5, we studied the effect of the blending ratio on the conversion of coal and biomass in co-firing.

We observed that during co-firing the presence of coal particles decreases the pyrolysis time of biomass particles, whereas it increases the combustion time of biomass particles. In contrast, the presence of biomass particles increases both the pyrolysis and combustion time of coal particles.

We also observed that the effect of blending ratio on coal conversion is higher in case of smaller biomass particles, which is caused by the higher number of biomass particles. The same effect is observed in case of higher solid mass loading where a larger number of solid particles in the domain increases the interaction between coal and biomass particles through the gas phase.

In our simulations, we observe that the biomass particles have a higher total conversion time than the coal particles. So the furnace should be operated such that all the biomass particles are burnt inside the furnance. In such a operation, all the coal particles will also be burnt as they have a smaller total conversion time. We observe that as we increase the blending ratio, the total conversion time of both the biomass and the coal increases. This effect is quite small for coal particles and modest for biomass particles. During co-firing, the relative differences in biomass conversion time due to changes in blending ratio will govern the operation of the

furnace.

For a furnace designed to be operated at a particular blending ratio, even the modest relative differences in conversion time for biomass can lead to serious operational problems. To avoid these problems, the operating conditions should be changed accordingly.

We also studied the effect of varying blending ratio on the maximum temperature inside the furnace as it is one of the critical operating parameters for a furnace. Using the co-firing model, we found that as the blending ratio increases the maximum temperature of the gas phase decreases. This is because of the difference in heating values of the coal and biomass. Coal has a higher heating value than biomass, so as the blending ratio, i.e., the fraction of biomass in the solid feed increases, the total heating value of the solid fuel decreases. This causes the maximum temperature of the gas phase to decrease.

6.2 Recommendations

The DNS model presented in this thesis incorporates several simplifying assumptions in describing various aspects of pyrolysis and combustion of biomass and coal particles. Some of these assumptions and possible improvements/recommendations are listed below.

- One of the main assumptions for biomass conversion is the spherical shape of the biomass particles. Biomass particles are highly unspherical in shape [13, 14, 15]. This is in contrast to coal particles which are very close to spherical in shape [23]. Although we use a point particle assumption in our model, the equations for particle tracking, heat transfer, and kinetic reaction rates have been formulated with an assumption of spherical shape for the biomass particles. An improvement of our model would be to remove this assumption for biomass particles. This can be done in two ways: Either use a correction factor to account for the non-spherical shape of the particles [87], or use a combination of standard non-spherical shapes to represent biomass particles [88]. In either case the orientation of the particles will play a role and equations describing the evolution of this orientation should be solved along with the other equations for the particle properties.

- As our main objective in this thesis was to present a framework for the DNS of biomass particle conversion, we used very simplified reaction kinetics for gas phase homogeneous reactions. The chemistry in the gas phase is represented by a single methane combustion reaction in our model. Other studies on coal combustion [23, 48] use a detailed chemical kinetics consisting of several elementary reactions to represent the chemistry of gases present in the gas

phase. Similar gas phase reaction models can be included in the DNS of biomass conversion to improve its predictive capability.

- The assumption of point particle in our model becomes questionable for larger particles. If the particle is larger than the typical length scales of the the flow, the expressions used for the drag force and the convective heat transfer between gas and particles are no longer valid and finite-size effects need to be incorporated.

- Multiple other issues with the numerical method need to be addressed in order to obtain a stable numerical method for a wide range of particle sizes. Currently, the stability issues in our model limit us to a smallest particle size of 0.025 mm and a largest particle size of 3 mm. Moreover, the presence of a large particle near the wall may lead to instability because its influence on the gas properties in the control volume where the particle is located may be too high. This presents a problem in particular in the region close to the walls, since the size of the control volume is smallest there. If the particle is larger than the control volume, the two-way coupling terms in the gas equations should be distributed over more control volumes.

In light of these assumptions, the DNS model presented in this thesis captures the main qualitative nature of the multitude of dynamic interactions between the gas flow, the particles, and the processes occuring. The presented approach shows that such models for biomass and coal conversion can be developed with sufficient accuracy without increasing the computational costs too much. Fewer model assumptions as outlined above can further improve the model's accuracy but this would also lead to an increase in computational time. More research is needed to quantify the impact of such potential improvements. Such research will benefit from ongoing rapid advancements in computing technology which will drive further computational discoveries and analysis in this field. The advancements in computing technology will make it possible in the near future to run detailed simulations for biomass and coal conversion in a reasonable amount of time.

References

[1] M. F. Demirbas, M. Balat, H. Balat, Potential contribution of biomass to the sustainable energy development, Energy Conversion and Management, 50(7), 1746-1760 (2009).

[2] A. Zervos, Renewables 2013 global status report, Renewable Energy Policy Network for the 21st Century, Paris, France (2013).

[3] S. van Loo, J. Koppejan (Eds.), The Handbook of biomass combustion and cofiring, Taylor and Francis, United Kingdom (2002).

[4] P. Basu, J. Butler, M. A. Leon, Biomass co-firing options on the emission reduction and electricity generation costs in coal-fired power plants, Renewable Energy, 36, 282-288 (2011)

[5] J. J. Battista, E. E. Hughes, D. A. Tillman, Biomass co-firing at Seward station, Biomass and Bioenergy, 19, 419-427 (2000)

[6] X. Wang, H. Tan, Y. Niu, M. Pourkashanian,L. Ma, E. Chen, Y. Liu, Z. Liu, T. Xu, Experimental investigation on biomass co-firing in a 300MW pulverised coal-fired utility furnace in China. Proceedings of the Combustion Institute, 33, 2725-2733 (2011)

[7] L. Baxter, Biomass-coal co-combustion: opportunity for affordable renewable energy, Fuel, 84(10), 1295-1302 (2005).

[8] L. Gustavsson, P. Borjesson, B. Johansson, P. Svenningsson, Reducing CO_2 emissions by substituting biomass for fossil fuels, Energy, 20(11), 1097-1113 (1995).

[9] P. McKendry, Energy production from biomass (part 1): overview of biomass, Bioresource technology, 83(1), 37-46 (2002).

[10] A. Demirbas, Sustainable cofiring of biomass with coal, Energy Conversion and Management, 44(9), 1465-1479 (2003).

[11] T. Abbas, P. G. Costen, F. C. Lockwood, Solid fuel utilization: from coal to biomass, In Symposium (International) on Combustion, Elsevier, 26(2), 3041-3058 (1996).

[12] Y. Haseli, Modeling combustion of single biomass particle (PhD thesis) Eindhoven University of Technology (2012).

[13] C. Di Blasi, Modeling chemical and physical processes of wood and biomass pyrolysis, Progress in Energy and Combustion Science, 34(1), 47-90 (2008).

[14] C. Di Blasi, Influences of physical properties on biomass devolatilization characteristics, Fuel, 76(10), 957-964 (1997).

[15] A. Galgano, C.Di Blasi, Modeling wood degradation by the unreacted-core-shrinking approximation, Industrial and engineering chemistry research, 42(10), 2101-2111 (2003).

[16] H. Lu, W. Robert, G. Peirce, B. Ripa, L. L. Baxter, Comprehensive study of biomass particle combustion, Energy and Fuels, 22(4), 2826-2839 (2008).

[17] Y. B. Yang, V. N. Sharifi, J. Swithenbank, L. Ma, L. I. Darvell, J. M. Jones, M. Pourkashanian, A. Williams, Combustion of a single particle of biomass, Energy and Fuels, 22(1), 306-316 (2007).

[18] K. Luo, H. Wang, J. Fan, F. Yi, Direct numerical simulation of pulverized coal combustion in a hot vitiated co-flow, Energy and Fuels, 26(10), 6128-6136 (2012).

[19] Q. Shang, J. Zhang, Simulation of gas-particle turbulent combustion in a pulverized coal-fired swirl combustor. Fuel, 88(1), 31-39 (2009).

[20] R. Kurose, H. Makino, Large eddy simulation of a solid-fuel jet flame, Combustion and Flame, 135(1), 1-16 (2003).

[21] K. Yamamoto, T. Murota, T. Okazaki, M. Taniguchi, Large eddy simulation of a pulverized coal jet flame ignited by a preheated gas flow, Proceedings of the Combustion Institute, 33(2), 1771-1778 (2011).

[22] C. Ghenai, I. Janajreh, CFD analysis of the effects of co-firing biomass with coal, Energy Conversion and Management, 51(8), 1694-1701 (2010).

[23] T. Hara, M. Muto, T. Kitano, R. Kurose, Direct numerical simulation of a pulverized coal jet flame employing a global volatile matter reaction scheme based on detailed reaction mechanism, Combustion and Flame, 162, 4391-4407 (2015).

[24] T. Brosch, D. Patel, D. Wacks, N. Chakraborty, Numerical investigation of localised forced ignition of pulverised coal particle-laden mixtures: A Direct Numerical Simulation (DNS analysis, Fuel, 145, 50-62 (2015).

[25] F. R. Shafizadeh, P. P. Chin, Thermal deterioration of wood, In ACS Symposium Series American Chemical Society (1977).

[26] C. A. Koufopanos, A. Lucchesi, G. Maschio, Kinetic modelling of the pyrolysis of biomass and biomass components, The Canadian Journal of Chemical Engineering, 67(1), 75-84 (1989).

[27] Y. Haseli, J. A. van Oijen, L. P. H. de Goey, A simplified pyrolysis model of a biomass particle based on infinitesimally thin reaction front approximation, Energy and Fuels, 26(6), 3230-3243 (2012).

[28] E. Russo, J. G. M. Kuerten, B. J. Geurts, Delay of biomass pyrolysis by gas-particle interaction, Journal of analytical and applied pyrolysis, 110, 88-99 (2014).

[29] E. Russo, DNS of turbulent particle-laden channel flow with heat and mass transfer (Ph.D. Thesis), Eindhoven University of Technology, The Netherlands (2014).

[30] Haseli Y., van Oijen J. A., de Goey L. P. H., A quasi-steady analysis of oxy-fuel combustion of a wood char particle. Combustion Science and Technology, (2012)

[31] A. Esmaeeli, G. Tryggvason, Direct numerical simulations of bubbly flows Part 1: Low Reynolds number arrays, Journal of Fluid Mechanics, 377, 313-345 (1998).

[32] A. Esmaeeli, G. Tryggvason, Direct numerical simulations of bubbly flows Part 2: Moderate Reynolds number arrays, Journal of Fluid Mechanics, 385, 325-358 (1999).

[33] S. Elghobashi, On predicting particle-laden turbulent flows, Applied Scientific Research, 52(4), 309-329 (1994).

[34] C. Marchioli, M. Picciotto, A. Soldati, Particle dispersion and wall-dependent turbulent flow scales: implications for local equilibrium models. Journal of Turbulence, 7, N60 (2006).

[35] C. Marchioli, A. Soldati, J. G. M. Kuerten, B. Arcen, A. Taniere, G. Goldensoph, K. D. Squires, M. F. Cargnelutti, L. M. Portela, Statistics of particle dispersion in direct numerical simulations of wall-bounded turbulence: results of an international collaborative benchmark test, International Journal of Multiphase Flow, 34(9), 879-893 (2008).

[36] F. Toschi, E. Bodenschatz, Lagrangian properties of particles in turbulence, Annual Review of Fluid Mechanics, 41, 375-404 (2009).

[37] S. Balachandar, J. K. Eaton, Turbulent dispersed multiphase flow, Annual Review of Fluid Mechanics, 42, 111-133 (2010).

[38] A. Ferrante, S. Elghobashi, On the physical mechanisms of two-way coupling in particle-laden isotropic turbulence, Physics of Fluids, 15(2), 315-329 (2003).

[39] L. Ma, M. Gharebaghi, R. Porter, M. Pourkashanian, J. M. Jones, A. Williams, Modelling methods for co-fired pulverised fuel furnaces, Fuel, 88(12), 2448-2454 (2009).

[40] B. Arias, C. Pevida, J. Fermoso, M. G. Plaza, F. Rubiera, J. J. Pis, Influence of torrefaction on the grindability and reactivity of woody biomass, Fuel Processing Technology, 89(2), 169-175 (2008).

[41] W. E. Hillis, Wood and biomass ultrastructure. In Fundamentals of Thermochemical Biomass Conversion, Springer, 1-33 (1985).

[42] M. G. Gronli, A theoretical and experimental study of the thermal degradation of biomass (Ph.D. Thesis), NTNU, Trondheim, Norway (1996).

[43] A. Galgano, C. Di Blasi, Modeling the propagation of drying and decomposition fronts in wood, Combustion and Flame, 139(1), 16-27 (2004).

[44] B. J. P. Buhre, L. K. Elliott, C. D. Sheng, R. P. Gupta, T. F. Wall, Oxy-fuel combustion technology for coal-fired power generation, Progress in Energy and Combustion Science, 31, 283-307 (2005).

[45] T. Wall, Y. Liu, C. Spero, L. Elliott, S. Khare, R. Rathnam, An overview on oxyfuel coal combustion – State of the art research and technology development, Chemical Engineering Research and Design, 87, 1003-1016 (2009).

[46] R. Johansson, K. Andersson, B. Leckner, H. Thunman, Models for gaseous radiative heat transfer applied to oxyfuel conditions in boilers, International Journal of Heat and Mass Transfer, 53, 220-230 (2010).

[47] C. Yin, L. C. R. Johansen, L. A. Rosendahl, S. K. Kaer, New weighted sum of gray gases model applicable to computational fluid dynamics (CFD) modeling of oxy-fuel combustion: derivation, validation, and implementation, Energy and Fuels, 24, 6274-6282 (2010).

[48] L. Ma, J.M. Jones, M. Pourkashanian, A. Williams, Modelling the combustion of pulverized biomass in an industrial combustion test furnace, Fuel, 86(12), 1959-1965 (2007).

[49] P. J. Linstrom, NIST chemistry webbook. Gaithersburg, MD: National Institute of Standards and Technology (2001).

[50] J. Warnatz, U. Maas, R. W. Dibble, Combustion, Springer Verlag, Berlin (1996).

[51] F. A. Williams, Combustion Theory, Addison-Wesley Publishing Company, Redwood city (1985).

[52] J. O. Hirschfelder, C. F. Curtis, R. B. Bird, Molecular theory of gases and liquids, Wiley, New York (1964).

[53] G. Dixon-Lewis, Flame structure and flame reaction kinetics II Transport phenomena in multi-component systems, Proc. Roy. Soc. A, 307(1488), 111-135 (1968).

[54] P. R. Spalart, R. D. Moser, M. M. Rogers, Spectral methods for the Navier-Stokes equations with one infinite and two periodic direction, Journal of Computational Physics, 96(2), 297-324 (1991).

[55] J. G. M. Kuerten, A. W. Vreman, Effect of droplet interaction on droplet-laden turbulent channel flow, Physics of Fluids, 27(5), 053304 (2015).

[56] A. Bukhvostova, E. Russo, J. G. M. Kuerten, B. J. Geurts, Comparison of DNS of compressible and incompressible turbulent droplet-laden heated channel flow with phase transition, International journal of multiphase flow, 63, 68-81 (2014).

[57] P. Rosin, E. Rammler, The laws governing the fineness of powdered coal, Journal of the Institute of Fuel, 7, 29-36 (1933).

[58] L. Yang, X. Chen, X. Zhou, W. Fan, The pyrolysis and ignition of charring materials under the external heat flux, Combust. Flame, 133, 407-13 (2003).

[59] M. Vascellari, S. Schulze, P. Nikrityuk, D. Safronov, C. Hasse, Numerical simulation of pulverized coal MILD combustion using a new heterogeneous combustion submodel. Flow, turbulence and combustion, 92(1-2), 319-345 (2014).

[60] J. Bibrzycki, T. Poinsot, Investigation of laminar flame speed of CH4/N2/O2 and CH4/CO2/O2 mixtures using reduced chemical kinetic mechanisms, Archivium Combustionis, 30, 287 (2010).

[61] S.V. Apte, K Mahesh, P. Moin, J.C. Oefelein, Large-eddy simulation of swirling particle-laden flows in a coaxial-jet combustor, International Journal of Multiphase Flow, 29, 1311-1331 (2003).

[62] R. I. Backreedy, L. M. Fletcher, L. Ma, M. Pourkashanian, A. Williams, Modelling pulverised coal combustion using a detailed coal combustion model, Combustion Science and Technology, 178, 763-787 (2006).

[63] P. Edge, S. R. Gubba, R. Porter, M. Pourkashanian, J. M. Jones, A. Williams, LES modelling of air and oxy-fuel pulverised coal combustion – Impact on flame properties. Proceedings of the Combustion Institute, 33, 2709-2716 (2011).

[64] R. Kurose, H. Watanabe, H. Makino, Numerical simulations of pulverized coal combustion, KONA Powder Part. Journal, 27(0),144–156 (2009).

[65] N. Hashimoto, R. Kurose, S. M. Hwang, H. Tsuji, H. Shirai, A numerical simulation of pulverized coal combustion employing a tabulated-devolatilization process model (TDP model), Combustion & Flame, 159(1), 353–366 (2012).

[66] A. H. Al-Abbas, J. Naser, E. K. Hussein, Numerical simulation of brown coal combustion in a 550 MW tangentially-fired furnace under different operating conditions,Fuel, 107, 688–698 (2013).

[67] R. Kurose, H. Makino, Large eddy simulation of a solid-fuel jet flame, Combustion & Flame, 135(1), 1–16 (2003).

[68] O. Stein, G. Olenik, A. Kronenburg, F. C. Marincola, B. Franchetti, A. Kempf, M. Ghiani, M. Vascellari, C. Hasse, Towards comprehensive coal combustion modelling for LES, Flow Turbulence & Combustion, 90(4), 859–884 (2013).

[69] G. Olenik, O. Stein, A. Kronenburg, LES of swirl-stabilised pulverised coal combustion in IFRF furnace No.1, Proceedings of the Combustion Institute, 35(3), 2819–2828 (2015).

[70] M. Muto, H. Watanabe, R. Kurose, S. Komori, S. Balusamy, S. Hochgreb, Large-eddy simulation of pulverized coal jet flame - Effect of oxygen concentration on NOx formation,Fuel, 142(15), 152–163 (2015).

[71] M. Rabacal, B. Franchetti, F. C. Marincola, F. Proch, M. Costa, C. Hasse, A. Kempf, Large eddy simulation of coal combustion in a large-scale laboratory furnace, Proceedings of the Combustion Institute, 35(3), 3609–3617 (2015).

[72] S. M. Hwang, R. Kurose, F. Akamatsu, H. Tsuji, H. Makino, M. Katsuki, Direct numerical simulation of pulverized coal combustion in a hot vitiated coflow, Energy & Fuels, 19(2), 382–392 (2005).

[73] E. Korytnyi, R. Saveliev, M. Perelman, B. Chudnovsky, R. Bar-Ziv E, Computational fluid dynamic simulations of coal-fired utility boilers: an engineering tool, Fuel, 88, 9–18 (2009).

[74] X. Y. Zhao, D. C. Haworth, Transported PDF modeling of pulverized coal jet flames, Combustion & Flame, 161, 1866–82 (2014).

[75] R. Jovanovic, B. Rašuo, P. Stefanovic, D. Cvetinovic, B. Swiatkowski, Numerical investigation of pulverized coal jet flame characteristics under different oxyfuel conditions, International Journal of Heat and Mass Transfer, 58, 654–62 (2013).

[76] B. M. Franchetti, M. F. Cavallo, S. Navarro-Martinez, A. M. Kempf, Large Eddy simulation of a pulverised coal jet flame, Proceedings of the Combustion Institute, 34, 2419 (2013).

[77] H. Kobayashi, J. B. Howard, A. Sarofim, Coal devolatilization at high temperatures, Proceedings of the Combustion Institute, 16, 411 (1977).

[78] J. M. Jones, M. Pourkashanian, D. J. Waldron, A. Williams, Prediction of NOx and unburned carbon in ash in highly staged pulverised coal furnace using overfire air, Journal of the Energy Institute, 83(3), 144-150 (2010).

[79] W. Lin, P. A. Jensen, A. D. Jensen AD, Biomass Suspension Combustion: Effect of two-stage combustion on NOx emissions in a laboratory-scale swirl burner, Energy and Fuels, 23, 1398-1405 (2009).

[80] Department of Energy, Energy Information Administration, Annual energy outlook 1998, DOE/EIA-0383(98), Washington, DC, December, 1997.

[81] K. R. G. Hein, J. M. Bemtgen, EU clean coal technology, co- combustion of coal and biomass, Fuel Processing & Technology, 54, 159–69 (1988).

[82] E. E. Hughes, D. A. Tillman, Biomass cofiring: status and prospects, Fuel Processing & Technology, 54, 127–42 (1998).

[83] T. Abbas, P. Costen, N. H. Kandamby, F.C. Lockwood, J. J. Ou, The influence of burner injection mode on pulverized coal and biosolid co-fired flames, Combustion & Flame, 99, 617–25 (1994).

[84] S. Dhanaplan, K. Annamalai, P. Daripa, Turbulent combustion modeling coal: biosolid blends in a swirl burner. Energy Week, vol. IV, ETCE, ASME, 415–23January (1997).

[85] S. K. Kaer, L. Rosendahl, P. Overgaard, Numerical analysis of co-firing coal and straw. In: Proceedings of the 4th European CFD Conference, Athens, Greece, 7–11 September, 1194-9 (1998).

[86] M. Sami, K. Annamalai, S. Dhanapalan, M. Wooldridge, Numerical simulation of blend combustion of coal and feedlot waste in a swirl burner. In: ASME Conference, Nashville, TN (1999).

[87] R. P. Chhabra, L. Agarwal, N.K. Sinha, Drag on non-spherical particles: an evaluation of available methods, Powder Technology, 101, 288-295 (1999).

[88] E. Loth, Drag of non-spherical solid particles of regular and irregular shape, Powder Technology 182, 342-353 (2008)

Societal Summary

Renewable energy is key to meet the ever increasing needs in a climate-constrained world. An increased awareness about the depleting fossil fuel resources coupled with a higher sensibility towards environmental pollution has made biomass an attractive alternative energy source. Being the only carbon based renewable fuel in our fossil fuel based economy and due to its large availability in many regions of the world, biomass has attracted the attention of both scientific researchers and industrial companies. Consequently, biomass utilization, as an energy source, has continued to increase and now accounts for over 10% of global primary energy supply.

The word biomass refers to all kinds of materials derived from living organisms. This inludes plant matter and its derivatives, such as wood, wood-derived fuels, fuel crops, agricultural wastes and by-products, and animal waste. This list comprises the solid, liquid, and gaseous forms of biomass. All these forms of biomass are used to generate energy in the form of renewable energy sources.

The solid biomass, mainly wood and wood-derived fuels, can be burned in furnaces to generate power. This is one of the main, and more mature, biomass-to-energy pathways. It involves generation of power by burning solid biomass along with coal in commercial power plants. This process of co-firing biomass with coal is one of the most economic and easily adaptable methods to increase the proportion of energy generated from renewable sources. The carbon neutrality of biomass is instrumental in reducing the carbon footprint of these co-firing plants. This is particularly beneficial if the biomass used in co-firing is a waste agricultural residue. The idea behind coal-biomass co-firing is to utilize existing coal combustion equipment for burning biomass in order to save on new capital expenditure. Experimental studies have also shown improvement in NOx and SOx emissions when comparing coal firing and co-firing.

However, biomass differs significantly from coal in its low carbon, high volatile matter and higher oxygen content. This results in lower heating values for biomass as compared to coal, and significant differences in conversion times of the fuel particles during co-firing. These differences in fuel properties result in suboptimal utilization of biomass while burning it in equipment primarily designed for coal. To achieve higher efficiencies in the co-firing process, a better understanding of biomass particle behavior and gas-particle interactions inside the furnace is desired. A deeper

knowledge of biomass particle interactions with the gas inside the furnace will be helpful in improving the design of furnaces and optimizing operating conditions by changing for example the properties of the biomass particles.

In this thesis, we focus our attention on studying the biomass-coal co-firing by developing a computational model for the process. In the past, much attention has been focused on the modeling of coal combustion. The success of such efforts is illustrated by the incorporation of coal conversion models into standard CFD commercial software packages. Modeling of other solid fuels, such as biomass, is still a relatively new field. Existing models for coal conversion can not be directly adopted for biomass because the fundamental assumptions in coal conversion process are not applicable to biomass particles.

We use single particle models for biomass pyrolysis and combustion and adopt them for their use in a CFD model of solid particles and gas. We combine the models for biomass conversion and coal conversion to study the co-firing process inside a furnace. The CFD model presented in this thesis captures the main qualitative nature of the multitude of dynamic interactions between the gas flow, the particles, and the processes occuring. The presented approach shows that such models for biomass and coal conversion can be developed with sufficient accuracy without increasing the computational costs too much.

In future, such research will further benefit from ongoing rapid advancements in computing technology which will drive further computational discoveries and analysis in this field. The advancements in computing technology will make it possible in the near future to run detailed simulations for biomass and coal conversion in a reasonable amount of time.

Acknowledgements

This thesis is the summary of four years of work on my Ph.D. project. There are a lot of people who accompanied me on this journey and I would like to express my gratitude to all of them.

First and foremost I would like to thank my thesis supervisor, Hans. I couldn't thank you enough. Your guidance is probably the most important factor that I was able to complete this project. Your patience while dealing with me was remarkable. I kept on missing the deadlines but you never lost your patience. My thanks are not only for your professional support and help but mainly for the growth I went through by working with you every day. I have learnt a lot from you that will help me in my life.

Next I would like to thank my co-supervisor Bernard. Your contribution to my work was immense. Our productive discussions helped in improving the quality of my work. These discussions helped me to develop and establish my ideas. The quality of my writing has also improved, all thanks to you.

I use this opportunity to express my gratitude to all my colleagues at the (old) Process Technology group, in particular to my colleague Julien. Your help and support during the initial years of my Ph.D. was immense. I would also like to thank my office-mate Haiyu. Our lunch table discussions were very interesting.

My stay in Netherlands would have been incomplete without my friends from India: Amar, Abhineet, Nikhil, And Shauvik. I will forever remember our friday night hangouts. Without you guys, my stay in Netherlands would not have been the same. All of you will always be a part of my life.

A special thanks to Vikrant. You are the reason I was able to settle in Netherlands without any problems.

During this journey I met special people, in Eindhoven and elsewhere, and I want to take this opportunity to express my gratitude to all of them: Prof. Niels Deen, Wiktor, Christian, Joris, Giel, Manoj, David, Coen, Boaz, Emanuele, Ashish, Mayank, Amit, Marjan, Marianne, Sina, Maria, and Erwin. I thank all of you for your help and support in my work.

Last but not the least, I would like to thank my mother and my elder brother. They have been supporting me like a rock. I owe them everything in my life.

Curriculum vitae

Abhijay Awasthi was born on March 14, 1987 in Jabalpur, India. He finished his schooling in 2005 and joined Indian Institute of Technology at Delhi (IIT Delhi) in India. There he studied chemical engineering at for 5 years and completed a dual degree course (Bachelor's and Master's). During the second year at college, he worked as a summer intern at Lupin Pharmaceuticals where he worked on the optimization of a solvent recovery process at the manufacturing plant. During the summer of third year at college, he worked as an intern at Larsen and Toubro (L&T) where he worked on the modeling of a fixed bed coal gasifier. In 2010, he completed his masters in computer applications in chemical engineering. During the convocation at IIT Delhi, he was awarded the Best Industry Relevant Thesis award for the year 2010.

After completing his Bachelor's and Master's studies, he joined Reliance Industries Limited (RIL) as a process engineer at their Jamnagar Refinery in India. He worked at RIL for 3 years where he was involved in several computational modeling projects. During his tenure at Reliance he was part of a special task force and worked on RIL's Jamnagar Mega Petcoke Gasification project.

In 2013, he was selected by Shell and NWO for their 'Computational Sciences in Energy Research Program' to pursue his Ph.D. in the Netherlands. He was selected to work under Prof.Dr. J. G. M. Kuerten at the Mechanical Engineering Department of University of Technology at Eindhoven (TU/e). He started his Ph.D. in September 2013. His doctoral research focussed on the mathematical modeling of biomass conversion for co-firing power plants. The modeling of the dispersed biomass particles was done with an point particle assumption. An Eulerian-Lagrangian approach was used to model the gas-particle system in a channel flow. The research involved using single particle models for biomass and coal conversion and adopt them for their use in Direct Numerical Simulation.

During his PhD research, he presented his work in several international conferences. During the four years at TU/e, he also tutored groups of Bachelors students and supervised projects of Bachelor students.